uOttawa

L'Université canadienne
Canada's university

FACULTÉ DES ÉTUDES SUPÉRIEURES ET POSTOCTORALES

uOttawa

L'Université canadienne
Canada's university

FACULTY OF GRADUATE AND POSDOCTORAL STUDIES

Patrick James Villeneuve
AUTEUR DE LA THÈSE / AUTHOR OF THESIS

Ph.D. (Biochemistry)
GRADE / DEGREE

Department of Biochemistry, Microbiology and Immunology
FACULTÉ, ÉCOLE, DÉPARTEMENT / FACULTY, SCHOOL, DEPARTMENT

The Aging Lung and Cancer:
Evidence of Field Cancerization from Transcriptional Profiles of Normal Human and Mouse Lung Tissues

TITRE DE LA THÈSE / TITLE OF THESIS

Douglas Gray
DIRECTEUR (DIRECTRICE) DE LA THÈSE / THESIS SUPERVISOR

CO-DIRECTEUR (CO-DIRECTRICE) DE LA THÈSE / THESIS CO-SUPERVISOR

John Bell

Christopher Kennedy

David LeBrun (Queen's University)

Bruce McKay

Gary W. Slater
Le Doyen de la Faculté des études supérieures et postdoctorales / Dean of the Faculty of Graduate and Postdoctoral Studies

The Aging Lung and Cancer:
Evidence of Field Cancerization from Transcriptional Profiles of Normal Human and Mouse Lung Tissues

Patrick James Villeneuve

Thesis submitted to the
Department of Biochemistry, Microbiology and Immunology
in partial fulfilment of the requirements for the degree of Doctor of Philosophy

University of Ottawa
Ottawa, ON, Canada
2010

Your file Votre référence
ISBN: 978-0-494-66253-3
Our file Notre référence
ISBN: 978-0-494-66253-3

ABSTRACT

The effect of increased age on gene expression has not previously been evaluated in lung tissues. Cancer incidence increases with age, and lung cancer in particular has been found to have an incidence that peaks in the later decades of life. Based on previously published studies of aging effects in human muscle, kidney and retinal tissues, significant transcriptional changes are anticipated in both mouse and human aged lung tissues that may predispose to the development of cancer.

We examined lung aging between young and old mice (6 vs. 30 months), using a hybrid mouse model (CB6F1) and an experimental colorectal metastasis model (CT26 cells). We also recruited young (<30 years) and aged (>60 years) human patients. Microarray analysis of mouse lung tissues using MOE430v2 and human lung tissues suing HG U133 2.0+ Affymetrix arrays was performed using total lung RNA, after which expression values were computed from .CEL files by applying RMA normalization within sets of replicate samples. Statistical testing was performed using the significance analysis of microarrays algorithm. Statistically significant transcripts were validated by histochemical staining and quantitative polymerase chain reactions (PCR).

In mouse tissues, induced metastatic disease was found to be associated with reduced overall survival in older mice. The pattern of pulmonary metastases was more diffuse as compared to younger mice. Age-related transcriptional changes in the lung of extremely old hybrid mice were related to altered effectors of the immune system, regulators of angiogenesis and elements of DNA repair mechanisms, likely explaining the molecular basis behind the altered patterns of pulmonary metastasis observed in the extremely old mice.

In human tissues, eighty-two genes were differentially expressed in a statistically significantly manner. Most genes were downregulated in aged lung tissue and included collagen isoforms and proteins responsible for extracellular matrix synthesis and turnover. A single upregulated transcript was a MYC binding protein. Selected transcripts were validated by PCR and histochemical staining.

This is the first examination of lung metastases and the molecular biology of lung tissues at the extremes of age. Alterations to gene expression profiles was observed in both mouse and human lung tissues, and supports the concept of a field defect in normal lung tissues that develops with increased age.

ACKNOWLEDGEMENTS

- Dr. Douglas Gray and Dr. Sudhir Sundaresan for unstinting support and guidance as thesis supervisors and mentors.
- Dr. Robin Fairfull-Smith for granting time within the General Surgery residency program to pursue this research opportunity.
- Dr. Eric Poulin (Department of Surgery), Dr. Farid Shamji (Division of Thoracic Surgery), Dr. Hartley Stern (Ottawa Hospital Cancer Centre) and Dr. Michael McBurney (Centre for Cancer Therapeutics) for salary support.
- Dr. Andrew Seely, Dr. Donna Maziak and attending staff in the Division of Thoracic Surgery for patient referrals.
- The Terry Fox Foundation through an award from the National Cancer Institute of Canada for salary support.
- Dr. Bruce McKay and Dr. Miguel Andrade-Navarro for valuable advice and assistance as part of my Thesis Advisory Committee.
- Lab colleagues for many valuable discussions, advice and assistance throughout my stay in the lab.
- Carol Ann Kelly for coping with the unpredictable schedule of a surgical resident in graduate studies.
- Finally, to my dears: Anne, Kate and Sarah for their limitless patience, support, inspiration and guidance without which it would have been impossible to have achieved any of this.

TABLE OF CONTENTS

LIST OF ABBREVIATIONS

AAH – atypical adenomatous hyperplasia
ACVS – Animal care and veterinary services
ATM – ataxia telangiectasia mutated homolog
BASC – bronchoalveolar stem cell
cAMP – cyclic adenosine monophosphate
COL1A1 – collagen 1 alpha 1
COPD – chronic obstructive pulmonary disease
CpG – cytosine-guanosine dinucleotide repeat
DNA – deoxyribonucleic acid
DNMT – DNA methyltransferase
ECMV – encephalomyocarditis virus
EDTA - ethylenediaminetetraacetic acid
EphB2 – ephrin B2
FACS – fluorescent activated cell sorting
FDR – false discovery rate
GFP – green fluorescent protein
GO – gene ontology
HAT – histone acetyltransferase
HDAC – histone deacetylase
IGF1 – insulin-like growth factor 1 (somatomedin C)
IRES – internal ribosomal entry site
LOH – loss of heterozygosity
LOX – lysyl oxidase
LOXL2 – lysyl oxidase-like 2
Mpa2l – macrophage activation 2 like
MYCBP – MYC binding protein (AMY-1, associate of MYC 1)
Narg-1 – NMDA receptor-regulated gene 1 (tubedown 1)
NSCLC – non-small cell lung cancer
OHREB – Ottawa Hospital research ethics board
OHRI – Ottawa Hospital Research Institute
PBS- phosphate-buffered saline
Plek – Plekstrin
QPCR – quantitative polymerase chain reaction
RARRES1 – RAR-responsive protein 1 (TIG1, tazarotene-induced gene 1)
RBC – red blood cell
RMA – robust multichip average
RNA – ribonucleic acid
SAM – significance array of microarrays
SD – standard deviation
SLK - STE20-like kinase
SPARC - secreted protein, acidic, cysteine-rich (osteonectin)
SULF1 – sulfatase 1
TFPI2 – tissue factor pathway inhibitor 2
TIMP1 – tissue inhibitor of metalloproteinases 1
TLR1 – toll-like receptor 1
YAP – *Yes* associated protein

LIST OF TABLES

LIST OF FIGURES

INTRODUCTION

LUNG CANCER AS A DISEASE OF ADVANCING AGE

The causation of age-associated diseases has long been associated with the fundamental molecular and cellular alterations noted to occur with advancing age (94). Cancer incidence increases with age, and lung cancer in particular has been found to have incidence that peaks in the later decades of life (21,131), both in current and former smokers (59) (Figure 1A). Lung cancer is the leading cause of cancer-related mortality in both males and females: Over 9000 women and 11 000 men will die of lung cancer this year in Canada. There is a relative reduction in lung cancer survival noted with increasing age (21). Mortality related to lung cancer has been stratified by age at cessation of smoking (Figure 1B). A plateau is evident in mortality rates up to the age of 75, at which point the mortality shows a sharp rise. These data implicate advancing age as a modulating factor. Several perturbations in lung function have been associated with advancing age (97), and can be broadly related to respiratory mechanics (decreased chest wall compliance and reduced respiratory muscle strength) and parenchymal alterations (loss of elastin, altered collagen cross-linking and decreased gas-exchange area). It becomes important to understand the biology of aging to gain insight into the changes related to age.

THEORIES OF AGING

The evolutionary basis for organismal aging has been encapsulated in distinct but complementary theories. The mutation accumulation theory of Medawar postulates that

organisms accumulating deleterious mutations whose effects become manifest later in life are not subject to evolutionary pressures, as these post-reproductive members of a population minimally affect gene transfer to subsequent generations. The antagonistic pleiotropy model suggested by Williams identifies a subset of genes whose multiple functions and targets are thought to lead to organismal aging. The antagonism suggests by Williams' model stems from the duality of beneficial effects observed in younger organisms related to gene function, the same gene function that in post-reproductive individuals becomes harmful. Two well-known examples of antagonistic pleiotropy are those of replicative senescence and p53 function; which abrogate tumorigenesis in early years, but enhance malignancies later in life by impaired stem cell-mediated tissue repair. An extension of the antagonistic pleiotropy model was proposed by Kirkwood and Holliday, which postulates a necessary trade-off between preservation of reproductive potential versus ongoing somatic maintenance and repair, reviewed in (91).

THEORIES OF CARCINOGENESIS

Hanrahan and Weinberg have outlined (60) the cellular acquisition of several capabilities which are permissive to the development of cancer. These include self-sufficiency in growth signals; insensitivity to anti-proliferative signals; evasion of apoptosis; sustained

A

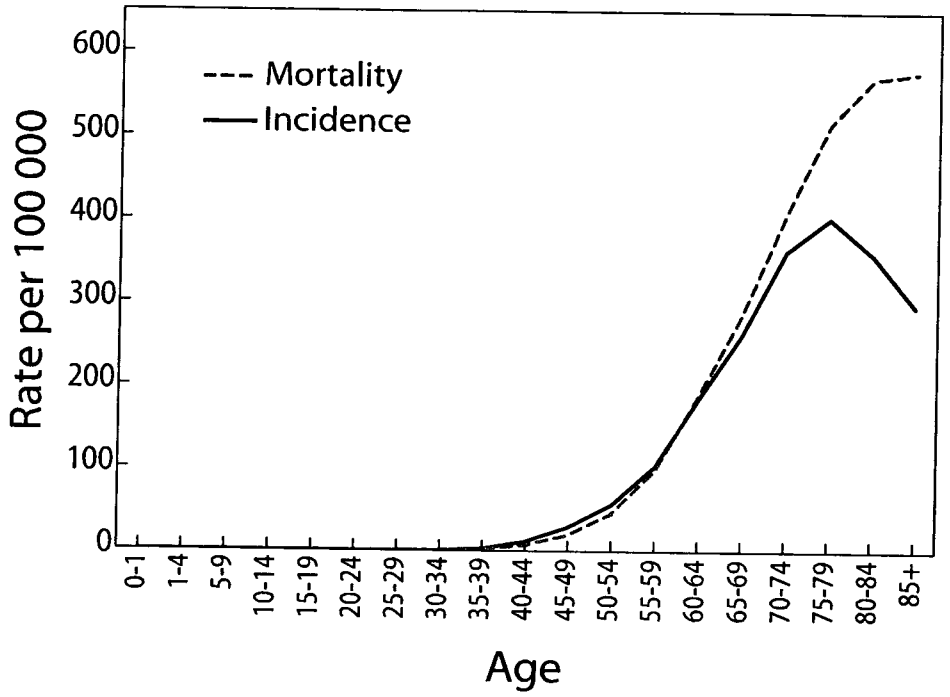
Mortality
Incidence
Rate per 100 000
600
500
400
300
200
100
0
0-1
1-4
5-9
10-14
15-19
20-24
25-29
30-34
35-39
40-44
45-49
50-54
55-59
60-64
65-69
70-74
75-79
80-84
85+
Age

B

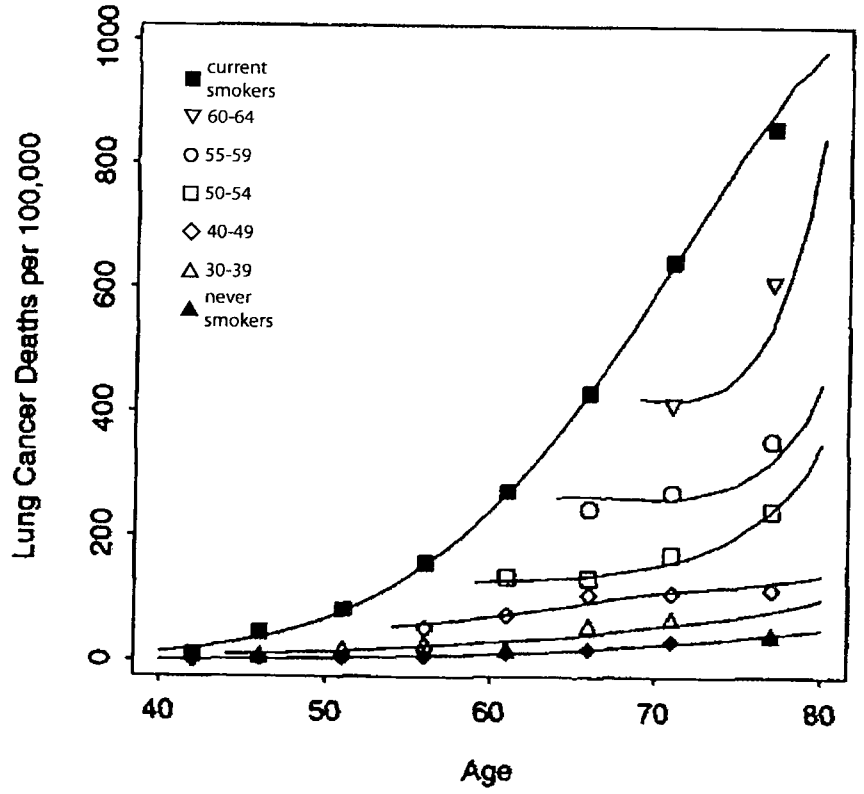
current smokers
60-64
55-59
50-54
40-49
30-39
never smokers
Lung Cancer Deaths per 100,000
1000
800
600
400
200
0
40
50
60
70
80
Age

Figure 1: Non-small cell lung cancer is a disease of aging.

Panel (A) demonstrates that lung cancer age-standardized incidence (solid line) and mortality (dashed line) rates spanning the years 1995-2004 begin to rise in the 6th decade of life. A decreased incidence is noted in the 8th decades. Data obtained from the Public Health Agency of Canada, Cancer Statistics On-Line for cancer of the Lung and Bronchus, both sexes combined. (B) Figure taken from (59) demonstrates cumulative NSCLC mortality rates, and is subdivided by age at complete cessation of cigarette smoking. Note is made of the long plateau in lung cancer mortality, which demonstrates a marked increase at age 75. The uppermost curve represents mortality of current smokers, while the lowermost curve represents mortality of never smokers.

angiogenesis; limitless replicative potential and tissue invasion/metastasis. These acquired characteristics have been adapted from the histologic and genetic studies of several cancer cell types, including colorectal (40) and lung (33) cancers. Tumorigenesis can be considered a multistep process which drives the transformation of normal epithelial cells towards malignant phenotypes. There are many examples of progressive passage of normal cells through premalignant states – these dysplastic cells are readily identified in the development of human cervical cancers and colorectal polyps (40). Genetic and epigenetic alterations mediate the acquisition of these hallmarks. Gatenby and Gillies have proposed a model (50) which examines anatomic (e.g., basement membrane) and physiologic barriers (e.g., hypoxia) to the development of cancer and matches these barriers with each of the specific hallmarks of cancer cells outlined by Hanrahan and Weinberg.

Armitage and Doll, in their studies of lung cancer incidence in British medical doctors, modeled a sequential six-step acquisition of rare mutations that was found to match the observed incidence rates in their study cohort (3). A more recent interpretation of this multi-step model of carcinogenesis has taken into account the presence of asymmetrically dividing stem cell populations (67). The two-stage clonal expansion model postulates that a genetic mutation in a progenitor cell allows for a clonal population to proliferate. This clonal patch need only accumulate one further mutation in order to achieve malignant potential. Recent in-vivo findings of lung epithelial stem cells have given further validity to the two-stage clonal expansion model's applicability to lung cancer.

Lung-resident stem cells (referred to as bronchoalveolar stem cells – BASC) repopulate alveolar and bronchiolar epithelia from their location at the bronchoalveolar junction (BAJ). BASC are characterized by the expression of both surfactant protein C, a type II pneumocyte (AT2) marker, and CC-10, a Clara-cell marker (76). In injury models using either bleomycin to deplete AT2 cells or naphthalene to deplete Clara cells, BASC were found to proliferate at the BAJ. These lung progenitor cells were initially identified with the surface marker profile Sca-1+CD31-CD45- . Subsequent identification of fetal cells with the Sca-1+CD34+Oct-4+SSEA-1+CK7+ profile also found co-expression of SpC and CC-10 ; this subpopulation was found to be susceptible to SARS coronavirus infection, suggesting that the devastating severity of SARS pneumonitis might be related to impaired epithelial repair mechanisms. Expansion of the BASC population by KRAS expression alone (71) or in combination with naphthalene injury, led to increased numbers of adenomas and areas of hyperplasia in the BAJ region . No reports studying Sca-1+CD31-CD45- BASC populations in young and extremely old mice have been reported to date, and it is unknown if the tissue repair mediated by these lung progenitor cells varies with advancing age.

PROGEROID SYNDROMES AND CANCER

The progeroid syndromes Werner syndrome (WS) and Hutchinson-Gilford progeria syndrome (HGPS) are characterized by early onset of aging features, a phenomenon referred to as segmental aging (as all features of normal aging are not evidenced). Patients with progeroid syndromes suffer increased epithelial and mesenchymal cancers at an increased rate. The relevant mutations to the DNA helicase activity (in WS) imply a tumour

suppressor function, a finding common to many age-associated cancers. Lamin A/C, the relevant mutation responsible for HGPS, functions as a regulator of gene expression and has been observed to be hypermethylated in adult Non-Hodgkin's and B-cell lymphomas (44).

FIELD CANCERIZATION

The term field cancerization was first introduced by Slaughter (138) to account for the observations that oral cancers (i) developed in multifocal areas of precancerous change; (ii) histologically abnormal tissues were observed adjacent to tumour masses; (iii) multiple smaller lesions were noted to occasionally coalesce; and (iv) second primary tumours were found to arise in abnormal tissues. These findings have also been described for cancers arising in other tissues, including lung. Sequential accumulation of mutations causes a progression from normal tissues to clonal aggregates of progenitor and daughter cells (known as a patch). Ongoing mutation allows expansion of abnormal cells into a field, a process occurring at the expense of normal epithelia. Subsequent carcinomas arise from the abnormal field (14). Figure 2 illustrates field cancerization within the context of lung cancer (63). Genetic changes related to cellular proliferation have been associated with field cancerization.

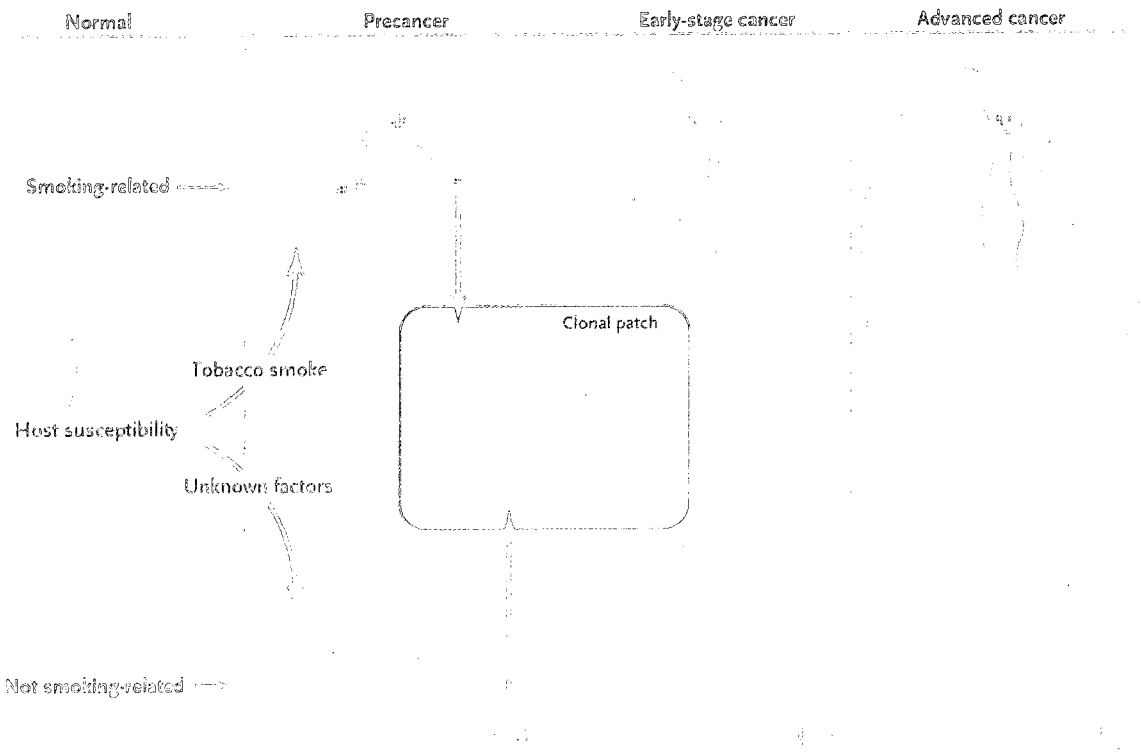

NEJM (2008) 359:1367-1380

Figure 2: Manifestations of field cancerization in the context of lung cancer

The process of field cancerization begins with the development of a clonal patch (second panel from left) after an insult to normal lung epithelium. Further accumulation of injury with concomitant genetic alterations commits tissues within clonal patches to neoplastic proliferation (third panel from left). Early stage cancers arising from clonal patches continue proliferation and accumulation of genetic lesions, with eventual cancer progression. (63)

THE MYC PATHWAY IN CARCINOGENESIS

The myelocytomatosis viral oncogene homolog MYC was first identified in Burkitt's lymphoma chromosomal translocations. Mutations in MYC are among the most common in human cancers, effecting oncogenesis by (i) cellular transformation by recruitment of histone acetyltransferase activity; (ii) immortalization by modulation of telomere length; (iii) blocking cellular differentiation; (iv) blocking apoptosis; (v) altering cell cycle programs (31). MYC overexpression has been shown to be sufficient in mediating lung cancer metastasis, however tumour progression required activation of an additional oncogene(120). The binding protein, MYCBP (130), is a 103 residue protein whose C-terminus binds to the N-terminal domain of MYC. The cellular functions of MCYBP remain ill-defined due to a paucity of published reports, however, it is known that MYCBP binding stimulates E-box dependent MYC:MAX transcriptional activity (149). MYCBP has been noted to translocate from the cytoplasm to the nucleus with MYC in conditions of overexpression, as well as in S-phase. MYCBP has been identified in as a target of the β-catenin/Lef-1 pathway at a binding site in its promoter sequence , and has been found to be upregulated in colon cancer cell lines, as compared to comparable normal cells in culture. Micro-RNA sequences (Let-7a in particular) have also been identified as regulating MYC levels and activity (132).

MUTATIONS IN LUNG CANCER ARE CONSISTENT WITH A FIELD DEFECT

Lung cancer has two main forms, small-cell (15% of all cases) and non-small-cell (85%). Non-small cell lung cancer (NSCLC) is composed of four histologic subtypes: Adenocarcinoma

(40% of NSCLC cases), squamous cell (25%), large-cell (7%) and bronchoalveolar (a subtype of adenocarcinoma, 2%, also considered to be carcinoma-in-situ). The molecular pathogenesis leading to adenocarcinoma of the lung follows a stepwise progression: Early molecular events include increased levels of circulating IL-8 and progressive allelic losses at multiple 3p tumour suppressor gene loci (3p21.3 (RASSF1A, FUS1) 3p14.2 (FHIT), 3p22-24, 3p12). These early genetic events are followed by chromosomal alterations involving DNA repair genes at 8p21-23, 13q14 (pRB) and 17p13 (p53) (158). Subsequent alterations are associated with premalignant and in-situ carcinomas, and relate to tobacco exposure: Epidermal growth factor receptor (EGFR) mutations are most often found in non-smokers, while Kirsten rat sarcoma-2 viral oncogene homolog (KRAS) mutations are observed in smokers. Multiple sites of hypermethylation are also noted in normal tissues at the periphery of tumours. (63). Half of all NSCLC are found to have mutations in the RAS-RAF-MEK-ERK signal transduction cascade, which converges upon MYC, which is itself a target of the Wnt signalling pathway. Atypical adenomatous hyperplasia (AAH) represents a putative preneoplastic lesion, being concurrently identified in up to 20% of lungs harbouring adenocarcinoma. Several early molecular events are mirrored in AAH and adenocarcinoma, namely *KRAS* mutations (up to 40% of cases) and *hTERT* overexpression (30-80% of cases). AAH lesions are found to be clonal and represent preneoplastic patches, thus suggesting that lung cancer satisfies the criteria of field cancerization outlined by Slaughter (158,159). A 15-gene signature has been identified by microarray analysis (143) that demonstrates perturbed antioxidant and cellular ion transport functions in normal airway epithelia, this most likely represents the field defect caused by tobacco smoke exposure.

Genetic and epigenetic alterations are noted with advanced age. Mutations due to DNA damage or replicative errors may activate oncogenes or abrogate appropriate tumour suppressor function. The epigenetic dysregulation associated with aging results two distinct phenomena: (1) global genomic hypomethylation, with an attendant predisposition to oncogenic expression and genomic instability, and (2) hypermethylation of tumour suppressor gene promoter sequences (44,75). Atypical adenomatous hyperplasia represents a precursor lesion to NSCLC and is characterized by tumour suppressor methylation (87), an finding that has also been noted in lung cancer tissues (10,32,41,70,90,121).

MICROARRAYS IDENTIFY MOLECULAR ALTERATIONS ASSOCIATED WITH AGING

Biomarkers are lacking to accurately describe or predict tissue or organismal aging; to this end high-throughput microarray platforms have been used to generate aggregate transcriptional signatures associated with advanced age. Tissues studied to date include kidney (125), retina (163), and brain (45). A recent study (165) of human muscle tissue identified age-associated changes in pathways of symporter activity, sialyltransferase activity and of chloride transport. Muscle microarray data was then compared to published array profiles of aged kidney and brain tissues. Six common pathways were found to be perturbed, four showing upregulation with age (extracellular matrix, cell growth, complement activity and cytosolic ribosome) while age-related reductions in chloride and electron transport chain were noted. The authors have suggested a common cross-species aging effect, since the alterations in electron transport chain transcripts were altered

congruently in mice, fruit flies (*Drosophila melanogaster)* and nematodes (*Caenorhabditis elegans*). Clearly, microarray approaches hold great promise in identifying age-related transcriptional changes. Recent studies of cadaveric human lung tissues applying similar methodologies (57) have also identified a gene signature related to advancing lung age within a subgroup analysis.

RATIONALE FOR EXPERIMENTAL METASTASIS MODEL

In order to study the molecular basis of a possible association of aging and cancer and metastasis, we began our study with a murine model of colorectal metastases. The lung is a common site of cancer metastasis, the most common of which arise from primary colorectal cancers (1). Metastases are formed through sequential steps, allowing tumour cells to (i) invade normal tissue, (ii) travel to distant organ sites and (iii) form new tumour colonies. Since each step in the metastatic process is inefficient , the successful formation of distant metastases is dependent upon cancer cell interactions with target tissues – originally described in 1889 by Stephen Paget as the interaction between 'seed and soil' (42). Two methodologies to study metastases have been described: (i) Orthotopic models, where metastases develop spontaneously from primary tumours, are able to assess all three stages of metastasis formation; while (ii) experimental models rely on direct vascular embolization of tumour cells after intravenous or intracardiac injections and consequently are limited to studies of tumour transport and colonization (145).

Historically, experimental metastasis models have been examined in inbred mouse strains, using cell types which rarely metastasize to lung in the usual clinically relevant scenarios,

and analyses have been limited to arbitrarily fixed endpoints (Table 1). In our studies, we used first-generation hybrid mice (CB6F1 hybrid line, BALB/c x C57BL/6) as opposed to inbred strains (99). First generation hybrid rodents show less strain-specific pathologies than the inbred parental lines, and maintain identical genetic backgrounds amongst the hybrid cohort (106). As an additional benefit, hybrid strains are characterized by enhanced physical health and longer lifespan, making hybrid strains ideal for studies of aging – this is referred to as hybrid vigour, and ensures an increased level of stringency when observing cohorts for effects related to aging. The maximal murine lifespan of 36 months is roughly comparable to that of a centenarian human (119). The detection of a unique aging signature is enhanced with a wide separation in study group ages. We have chosen the mouse ages of 6 months and 30 months in order to be comparable to humans aged 25 and 90, respectively.

As the experimental model of metastatic colorectal carcinoma, we used the mouse CT26 cell line, which has been well-characterized and validated (117). Most previous experimental models examining the effect of age on metastases have employed cell lines which were not derived from colonic tissues (Table 1), despite evidence that colorectal carcinoma represents the most common source of lung metastases.

The studies reported herein incorporate both a cancer and an aging focus. Inbred mouse strains, with specific susceptibilities to lung cancer having been selected, would represent a ideal cohort for investigating isolated aspects of lung cancer. Since the main focus of this thesis was to determine the putative effects of aging on lung cancer susceptibility, a mouse

strain ideally suited for detection of robust aging signatures was selected. A metastasis model was used to ensure that: (1) an aged hybrid strain was used, and (2) the engraftment of metastatic deposits would depend solely on aged host tissue factors.

IMMUNE FUNCTION IS IMPAIRED WITH ADVANCING AGE

Cell-mediated immune function has been found to decrease with age (58,114), the result of a complex interplay (89) between thymic involution, a reduced naïve T-cell population (with concomitantly expanded memory pool) and decreased natural killer (NK) cell activity . Cytokine signalling, as assessed by interleukin-6 mediated phosphorylation of STATs -3 and -5, is inappropriately activated in advanced age (47). Macrophage responses to experimentally-induced tumours are also reduced (157), as is activation in response to silica-induced airway injury (29). The net result of these varied immunological alterations is the presence of chronic inflammation in aged lungs. Chronic inflammation has been linked with carcinogenesis (30), and of the many effectors of inflammation, the mitogen-activated protein (MAP) kinases figure prominently. MAP kinase p38α has been overexpressed in a mouse model and was found to facilitate the development of lung metastases (95) and has been implicated in ephrin-mediated signalling.

RATIONALE FOR STUDY

This thesis represents the first examination of the molecular basis of lung metastases at an extreme age. The extent and spread of experimental metastases using CT26 murine colon cancer cells was found to differ in older mice as compared to young cohorts. Employing

microarray methodology and validating selected transcripts, we describe the significant alteration of the patterns of gene expression in aged lung tissues, which we relate to the age-dependent increase in cancer malignancy. Taken together, the data highlight unique characteristics of extremely old lung tissue, and represent the only examination to date of metastatic disease patterns of a common cancer using a hybrid mouse strain.

This thesis also represents the first examination of transcriptional changes associated with advanced age in the human lung, in order to ascertain if age is sufficient field cancerization to facilitate the pathogenesis of NSCLC.

HYPOTHESIS

Our study hypotheses are the following:

(1) There is an aging effect on gene expression in normal lung tissue;

(2) Differences in gene expression noted in normal aged lung tissue will represent changes associated with field cancerization.

MATERIALS AND METHODS

MOUSE STUDY PROTOCOLS

ANIMALS AND TISSUES

All animal procedures were approved by the Animal Care committee of the University of Ottawa under protocol ME-214 and were cared for in accordance with standards approved by the University of Ottawa's Animal Care and Veterinary Services (ACVS). Young (6 month) and aged (30 month) male CB6F1 hybrid mice (F1 offspring of C57/BL6 x BALB/c crosses) were obtained from the Aged Rodent Colony (Harlan, Indianapolis IN, USA) of the National Institute of Aging (NIH, Bethesda MD, USA). Young BALB/c mice were obtained commercially (Charles River Laboratories, Wilmington MA, USA).

Mouse CT26.25 colon carcinoma cells (gift of Dr. John Bell, Ottawa Hospital Research Institute, OHRI, Ottawa ON) were cultured using Dulbecco's Modified Eagle's Medium (Hyclone, Logan UT, USA) supplemented with 10% fetal bovine serum (Gibco, Burlington ON) at 37°C in 5% CO_2 and subcultured every 72h.

All mice were anaesthetized using an injectable mixture provided by ACVS (100mg/mL ketamine, 20mg/mL xylazine, 10mg/mL acepromazine) and dosed by body weight. Lungs were perfused with 10mL of phosphate-buffered saline via the right cardiac ventricle until effluent from the transected abdominal aorta was clear. Specimens were immediately frozen in liquid nitrogen for future nucleic acid and protein analysis. For tissues later undergoing histochemical studies, a second lung perfusion step using 5mL fixative (10%

buffered formalin, Sigma-Aldrich, Oakville ON) was performed, followed by intratracheal injection of 2-4mL fixative until lung distension was achieved and held for 2min. Lungs were then removed and were stored in fixative for 24h and subsequently transferred to 70% ethanol. Tissues were embedded in paraffin blocks and triplicate 5μm sections at 100μm intervals were obtained for subsequent analyses.

CT26 TUMOUR STUDIES

To determine metastatic tumour counts, young (6-month) and aged (30-month) mice underwent intravenous administration of CT26 cells ($2.5x10^5$ or $1x10^5$ cells in 50μl PBS to induce pulmonary metastatic disease . Mice were sacrificed according to approved veterinary protocols at 14 days (after high dose, n=12) or upon exhibiting extreme respiratory distress or extreme weight loss (low dose, n=17) at the direction of veterinary staff. Sections (5μm thickness) were taken at 20μm intervals throughout paraffin-embedded lung tissue and stained with hematoxylin using standard histochemical techniques. Slides were scanned using a flatbed scanner at 2400dpi in greyscale and saved as 16-bit tiff files. Image morphometric analysis was performed using commercial software (Metamorph Offline 4.6r5, Molecular Devices, Downingtown PA, USA). Lung parenchyma was quantified by applying a 0-200 (arbitrary pixel intensity scale) threshold to the image; total lung area was approximated by a sum of all thresholded pixels. Tumour deposits were counted by applying a 0-140 threshold, ignoring aggregates smaller than 50 pixels in the cumulative count. Tumour counts were then indexed to total lung area analyzed.

PULMONARY BLOOD FLOW STUDIES

The accumulation of fluorescent markers was used to determine if pulmonary blood flow differed between age cohorts. Mice were injected intravenously with $1.8x10^5$ (in 50µL) fluorescent polystyrene microspheres (10µm diameter, orange fluorophore, Molecular Probes, Burlington ON). These do not perturb the pulmonary blood flow patterns (84), but arrest in pulmonary capillaries. Microspheres were allowed to circulate for 5 minutes, followed by immediate cervical dislocation, lung removal and embedding in water-soluble fixative (TissueTek OCT, Sakura-Finetek, Torrance CA, USA). Samples were stored in the dark at -80°C, followed by sectioning at 20µm intervals throughout embedded lung tissue. Fluorescence signal was acquired using a Scan Array Express Microarray Scanner with external laser source (Perkin-Elmer, Wilmington MA, USA) at 543 nm using the Cy3 filter set. Data was stored as 16-bit greyscale tiff files. Image morphometric analysis was performed using commercial software (Metamorph). In order to determine the total surface area of the lung sections being analysed, lung parenchyma was quantified by applying a 140-65535 (arbitrary pixel intensity scale) threshold to the image; total lung area was approximated by a sum of all thresholded pixels. Trapped RBC-sized microspheres were counted by applying a 30000-65535 threshold, ignoring aggregates smaller than 100 pixels in the cumulative count. Microsphere counts were then normalized to total lung area analyzed.

LUCIFERASE EXPRESSING CT26 CELLS ($CT26^{FLUC+}$)

CT 26 cells grown to 80% confluence were infected with an engineered lentivirus (gift of Dr. J. Wang, OHRI) in the presence of polybrene for 24 hours. The lentivirus contained a dual expression vector (Figure 5A) with both firefly luciferase, under control of the minimal elongation factor 1 alfa (EF1α) promoter, and green fluorescent protein (GFP), under control of the encephalomyocarditis virus (ECMV) internal ribosomal entry site (IRES) sequence. After a single passage in cell culture, GFP+ cells were selected by FACS (StemCore facility, OHRI, Ottawa ON) to >95% purity for further propagation and experimental use. The cell population was re-enriched for GFP+ cells after six months of serial passage to ensure >95% purity.

KINETICS OF TUMOUR GROWTH USING IN-VIVO IMAGING

Young and aged mice (6-month, 30-month) underwent intravenous administration of $CT26^{fLUC+}$ cells ($1x10^5$ cells in 50µl PBS). In-vivo luminescent imaging was performed 4 hours after tumour injection and every 48h thereafter using the IVIS 200 system (Xenogen, Hopkinton MA, USA). Anaesthesia was achieved with the use of inhaled 2% isoflurane (Baxter, Toronto ON) in oxygen. Luciferin potassium salt (Molecular Imaging Products Company, Ann Arbour MI, USA) dissolved in PBS (2mg per imaging session per mouse) was injected intraperitoneally. After an absorption time lapse of 6 minutes, luminescent signals were acquired over a 3 minute exposure time. Identical exposure, aperture and binning parameters were used for all image acquisition. Image processing and data analysis was performed using commercial software (Living Image 2.50.1, Wavemetrics, Almeda CA, USA).

Due to high inter-animal and inter-day variability in detected signals, mice were included in the kinetic analysis if the detected radiance signal was greater than 1000 photons/s/cm^2/sr at 19-21 days after injection of tumour cells (earlier if endpoint was reached prior to 21 days).

DETERMINATION OF LUNG ENDOTHELIAL AND LYMPHOCYTE POPULATIONS

Young and aged mice were injected with CT26^{fLUC+} cells (1x10^5 cells in 50µl PBS). After 14 days, lungs were removed and cells were isolated according to described methods . Cell suspensions were labelled with antibodies to mouse CD31 (PE conjugated, eBioscience, San Diego CA, USA) and a Mouse T Lymphocyte Antibody Cocktail (CD3e PE-Cy7, CD4 PE, CD8a APC, BD Biosciences, Mississauga ON). Spleens were also removed, minced in ice-cold RPMI-1640 (Hyclone) and separated by density gradient centrifugation (Lympholyte-M, Cedarlane Laboratories, Burlington ON). All data acquisition and cell sorting was done in the StemCore facility (OHRI) on a MoFlo cell sorter (DakoCytomation, Fort Collins CO, USA).

BRONCHOALVELOAR STEM CELL ISOLATION

The lungs of young and aged (11-month, 34-month) mice were removed and primary lung cells were isolated as described previously. Cell suspensions were labelled with antibodies to mouse Sca-1 (APC conjugate, BD Pharmingen), mouse CD45 (PE conjugate, BD Pharmingen) and mouse CD31 (PE conjugate, eBioscience). All data acquisition was done in the StemCore facility (OHRI) on a MoFlo cell sorter (DakoCytomation).

LUCIFERASE ASSAYS

Samples were processed using a dual luciferase assay kit (Promega, Madison WI, USA) according to the manufacturer's directions (tissues were homogenized using a rotor-stator apparatus) to produce total protein lysates. These were quantified using a dye-binding assay (BioRad, Hercules CA, USA). Samples were analysed on a Lumat LB9507 luminometer (Berthold Technologies, Bad Wildbad, Germany). Relative luminescence was normalized to protein concentration.

NORMAL MOUSE LUNG TISSUE MICROARRAY ANALYSIS

To determine global gene expression in normal young and old lung tissue, an Affymetrix-based microarray analysis was performed. Three mice of each age group were treated, for a total of twelve mice. Total lung RNA was isolated from lung using column-based kits (Qiagen Inc, Mississauga ON) or Trizol reagent (Invitrogen, Burlington ON) according to the manufacturer's protocol for total RNA isolation, followed by ethanol precipitation according to standard protocols. The RNA was submitted to the StemCore microarray facility (OHRI) for hybridization to the MOE430A (unperfused lung tissues) or MOE430v2 (perfused lung tissues) microarray chips (Affymetrix, Santa Clara CA, USA). Expression values were computed from .CEL files by applying RMA (robust multichip averaging) normalization under R (v2.3.1, www.r-project.org) within sets of replicate samples. Statistical testing was performed with the significance analysis of microarrays (SAM) algorithm (154), part of the SIGGENES (v1.2.11) package. The RMA and SIGGENES packages are part of the Bioconductor (www.bioconductor.org) package (52). Functional information (8) regarding the transcripts

in the significant gene lists was derived from gene ontology (4,22) information using GOstat software (gostat.wehi.edu.au) (9).

VALIDATION BY QUANTITATIVE POLYMERASE CHAIN REACTION

To validate selected transcripts identified in the microarray analysis, PCR methods were employed. Complementary DNA (cDNA) to messenger RNA pools were synthesized using oligo$(dT)_{12\text{-}18}$ primers and Moloney murine leukemia virus reverse transcriptase (Invitrogen) according to standard protocols. Products were stored at 4°C, quantified and diluted as required. Primer oligonucleotides were designed in Primer3 (MIT, Cambridge MA, USA) using nucleotide sequences from the NCBI (National Library of Medicine, NIH, USA) and synthesized commercially (SigmaGenosys, Mississauga, ON). Primer sequences listed in Table 6 were used to validate selected transcripts. Protocols were optimized for use with the LightCycler (Roche Diagnostics, Laval QC). A 20µL reaction master mix contained *Taq* polymerase, 10X PCR buffer, 10mM mixed deoxyribonucleotides (all from Invitrogen), 10X SYBR Green I dye (Cambrex, East Rutherford NJ, USA), and 50X bovine serum albumin (BSA heat shock fraction V, BioShop, Burlington ON). Magnesium chloride was adjusted as required for optimal reaction conditions. Reactions used temperature gradient slopes of 20°C/s unless otherwise specified with the following conditions: (1) denaturation (95°C for 20s); (2) amplification (forty cycles of 95°C for 2s, 55°C for 10s, 72°C for 10s with single fluorescent acquisition; (3) melting curve analysis (60-99°C with temperature gradient of 0.1°C/s and continuous fluorescence acquisition). LightCycler analysis software was used to determine reaction crossing points, relative product concentrations and the first derivative

of the fluorescence-temperature curve. Product amplification specificity was determined using melting curve peak profiles and standard agarose gel electrophoresis as needed.

VALIDATION BY WESTERN BLOT ANALYSIS

To further validate selected transcripts from the microarray analysis, protein analysis was undertaken. Lung tissues were harvested as outlined above, followed by homogenization in protein lysis buffer (20mM Tris pH 7.5, 150mM NaCl, 2mM EDTA, 1% Triton-X and 5% glycerol) containing the following protease and phosphatase inhibitors: 200 µg/ml phenylmethylsulfonyl fluoride, 5 µg/ml leupeptin, 2 µg/ml aprotinin, 200 µM sodium fluoride, 200 µM sodium pyrophosphate and Complete Protease Inhibitor Cocktail (Roche Diagnostics). Soluble protein was quantified using a dye-binding assay (BioRad, Hercules CA, USA). Proteins were resolved on an 8% SDS-polyacrylamide gel and electroblotted onto a Hybond C nitrocellulose membrane (Amersham, Baie d'Urfé QC). The membranes were stained with Ponceau S (Sigma-Aldrich) to confirm transfer prior to immunoblotting with the appropriate primary antibody: Plekstrin (BD Biosciences, Mississauga ON), Yap (Santa Cruz Biotechnology, Santa Cruz CA, USA) and β-actin (Sigma) were diluted using 5% skim milk in TBST (10mM Tris pH 8.0, 150mM NaCl, 0.1% Tween-20); Ephrin B2 (R&D Systems, Minneapolis MN, USA), was diluted using 0.5% BSA in TBST. Blots were visualized using standard HRP-chemiluminescent techniques (Kirkegaard & Perry Laboratories, Gaithersburg MD, USA).

HUMAN STUDY PROTOCOL

STUDY DESIGN

A two-phase approach to this problem was implemented. A pilot phase encompassing six patient samples (3 young and 3 aged) was to examine the first hypothesis of altered gene expression with advanced age. The minimum number of samples needed to achieve statistical significance has been demonstrated to be six (three replicates per group (86)). Once the pilot phase of the proposed study and the genetic analysis has been completed, further patient recruitment will occur in order to address the second hypothesis. Three additional young patients will be recruited to serve as additional control subjects. Nine aged patients will be recruited - in this cohort of patients both normal tissue and a small portion of lung tumour will be removed. Both normal and tumour tissue will undergo microarray analysis.

STUDY PATIENT ENROLMENT

The study protocol, consent form and information sheet were approved by the Ottawa Hospital Research Ethics Board (Protocol 2004-484-01H). Patients were then identified by attending staff in the Division of Thoracic surgery at the General Campus of the Ottawa Hospital according to the inclusion and exclusion criteria outlined in Table 7.

TISSUE PROCUREMENT AND SAMPLING

Tissues were procured directly from the operating room of the Ottawa Hospital, General Campus. Sections of fresh lung tissue and tumour were sectioned by technicians in the Department of Pathology at the Ottawa Hospital, General Campus. Resected lung and tumour tissues were snap frozen in liquid nitrogen for future nucleic acid and protein analysis, while smaller samples were stored in 10% neutral buffered formalin (Sigma Aldrich, Oakville ON) fixative for 24h and subsequently transferred to 70% ethanol. Tissues were then embedded in paraffin blocks and triplicate 5μm sections at 100μm intervals were obtained and stained using hematoxylin and eosin or Masson's trichrome stains (Pathology services, University of Ottawa).

NORMAL HUMAN LUNG TISSUE MICROARRAY ANALYSIS

To determine global gene expression in young and old lung tissue, an Affymetrix-based microarray analysis was performed. Total lung RNA was isolated from lung using Trizol reagent (Invitrogen) according to the manufacturer's protocol for total RNA isolation, followed by ethanol precipitation according to standard protocols. RNA samples with an absorbance ratio ($A_{260/280}$) of 1.8 or greater were submitted to the StemCore microarray facility for quality assurance using an Agilent Bioanalyzer (Santa Clara CA, USA). Traces are presented in Appendix 1. Samples were selected for hybridization to HG U133 2.0+ microarray chips (Affymetrix, Santa Clara CA, USA) when intact 18S and 28S peaks and low amplitude baseline tracing were observed. Analysis of hybridization data was performed as outlined above (see Normal mouse lung microarray analysis). Heatmaps were generated

using the TM4 analysis package (www.tm4.org) (128). The quality of the raw microarray data was examined using the AffyQCReport package in Bioconductor.

VALIDATION BY QUANTITATIVE POLYMERASE CHAIN REACTION

To validate selected transcripts identified in the microarray analysis, PCR methods were employed. Protocols were as outlined above (see above Validation by quantitative polymerase chain reaction). Primer sequences are listed in Table 10.

MORPHOMETRIC ANALYSIS OF HISTOCHEMICAL STAINING

Three slides per patient were scanned using a flatbed scanner at 2400dpi in greyscale and saved as 16-bit tiff files. Image morphometric analysis was performed using commercial software (Metamorph Offline 4.6r5, Molecular Devices, Downingtown PA, USA). Lung parenchyma was quantified by applying a 0-185 (arbitrary pixel intensity scale) threshold to the image; total lung area was approximated by a sum of all thresholded pixels. Collagen content was estimated by applying a 0-120 threshold, subtracting hole area and ignoring aggregates smaller than 50 pixels in the cumulative count. Collagen pixel counts were then indexed to the total number of lung pixels analyzed. Analyses of MYC, MYCBP and Ki-67 from digital images captured using an Aperio SlideScope (Vista CA, USA) were quantified using a proprietary positive pixel count algorithm (Aperio). Briefly, this algorithm identifies brown staining using thresholded and binned intensity ranges, quantifies the total pixel count and stores this data for subsequent analysis. Figure 3 demonstrates standard immunohistochemical staining and the corresponding false colour overlay representing the

detection of positive pixels after application of the counting algorithm. All pixel counts were indexed to total tissue area in millimetres squared (mm^2).

TISSUE MICROARRAY ANALYSIS

Lung cancer-specific tissue microarrays (LC1201, US Biomax, Rockville MD, USA) were stained using standard immunohistochemical methods (Appendix 4) with antibodies to MYC (Clone Y69, Millipore, Billerica MA , USA), MYCBP (Aviva Systems Biology, San Diego CA, USA) and Ki-67 (BD Pharmingen, Mississauga ON). Digital images were captured using an Aperio SlideScope (Aperio) and quantified after immunohistochemical staining using a proprietary positive pixel count algorithm (Aperio). Demographic data provided by the TMA manufacturer was used to identify age cohorts; these were arbitrarily binned into young (0-35y), intermediate (36-59) and aged (60+) groups for analysis.

STATISTICAL ANALYSIS

Tests of significance were performed using a commercial software package (Prizm 4, GraphPad, San Diego CA, USA) and involved two-tailed t-tests for differences in the mean, using Welch's correction for unequal group variance. All other statistical tests fell within the structured microarray analyses outlined above.

Tumour tissue

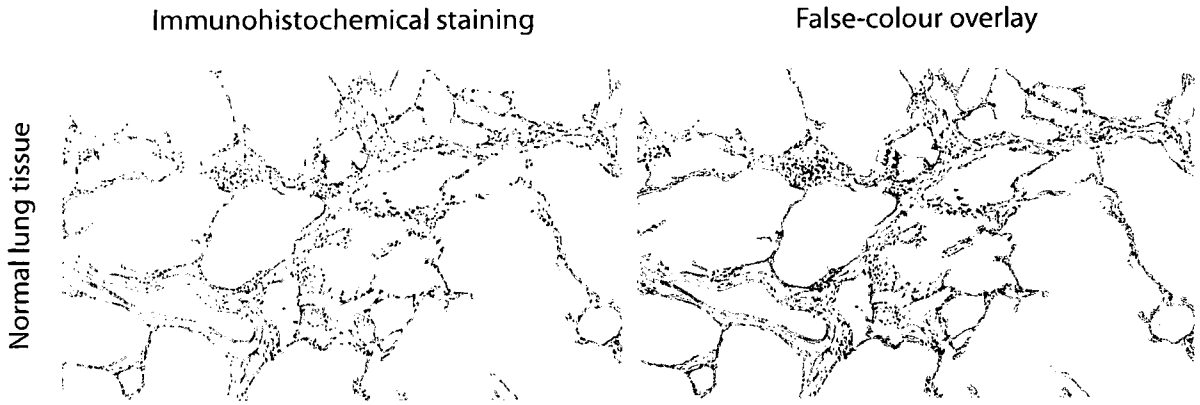
Immunohistochemical staining
False-colour overlay
Normal lung tissue

Figure 3: The positive pixel count algorithm accurately identifies areas of positive immunohistochemical staining in human lung tissue.

Tissue sections stained using immunohistochemical techniques for MYC from normal lung tissue from a 63-year old patient and the corresponding adenocarcinoma from the operative specimen. The right-hand column shows false colour overlays, demonstrating the recognition of positive staining by the Aperio Positive Pixel Count algorithm and confirming the technique's validity for staining analyses.

RESULTS

AGED MICE EXHIBIT A DISTINCT PATTERN OF METASTASES

The pattern and extent of pulmonary disease caused by intravenous injection of CT26 mouse colon carcinoma was studied. When allowing pulmonary metastases to develop for 14 days after injection of $2.5x10^5$ cells, there were no significant differences noted by morphometric analysis in the number (Figure 4A) or size (data not shown) of tumour deposits between the two age cohorts. All counts of tumour number or size were normalized to take into consideration the total area of the lung slice examined (in pixels). Qualitatively, there was a trend for diffuse, ill-demarcated disease in aged mice (Figure 4B, white arrowheads); while younger mice showed well-circumscribed lesions (Figure 4B, black arrowheads).

Since members of the initial test cohort were sacrificed at 14 days after tumour injection, a second group was considered to further examine survival in the context of metastatic disease. A reduced number of tumour ($1x10^5$ CT 26) cells was injected and mice allowed to succumb naturally to the metastatic disease. The metastatic patterns observed at endpoint were different from patterns noted at the 14d timepoint. Morphometric analysis revealed a significantly greater number of tumours to be present in the lungs of aged mice (Figure 4D). No difference was noted in tumour size between the two groups. As before, data were normalized to total lung area. The impact of age on survival was also examined. After administration of $1x10^5$ CT26 cells, thirty-month mice (n=14) survived a median 47 days, while the cohort of 6-month mice (n=15) still had greater than 50% survivorship at 70 days.

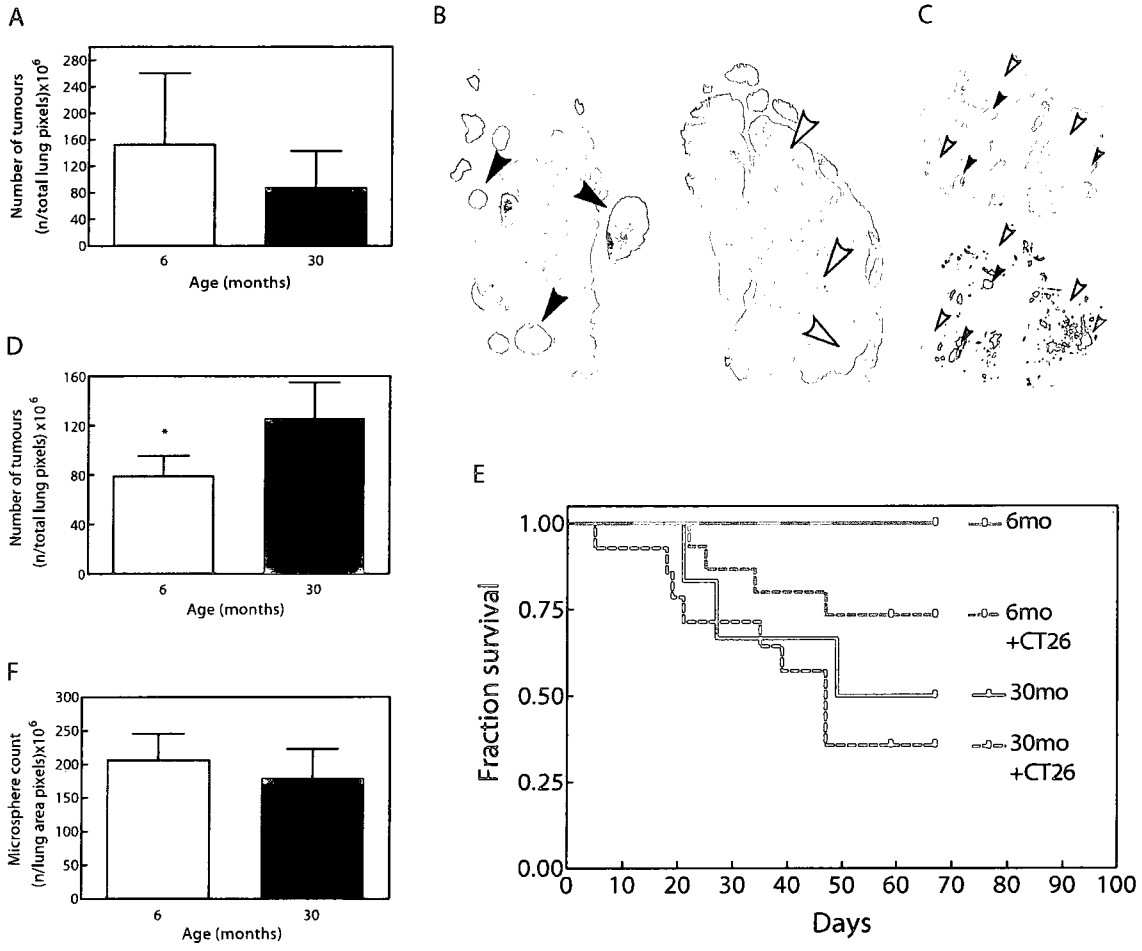
A
Number of tumours (n/total lung pixels)x10^6
280
240
200
160
120
80
40
0
6
30
Age (months)
B
C
D
Number of tumours (n/total lung pixels) x10^6
160
120
80
40
0
*
6
30
Age (months)
E
Fraction survival
1.00
0.75
0.50
0.25
0.00
0
10
20
30
40
50
60
70
80
90
100
Days
6mo
6mo +CT26
30mo
30mo +CT26
F
Microsphere count (n/lung area pixels)x10^6
300
250
200
150
100
50
0
6
30
Age (months)

Figure 4: Aspects of pulmonary metastatic disease in young (6-month) and old (30-month) CB6F1 mice after intravenous injection with $1x10^5$ syngeneic CT26 murine colon cancer cells.

Panel (A) No differences are noted in number of tumours when sacrificed at 14 days between 6-month and 30-month mice. (B) H&E stained histologic sections of mouse lung showing 6-month lung with well-demarcated tumour nodules (black arrowheads) and 30-month lung with more diffuse tumour deposits (open arrowheads). (C) H&E stained histologic section of mouse lung showing dark-staining tumour deposits (filled arrowheads) that are well-defined from normal lung parenchyma (open arrowheads). A modified image below shows correct identification of tumours by morphometric analysis. (D) Significantly greater numbers of tumour deposits are found in the lungs of old mice when allowed to live to endpoint (n=6 in each age cohort, $p<0.05$ by t-test with Welch's correction). (E) Survival of 30-month mice is not altered by tumour injection, but remains significantly reduced when compared to younger mice (n=14 in 30-month cohort, n=15 in 6-month cohort, $p<0.05$ by log-rank test). (F) No age-related differences in pulmonary blood flow exist as determined by lung trapping of 10μm diameter fluorescent microspheres (n=3 mice per group, triplicate lung sections analyzed for each mouse, error bars=SD). The hazard ratio was 3.02 (95% CI 1.02-9.69) which was statistically significant ($p<0.05$) by the log-rank test. CT26 model of pulmonary metastases relies on blood flow to carry injected cells to the lung; no age-related differences in pulmonary blood flow were observed (Figure 4F).

To further confirm the distinct pattern of metastatic spread between young and aged mice, the kinetics of lung tumour formation was studied using in-vivo imaging techniques. A luminescent CT26 cell line was created using a lentivirus expressing a dual reporter construct (Figure 5A). Confirmation of luciferase expression (Figure 5B) was performed on FACS-enriched GFP expressing cells and the parental wild-type cells. Imaging of luciferase expression was performed every 48 hours (see methods). Increases in signal intensity were noted in 30-month mice at day 9, which is a day earlier than in the 6-month group (Figure 5 bottom panel Figure 5and D). At day 16, the signal strength was roughly equal between the age groups. At day 21, signal intensity was greater in the 6-month age group. Luminescent signals were quantified (Figure 5D) using commercial software (Living Image). Aged mice showed a trend for early increases in tumour burden up to 20 days after injection, with absolute signal strength diminishing after day 15. Younger mice, although demonstrating slower increases in luminescence, sustained these increases for up to 30 days. Care must be taken in interpreting these results, as a non-linear relationship between tumour burden and luminescent signal appears to exist. Both CT26wt and CT26fLUC+ cells were injected into BALB/c mice and allowed to grow for 14 days. Nodules were removed and homogenized. Residual GFP activity was measured using flow cytometry on single-cell suspensions and gating for GFP. Luciferase activity was assessed using a luminometer and indexed to total protein in each sample. As expected, CT26wt cells did not express GFP (Figure 6A and C), while expression of GFP and luciferase activity was preserved in reporter cells (Figure 6B and D).

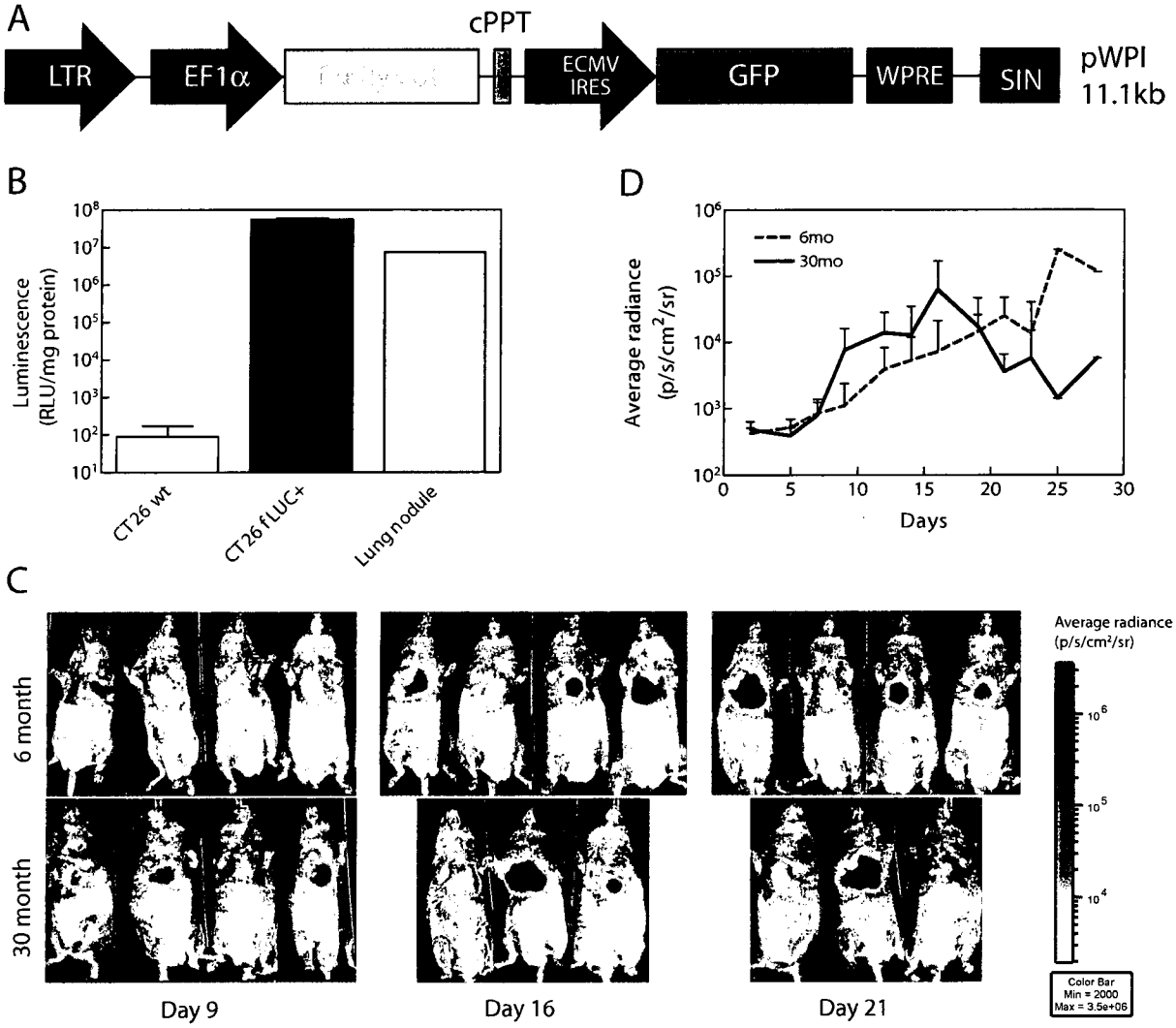
A
cPPT
LTR
EF1α
ECMV IRES
GFP
WPRE
SIN
pWPI 11.1kb
B
Luminescence (RLU/mg protein)
CT26 wt
CT26 fLUC+
Lung nodule
D
Average radiance (p/s/cm²/sr)
6mo
30mo
Days
C
6 month
30 month
Day 9
Day 16
Day 21
Average radiance (p/s/cm²/sr)
Color Bar
Min = 2000
Max = 3.5e+06

Figure 5: Aspects of disease kinetics in young (6-month) and old (30-month) CB6F1 mice after intravenous injection with $1x10^5$ syngeneic $CT26^{fluc+}$ murine colon cancer cells.

Panel (A) Lentiviral bicistronic vector used for all in-vivo imaging experiments. Reporter constructs subcloned into the 11.1kb pWPI backbone (LTR, long terminal repeat; EF1a, elongation factor 1 alpha promoter element; LUC, luciferase; cPPT, central polypurine tract; ECMV IRES, encephalomyocarditis virus internal ribosomal entry site; GFP, green fluorescent protein; WPRE, woodchuck hepatitis post-transcriptional regulatory element; SIN, self-inactivating LTR). (B) Luciferase assay demonstrating robust luciferase activity in infected cells and in lung nodules arising 16 days following intravenous injections of cell suspensions (CT26wt, parental cell line; CT26fLUC+, cells expressing luciferase and GFP; n=3 in each column, error bars = SD). (C) Kinetics of pulmonary metastases as monitored non-invasively by luminescent detection of CT26fLUC+ lung tumours. The average radiance has been normalized across all panels (min=2000, max=$3.5x10^6$). (D) Quantification of radiance values from Panel C (n=4 in each group; error bars = SD).

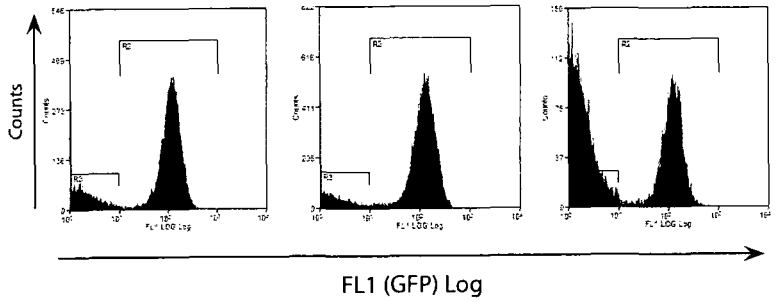
Counts
FL1 (GFP) Log

C

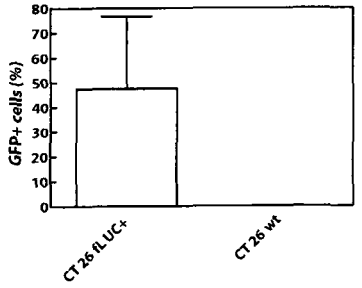
GFP+ cells (%)
80
70
60
50
40
30
20
10
0
CT 26 fLUC+
CT 26 wt

D

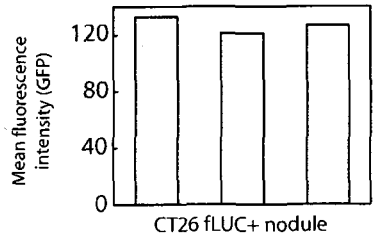
Mean fluorescence intensity (GFP)
120
80
40
0
CT26 fLUC+ nodule

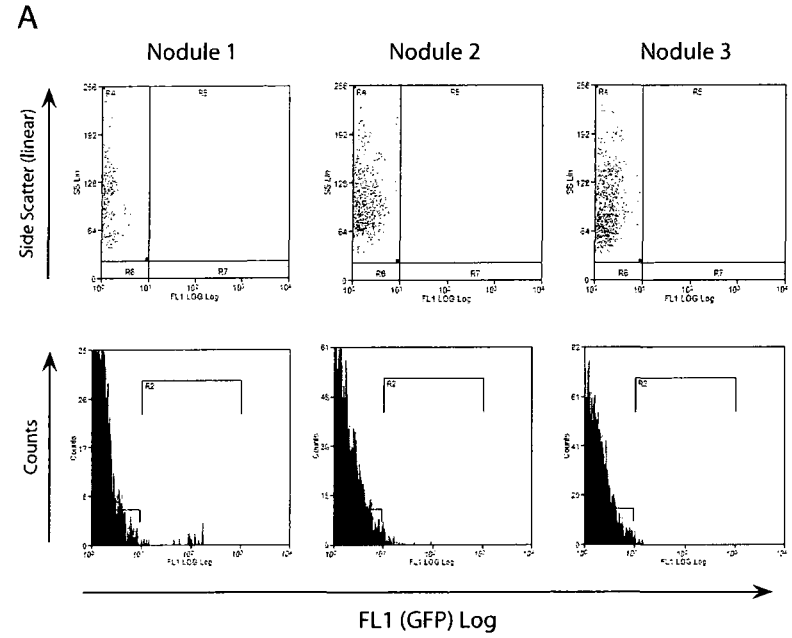
A
Nodule 1
Nodule 2
Nodule 3
Side Scatter (linear)
Counts
FL1 (GFP) Log
B
Nodule 1
Nodule 2
Nodule 3
Side Scatter (linear)

Figure 6: Flow cytometry on single lung nodules removed after 14 days in-vivo growth.

Panel (A) Three separate lung nodules from mouse treated with wild-type CT26 cells. (B) Three separate lung nodules from mouse treated with CT26fLUC+ cells. (C) Quantification of GFP+ cell numbers from samples in panels A and B (n=3 nodules per mouse per treatment group, error bars=SD). (D) Mean fluorescence intensity of GFP signal from tumour nodules in panel B. All counts relative and indexed for numbers of cells in suspension for flow cytometric analysis.

AGING MOUSE LUNG HAS A UNIQUE TRANSCRIPTIONAL SIGNATURE

To gain a broader insight into age-related changes in the lung, a high-throughput microarray-based approach was employed. Both perfused and unperfused tissues were studied in order to determine the relative contribution of circulating factors (unperfused) and lung parenchyma (perfused) to the aging phenotype observed. Our strategy for analysis was based on performing tests for statistical significance using analysis tools from Bioconductor (see Methods) to determine significantly altered transcription changes. Briefly, the SAM algorithm (154) determines the difference between the observed expression values and an arbitrary calculated value which approximates an expected value arising by chance. The calculation is approximated by permuting the data randomly. When observed and permuted expression values are plotted against each other, most will fall on the 45-degree line of equivalence. Significant transcripts will deviate above or below this line. The parameter delta is then selected to determine how much of a deviation from the 45-degree line is required to be called significant. Typically, the choice of delta is based on a sensitivity analysis performed within SAM in order to achieve a false discovery rate of less than 5%, which is in essence the statistical alpha. The p-values obtained are corrected using the Benjamini-Hochberg correction for multiple testing to arrive at a corrected p-value, known as the q-value.

Microarray hybridization quality was acceptable (Appendix 2). Our strategy for analysis was based on performing tests for statistical significance using analysis tools from Bioconductor (see Methods) to determine significantly altered transcripts. Under the analysis parameters

selected (delta = 4.8) the SAMplot visually demonstrates the significantly altered transcripts (Figure 7A). With delta = 4.8, the false-discovery rate was estimated to be 4.5% for the gene list (Figure 7B). The data reveal 465 transcripts found to be significantly expressed in a differential manner in aged normal lung tissue (referred to as the *gene list*). Statistically over-represented transcripts were subsequently examined: GO terms found to be statistically over-represented in the older, unperfused lung tissues are presented in Table 2. It is clear that there is evidence of perturbation in markers of immune function. Many of the transcripts represent effectors of airway inflammation receptors (Syk), cytokines (CCL5, 8) and toll-like receptors (TRL1) – these point to innate immune functions being upregulated with advancing age. Within this context, we sought to examine the transcription profile of parenchyma alone.

Similar microarray methodology was applied and the transcriptional profile in perfused lung tissues was examined. Gene ontology analysis identified angiogenesis (GO: 0001525, Table 3), immune response (GO: 0006955, Table 4) and DNA repair (GO: 0006281, Table 5); as statistically over-represented in the gene list, targets for validation were selected based on these data.

A

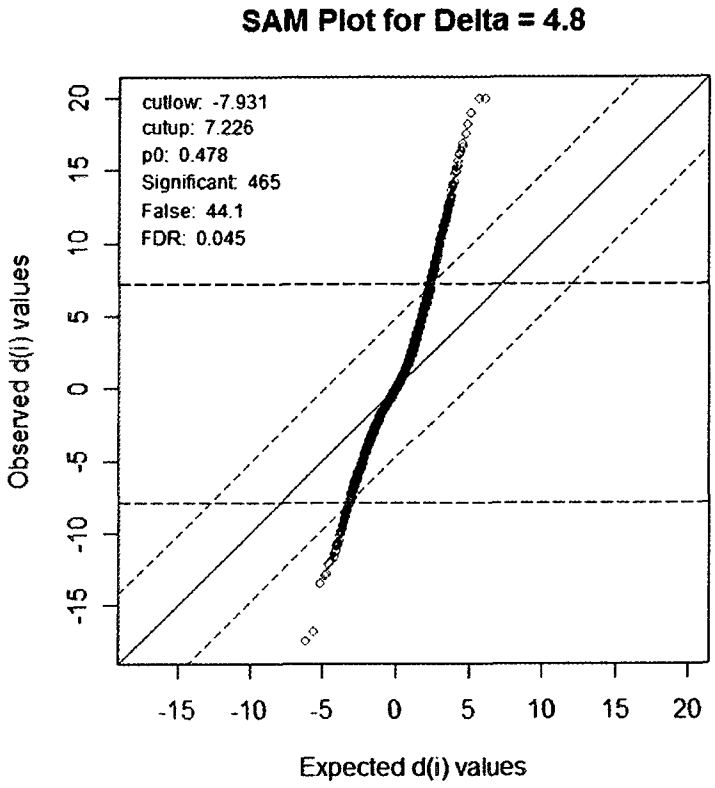
SAM Plot for Delta = 4.8
cutlow: -7.931
cutup: 7.226
p0: 0.478
Significant: 465
False: 44.1
FDR: 0.045
Observed d(i) values
Expected d(i) values
-15
-10
-5
0
5
10
15
20

B

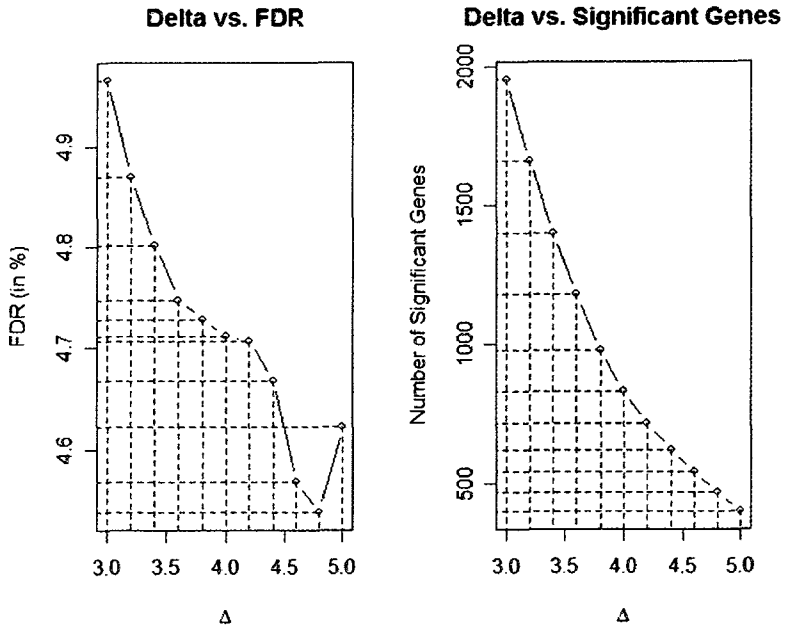
Delta vs. FDR
FDR (in %)
4.6
4.7
4.8
4.9
3.0
3.5
4.0
4.5
5.0
Δ
Delta vs. Significant Genes
Number of Significant Genes
500
1000
1500
2000
3.0
3.5
4.0
4.5
5.0
Δ

Figure 7: Differential expression and sensitivity analysis for parameters used in the structured microarray analysis of normal mouse lung tissue.

Panel (A) Observed versus expected intensity differences (SAMplot) for delta=4.8. The diagonal line and the dashed interval represent the confidence interval defined by the parameter delta. Non-significant transcripts falling within these bounds are marked in black. Transcripts whose differential expression lies beyond the dashed lines are marked in green, representing significant changers. The horizontal dashed lines indicate the lower and upper bounds of non-significant differential expression. (B) Sensitivity analysis showing the dependence of false discovery rates and number of significant genes to the stringency defined by the parameter delta.

In this case, a delta of 4.8 identified 465 significant transcripts with an estimated false discovery rate of 4.5%.

A

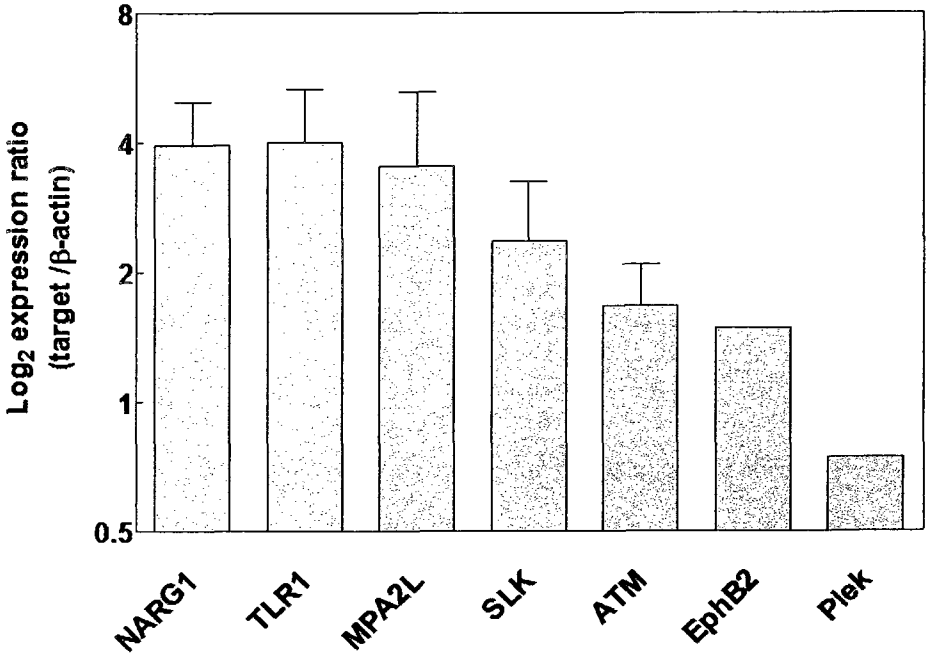
8
4
2
1
0.5
Log2 expression ratio
(target /β-actin)
NARG1
TLR1
MPA2L
SLK
ATM
EphB2
Plek

B

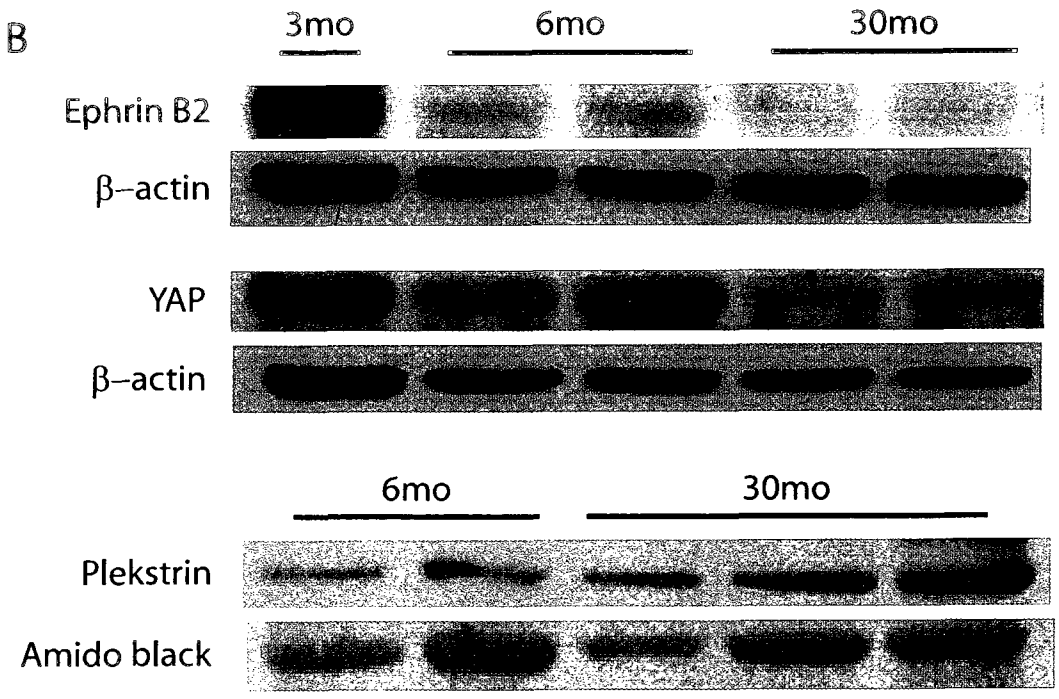
3mo
6mo
30mo
Ephrin B2
β–actin
YAP
β–actin
6mo
30mo
Plekstrin
Amido black

Figure 8: Validation of mouse microarray results by PCR and Western blotting.

Panel (A) A subset of transcripts annotated with Gene Ontology (GO) terms found to be significantly enriched in the set of differentially expressed genes were validated by quantitative PCR. All gene expression was compared to expression levels in young mice, normalized to expression levels of β-actin. **Narg-1**, NMDA receptor-regulated gene 1; **MPA2L**, macrophage activation 2 like; **TLR1**, toll-like receptor-1; **ATM**, ataxia telangiectasia mutated homolog; **Slk**, STE20-like kinase; **EphB2**, Ephrin B2; **Plek**, Plekstrin. Mean relative expression for triplicate runs plotted, error bars = SD. (B) Western blot analysis of young and aged lung tissue. Top panel shows protein levels of ephrin B2 to be decreased in lung tissue lysates with increasing age. Middle panel shows protein levels of Yap to be decreased in lung tissue lysates with increasing age; both blots were reprobed with actin-specific antibody to demonstrate relative loading. Lower panel shows protein levels of plekstin to be increased in lung tissue lysates with increasing age. Amido black stain shown as relative load control.

Quantitative PCR (Figure 8A) confirms that transcripts related to immune function (macrophage recruitment, MPA2L; toll-like receptor 1, TLR1); angiogenesis (NMDA receptor regulated gene 1, Narg-1; Ephrin B2, EphnB2); and DNA repair (ataxia telangiectasia mutated homolog, ATM; STE20-like kinase, Slk) are upregulated in perfused lungs of older mice. Protein analysis by western blot (Figure 8B) demonstrated reduced Ephrin B2 and *Yes*-associated protein with advancing lung age, while Plekstrin (a marker of immune activation) was upregulated.

To confirm that endothelial cell populations were not different between the age cohorts, flow cytometry was performed on perfused lung cell suspensions to enumerate CD31+ cells (Figure 9A), no differences were detected. To ascertain that observed differences in markers of immune function, flow cytometry was performed on perfused lung tissue cell suspensions to determine lung T-lymphocyte populations (Figure 9B). BASC progenitor pools were also not found to differ between age groups (Figure 9C).

DEMOGRAPHICS OF HUMAN STUDY POPULATION

A total of five patients were recruited into the study over the period 2005-2007. Two patients were enrolled in the young cohort, with the remainder joining the aged cohort (see Table 7). All patients in the young cohort were non-smokers and underwent operative treatment for unresolved spontaneous pneumothorax. All patients in the aged cohort underwent pulmonary resection for non-small cell lung cancer. Specific demographic information is presented in Table 8.

A

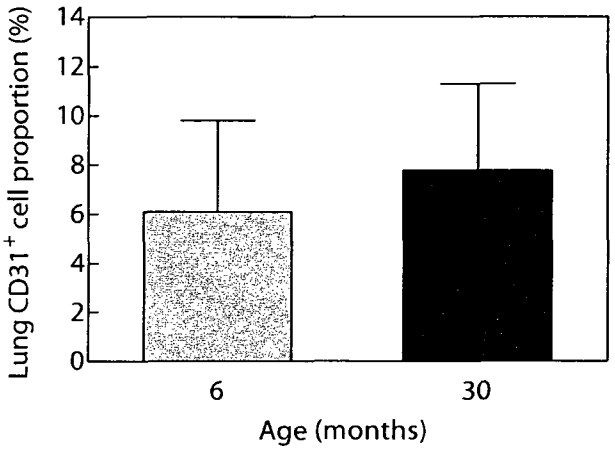
Lung CD31+ cell proportion (%)
14
12
10
8
6
4
2
0
6
30
Age (months)

B

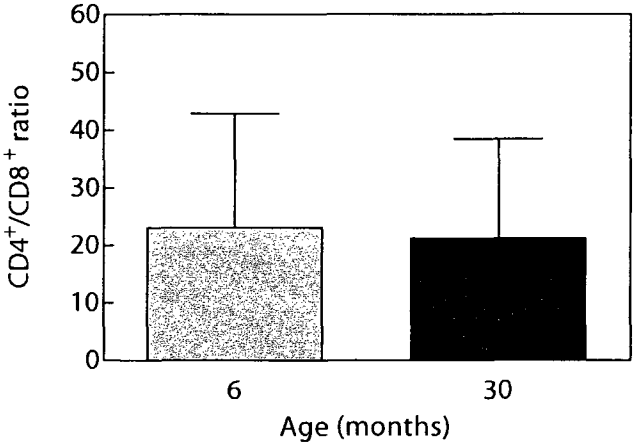
CD4+/CD8+ ratio
60
50
40
30
20
10
0
6
30
Age (months)

C

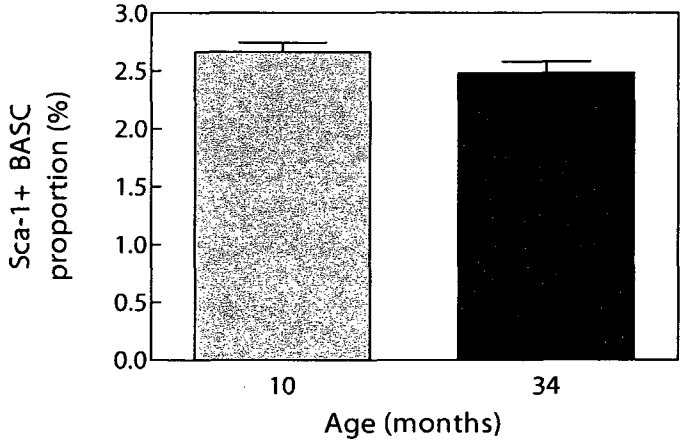
Sca-1+ BASC proportion (%)
3.0
2.5
2.0
1.5
1.0
0.5
0.0
10
34
Age (months)

Figure 9: Cellular subpopulations are not different between young and aged mouse lungs.

Panel (A) No significant differences in CD31+ endothelial cell population by flow cytometry (n=4 mice in each group, error bars = SD). (B) CD3+ T-lymphocyte populations in lung tissue are not different by flow cytometry (n=4 mice in each group, error bars = SD). (C) Lung progenitor cell populations are not different by flow cytometry. No tumour injections were performed in these mice (n=2 mice in each group, error bars = SD). Lung-resident endothelial and lymphocytic cell populations do not differ with age

As outlined above (Methods), the study design encompassed a preliminary pilot microarray study of 3 young and three aged patient samples of normal lung tissue. Having established the presence of transcriptional alteration with advancing age, further recruitment would allow for a second microarray comparison between aged normal lung tissues and the corresponding tumour tissue within the operative specimen. Study recruitment was unable to fulfill criteria for completion of the pilot phase of the study. The results presented herein represent an interim analysis.

AGING HUMAN LUNG TISSUE HAS A UNIQUE TRANSCRIPTIONAL SIGNATURE

Microarray hybridization quality was acceptable (Appendix 3). Our strategy for analysis was based on performing tests for statistical significance using analysis tools from Bioconductor (see Methods) to determine significantly altered transcripts. Under the analysis parameters selected (delta = 1.7) the SAMplot visually demonstrates the significantly altered transcripts (Figure 10A). With delta = 1.7, the false-discovery rate was estimated to be 29% (Figure 10B). The data reveal 82 transcripts found to be significantly expressed in a differential manner (Table 9) in aged normal lung tissue (referred to as the *gene list*). Since most of the genetic alteration appeared to be related to downregulation, transcripts were examined to ensure that a single chromosomal translocation was not responsible for the observed profile. Chromosomal locations of selected transcripts from the gene list (Table 11) are well-varied. A heat map was constructed based on the gene list in order to visualize the transcriptional profile in a global fashion. The age cohorts are well segregated by cluster analysis (Figure 11).

A

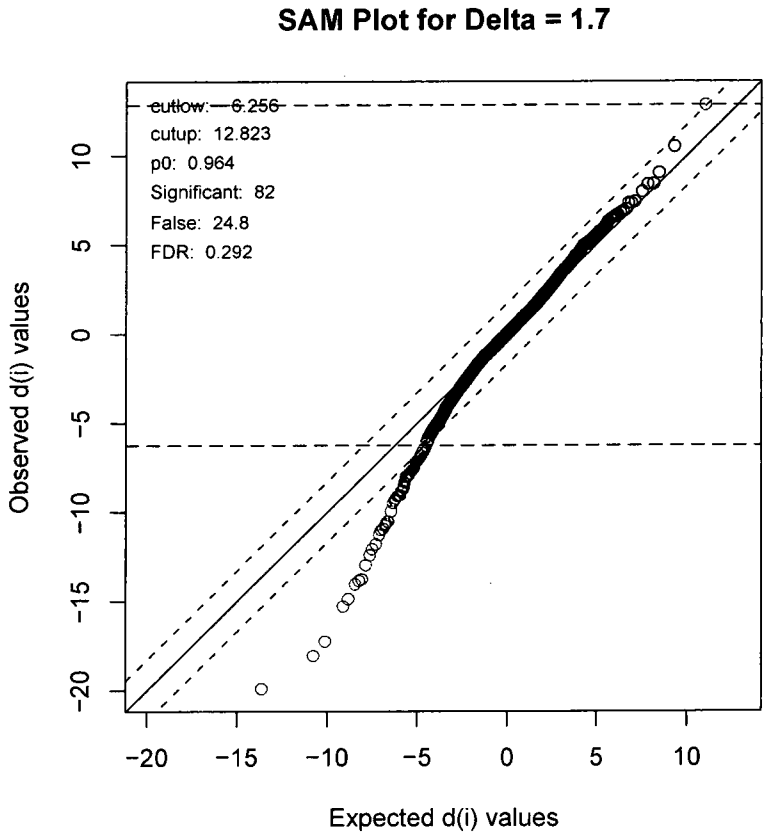
SAM Plot for Delta = 1.7
cutlow: −6.256
cutup: 12.823
p0: 0.964
Significant: 82
False: 24.8
FDR: 0.292
Observed d(i) values
Expected d(i) values
−20
−15
−10
−5
0
5
10

B

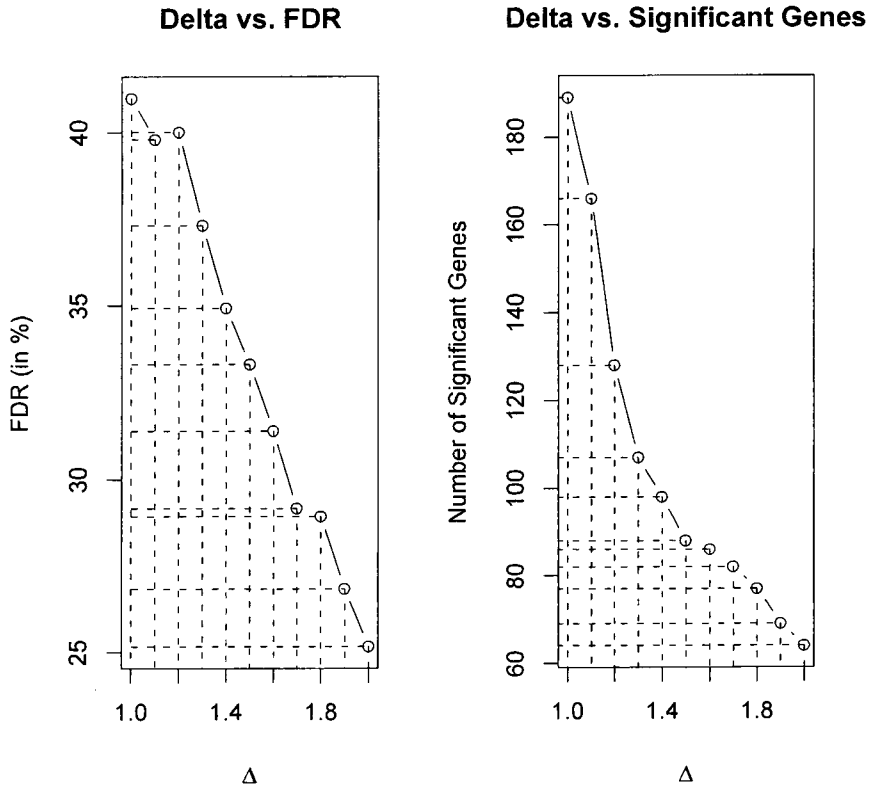
Delta vs. FDR
FDR (in %)
25
30
35
40
1.0
1.4
1.8
Δ
Delta vs. Significant Genes
Number of Significant Genes
60
80
100
120
140
160
180
1.0
1.4
1.8
Δ

Figure 10: Differential expression and sensitivity analysis for parameters used in the structured microarray analysis of normal human lung tissue.

Panel (A) Observed versus expected intensity differences (SAMplot) for delta=1.7. The diagonal line and the dashed interval represent the confidence interval defined by the parameter delta. Non-significant transcripts falling within these bounds are marked in black. Transcripts whose differential expression lies beyond the dashed lines are marked in green, representing significant changers. The horizontal dashed lines indicate the lower and upper bounds of non-significant differential expression. (B) Sensitivity analysis showing the dependence of false discovery rates and number of significant genes to the stringency defined by the parameter delta.

In this case, a delta of 1.7 identified 82 significant transcripts with an estimated false discovery rate of 29%.

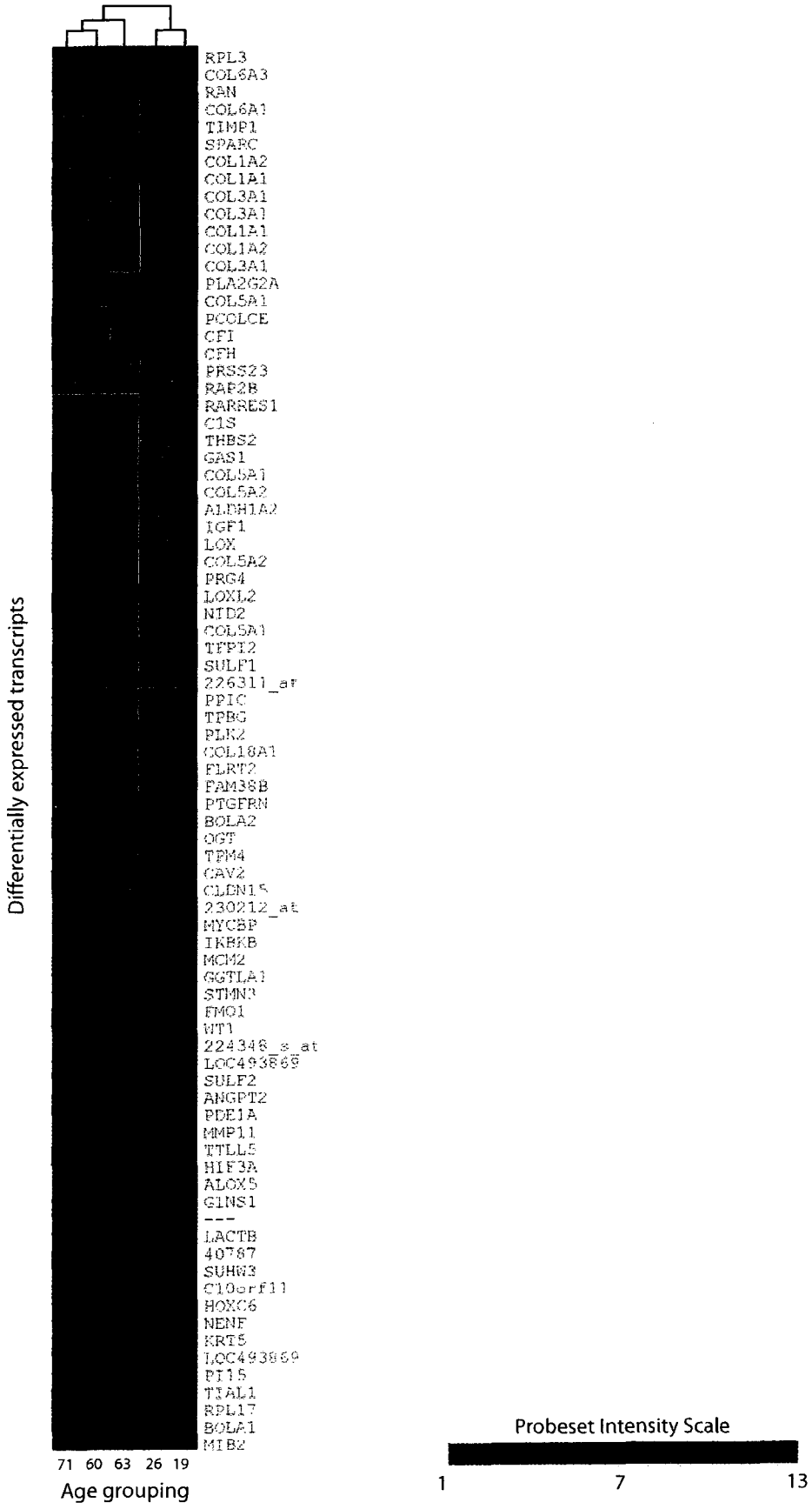
Differentially expressed transcripts
RPL3
COL6A3
RAN
COL6A1
TIMP1
SPARC
COL1A2
COL1A1
COL3A1
COL3A1
COL1A1
COL1A2
COL3A1
PLA2G2A
COL5A1
PCOLCE
CFI
CFH
PRSS23
RAP2B
RARRES1
C1S
THBS2
GAS1
COL5A1
COL5A2
ALDH1A2
IGF1
LOX
COL5A2
PRG4
LOXL2
NID2
COL5A1
TFPI2
SULF1
226311_at
PPIC
TPBG
PLK2
COL18A1
FLRT2
FAM38B
PTGFRN
BOLA2
OGT
TPM4
CAV2
CLDN15
230212_at
MYCBP
IKBKB
MCM2
GGTLA1
STMN3
FMO1
WT1
224348_s_at
LOC493869
SULF2
ANGPT2
PDE1A
MMP11
TTLL5
HIF3A
ALOX5
G1NS1

LACTB
40787
SUHW3
C10orf11
HOXC6
NENF
KRT5
LOC493869
PI15
TIAL1
RPL17
BOLA1
MIB2
71 60 63 26 19
Age grouping
Probeset Intensity Scale
1
7
13

Figure 11: Transcripts are clustered by age using heatmap analysis of significantly altered gene expression.

Heatmap analysis represents a hierarchical clustering of expression data by cohort and transcript. The intensity is a $\log_2$ scale and runs from 1 to 13 in arbitrary intensity units. Age grouping clusters into young and aged samples.

Gene ontology (GO) analysis (see Methods) revealed that transcripts relating to collagen and extracellular matrix were statistically over-represented in the gene list (Appendix 4). An examination of GO terms with collagen transcripts removed from the gene list does not show any statistically over-represented categories. A single transcript, MYC binding protein (MYCBP), showed increased expression with increasing age. The remaining 81 significantly altered transcripts were found to be downregulated. Nine transcripts were chosen to undergo further validation, based on over-expression (MYCBP), over-representation in the GO analysis (COL1A1), previous association with aging phenotypes (IGF1), potential role in extracellular matrix (ECM) remodelling (SPARC, LOX, TIMP1, TFPI2, SULF1) and potential role in retinoid signalling response (RARRES1).

MYC BINDING PROTEIN IS UPREGULATED IN TUMOUR TISSUES

Quantitative PCR (see Table 10 for primer sequences) confirmed that MYCBP was upregulated in aged lung tissue (Figure 12). The absolute magnitude of the overexpression was comparable. Further validation was undertaken to confirm MYCBP protein levels. Immunohistochemical techniques were employed on paraffin-embedded sections of normal lung tissue from young and aged patients (Figure 13). MYCBP-positive pixels were quantified using analysis software (Aperio) and were indexed to lung tissue area (mm^2). Visually, staining intensity was not found to differ with advancing age (Figure 13A), which was confirmed by pixel quantification (Figure 13B). Normal tissue samples from the LC1201 lung cancer tissue microarray were also examined, grouped by age cohort (Figure 14A), which did not demonstrate age-related differences in MYCBP staining.

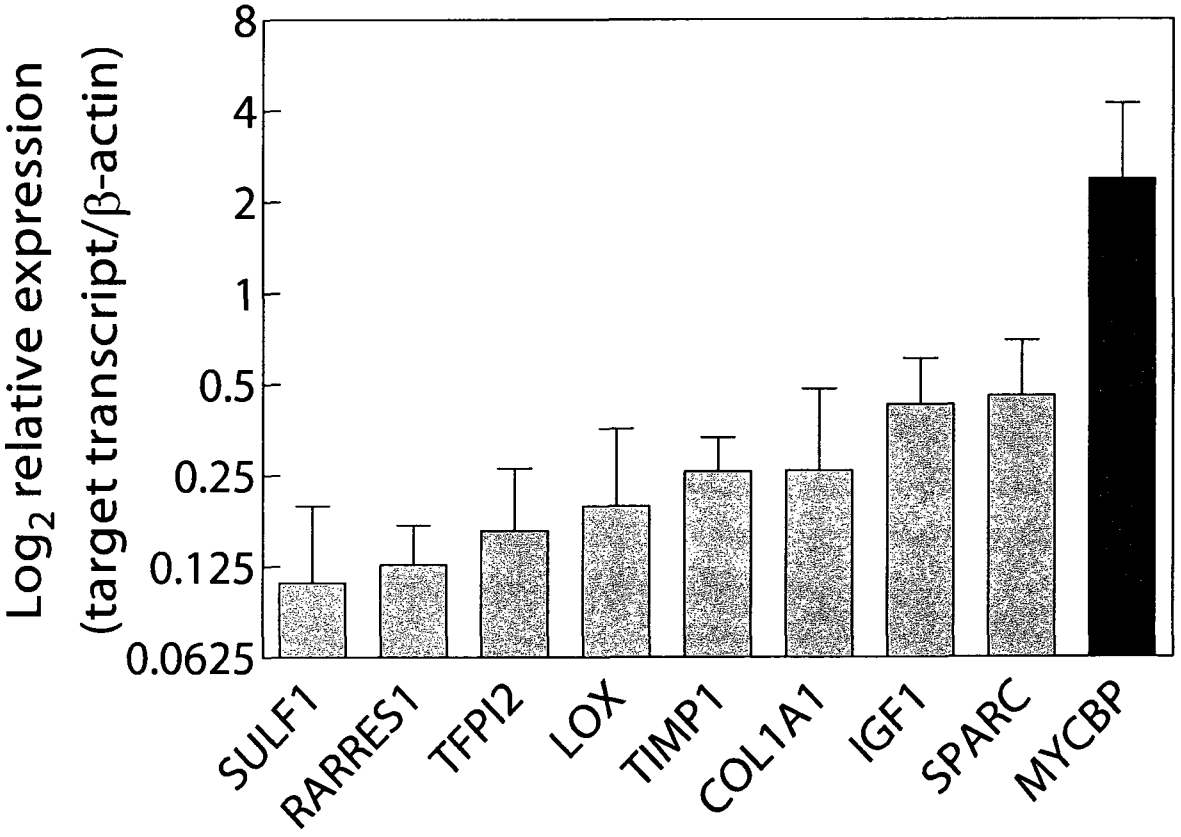
Log2 relative expression
(target transcript/β-actin)
8
4
2
1
0.5
0.25
0.125
0.0625
SULF1
RARRES1
TFPI2
LOX
TIMP1
COL1A1
IGF1
SPARC
MYCBP

Figure 12: Validation of normal human lung microarray results by quantitative PCR

A subset of transcripts found to be differentially expressed were validated by quantitative PCR. All gene expression was compared to expression levels in young lung tissues, normalized to expression levels of β-actin. **SULF1**, sulfatase-1; **RARRES1**, RAR responsive element 1; **TFPI2**, tissue factor pathway inhibitor 2; **LOX**, lysyl oxidase; **TIMP1**, tissue inhibitor of metalloproteinase 1; **COL1A1**, collagen 1 alpha 1; **IGF1**, insulin-like growth factor 1; **SPARC**, secreted protein, acidic, rich in cysteine; **MYCBP**, MYC binding protein. Mean relative expression for triplicate runs plotted, error bars = SD.

B

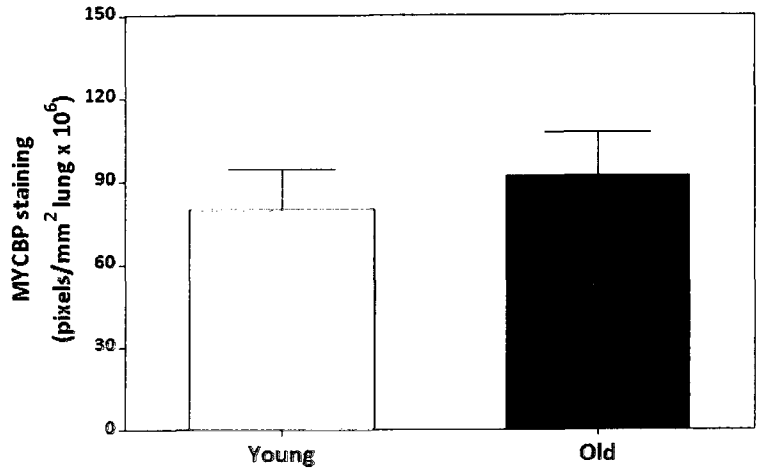
150
120
90
60
30
0
MYCBP staining
(pixels/mm^2 lung x 10^6)
Young
Old


A
26
71
19
60

Figure 13: No differences are found between young and aged normal human lung tissue levels of MYCBP by immunohistochemistry.

Panel (A) Low power digital images of microscope slides of normal lung tissues stained for MYCBP. Age of patient is indicated beside image. No difference in staining intensity is visually discernable. (B) Quantitative analysis of positive MYCBP staining does not reveal significant differences in expression levels. N=2 for young cohort, 5 for aged cohort, mean plotted, error bars = SD.

A

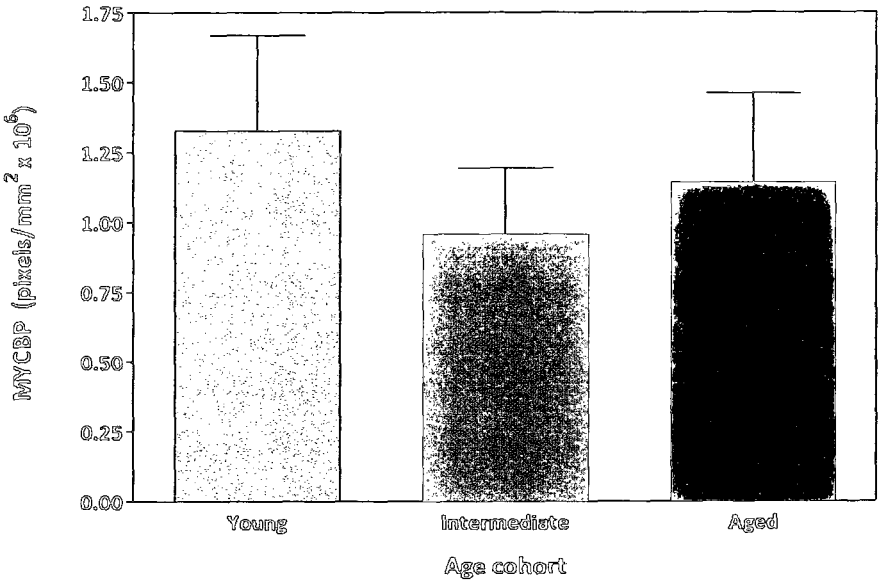
1.75
1.50
1.25
1.00
0.75
0.50
0.25
0.00
MYCBP (pixels/mm 2 x 10 6)
Young
Intermediate
Aged
Age cohort

B

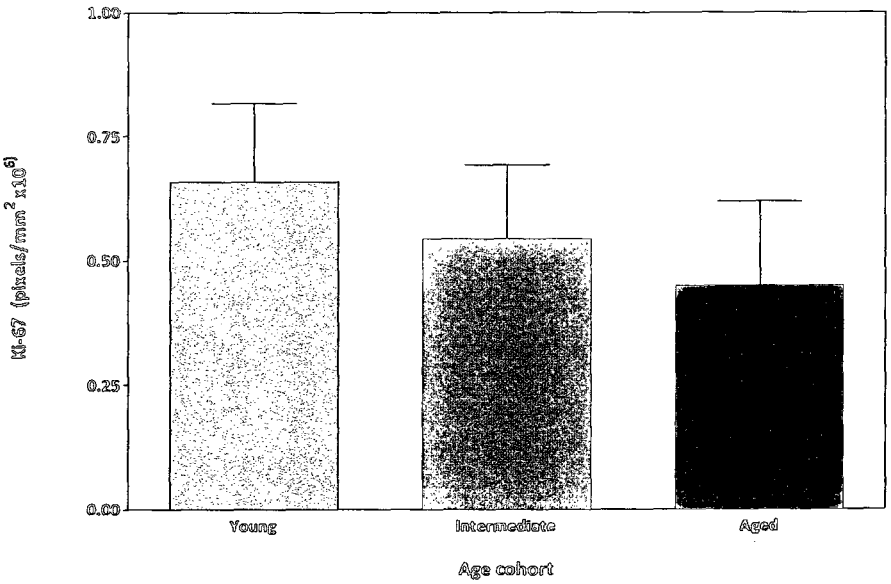
1.00
0.75
0.50
0.25
0.00
KI-67 (pixels/mm 2 x10 6)
Young
Intermediate
Aged
Age cohort

Figure 14: No differences are found between young and aged normal human lung tissue on tissue microarray analysis (TMA) of MYCBP and Ki-67 staining.

Panel (A) shows quantitative analysis of MYCBP and (B) Ki-67 staining from the LC1201 TMA. No differences between age groups are noted. Young represents samples from patients aged 18-35, n=4; intermediate represents samples from patients aged 36-59, n=4; aged represents samples from patients aged 60-65, n=4. Mean plotted, error bars = SD.

The pattern of MYCBP staining was overall increased in tumour tissues (Figure 15A) and was observed to be localized primarily to the cytoplasm in normal tissues, compared to the predominantly nuclear localization in tumour tissues. In normal tissues, MYCBP was not associated with increased Ki-67 expression (Figure 14B).

MYC IS NOT OVEREXPRESSED IN NORMAL OR TUMOUR TISSUES

To further explore the relevance of MYCBP in lung aging and carcinogenesis, we performed immunohistochemical staining on sections of normal lung and tumour tissue. The extent of positive staining for MYC was quantified by applying the positive pixel count algorithm. Subcellular localization was performed visually. There was no differences noted in MYC staining intensity or subcellular localization between young and old lung tissues (Figure 16A). A similar evaluation of tumour tissues also revealed no differences in MYC staining (Figure 16B) or subcellular localization (Figure 17).

COLLAGEN IS DOWNREGULATED IN NORMAL HUMAN LUNG TISSUES

Fifteen transcripts accounting for 8 collagen isoforms were found to be significantly downregulated in aged normal lung tissues (Figure 11Table 9: List of significantly altered transcripts in aging human lung tissue. and Table 9); these include collagens 1A1, 1A2, 3A1, 5A1, 5A2, 6A1, 6A3 and 18A1. The dominant structural isoform present in extracellular matrices is COL1A1 (11) (along with types 2 and 3), which was selected for further validation. Quantitative PCR (Figure 12) shows collagen to be downregulated in aged lung tissues.

A

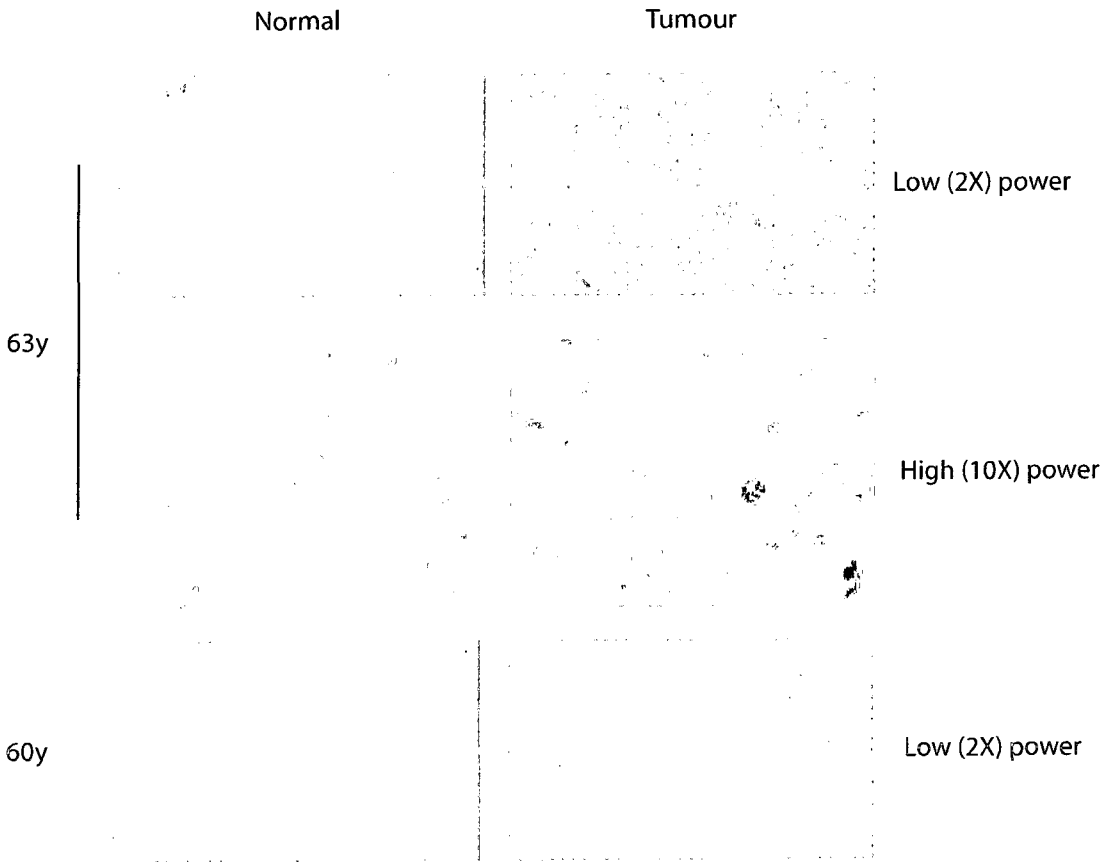
Normal
Tumour
Low (2X) power
63y
High (10X) power
60y
Low (2X) power

B

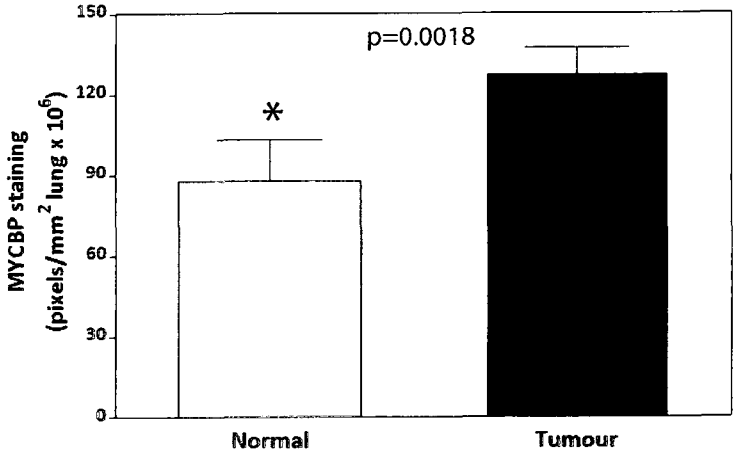
p=0.0018
*
MYCBP staining
(pixels/mm² lung x 10⁶)
150
120
90
60
30
0
Normal
Tumour

Figure 15: MYCBP is overexpressed and localized to the nucleus in human lung tumour tissue.

Panel (A) shows normal and matched lung tissues stained for MYCBP at low (upper row) and high (lower row) power. Compared to normal tissues, tumours exhibit intense staining for MYCBP, with a marked increase in nuclear localization. (B) Quantitative analysis reveals significantly greater MYCBP staining in tumour tissues ($p=0.002$, two-tailed t-test with Welch's correction), $n=4$ per group, mean plotted, error bars = SD.

A

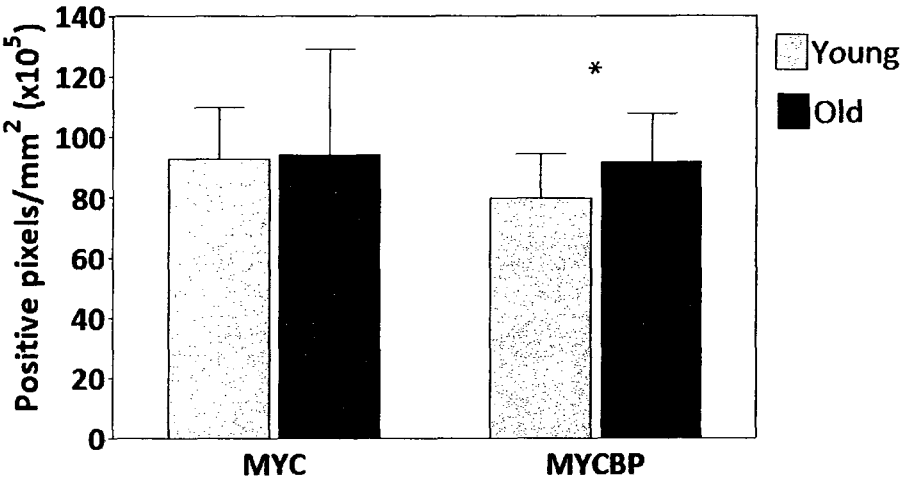
Positive pixels/mm^2 (x10^5)
140
120
100
80
60
40
20
0
*
Young
Old
MYC
MYCBP

B

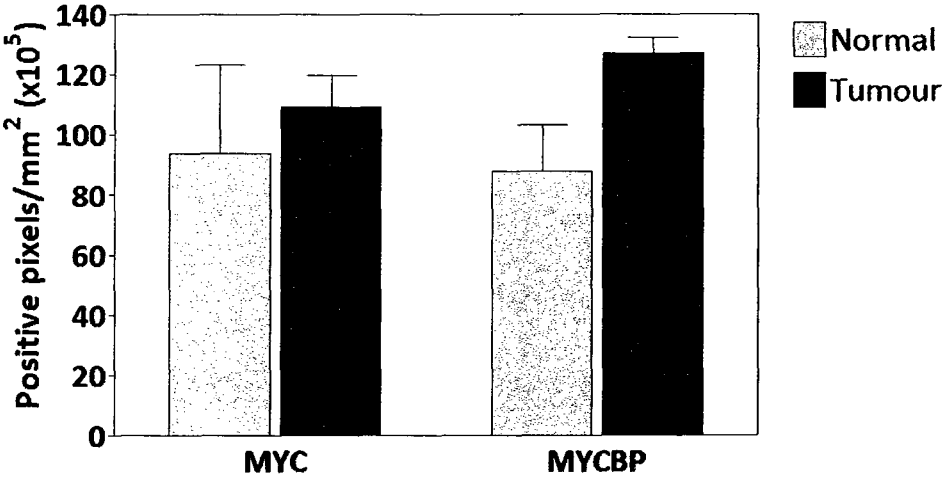
Positive pixels/mm^2 (x10^5)
140
120
100
80
60
40
20
0
Normal
Tumour
MYC
MYCBP

Figure 16: No differences are found between young and aged normal human lung tissue levels of MYC by immunohistochemical staining.

Panel A shows no difference in the magnitude of MYC staining in young and aged lung tissues. Comparison is made with MYCBP pixel counts, indexed staining intensity is equivalent. (B) Comparison of MYC and MYCBP staining in normal lung tissue and matched tumour tissues. No differences are apparent for MYC staining, while a statistical difference is noted in MYCBP levels. Young cohort n=2; aged cohort n=4, mean plotted, error bars = SD. Level of significance p=0.002 for MYCBP levels between normal and tumour by two-tailed t-test with Welch's correction.

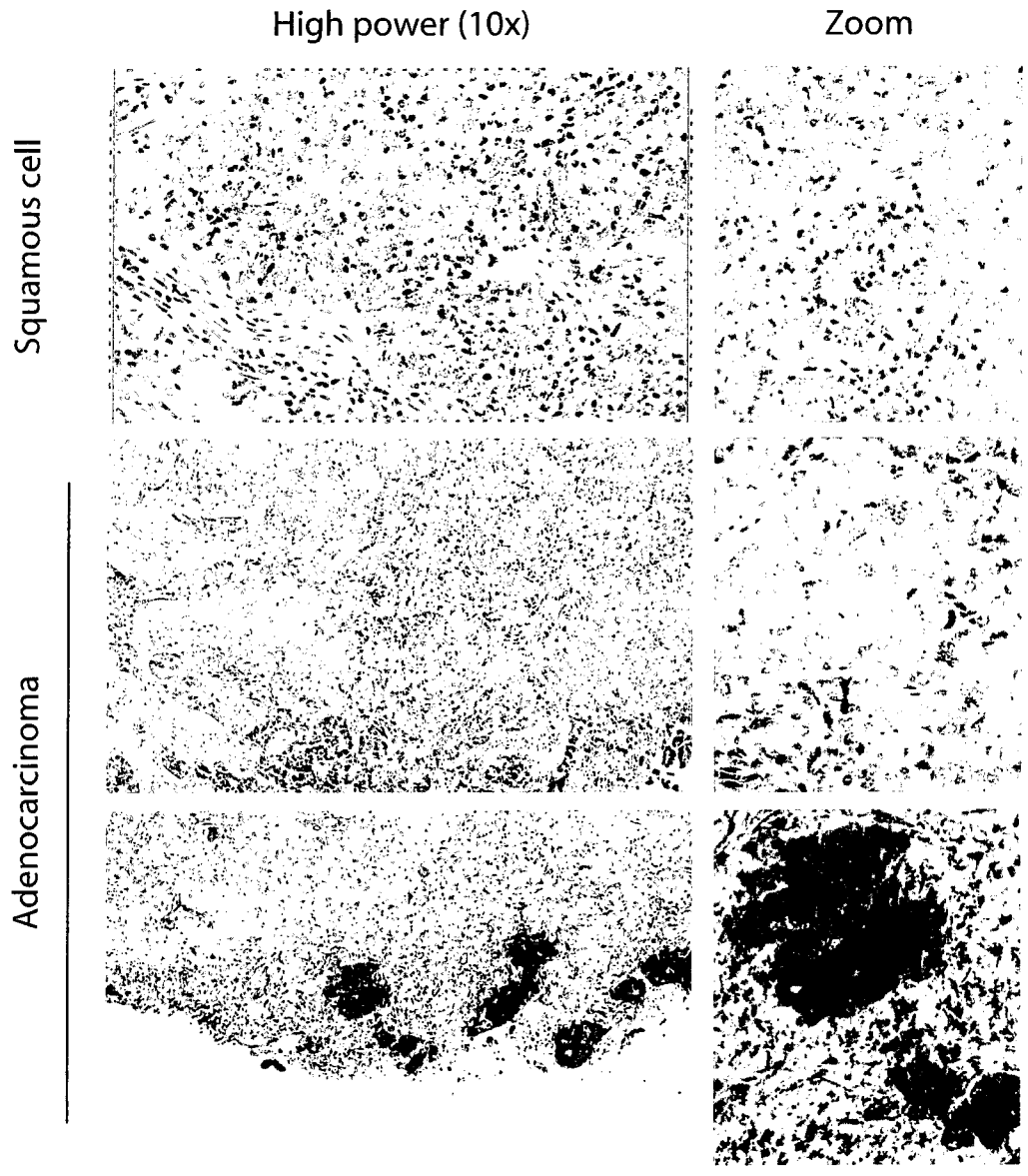
High power (10x)
Zoom
Squamous cell
Adenocarcinoma

Figure 17: MYC is not localized to the nucleus in human lung tumour tissue.

Tissue sections of human lung tumours stained for MYC do not demonstrate nuclear localization. High power and zoomed images demonstrate staining patterns. A squamous cell cancer is shown in the top row; the remaining images are from two adenocarcinoma samples. The intensity of the cytoplasmic staining is greatest in the adenocarcinoma with abundant peritumoral hypocellular tissue.

This was examined at the tissue level using the collagen-specific Masson's trichrome stain (Figure 18). The number of collagen-staining pixels was quantified and indexed to total lung area in pixels, showing a statistically significant decrease in collagen in aged lung tissue ($p=0.0012$, two-tailed t-test with Welch's correction).

Quantitative PCR was used to validate the downregulation of SULF1, RARRES1, TFPI2, LOX, IGF-1, SPARC and TIMP1 (Figure 12). Transcript levels assessed by PCR were concordant with the microarray data.

A

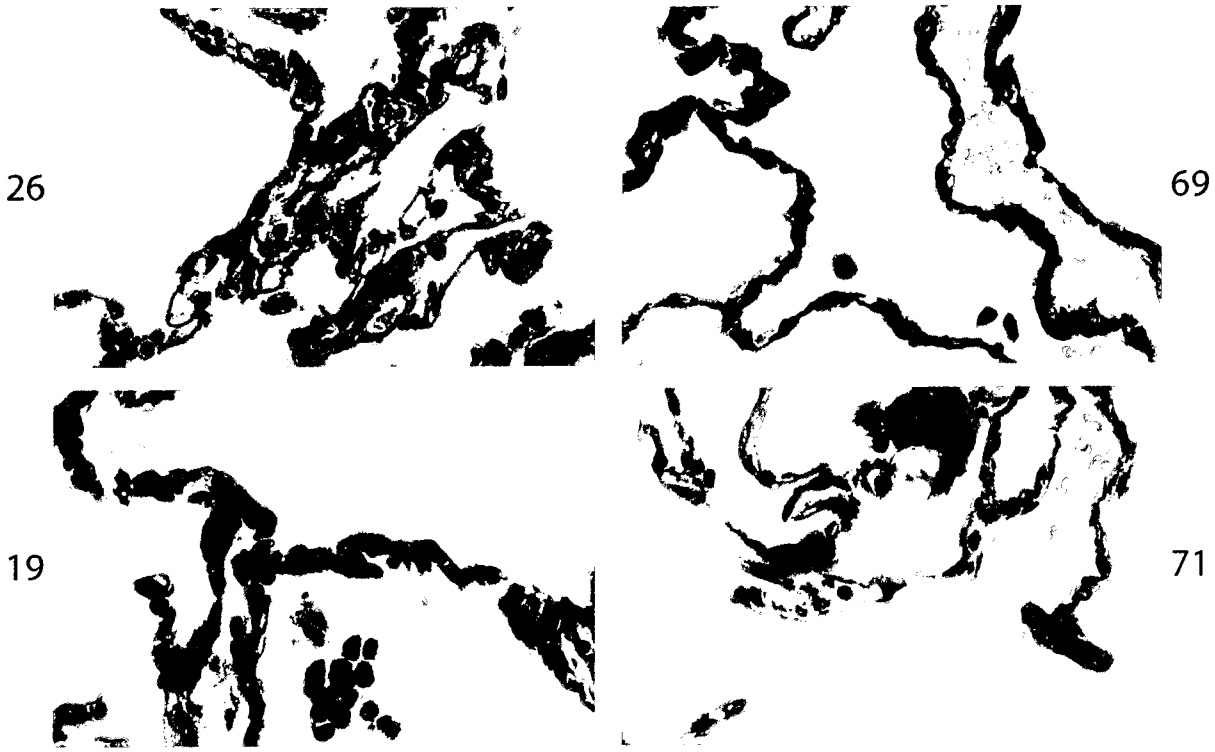
26
69
19
71

B

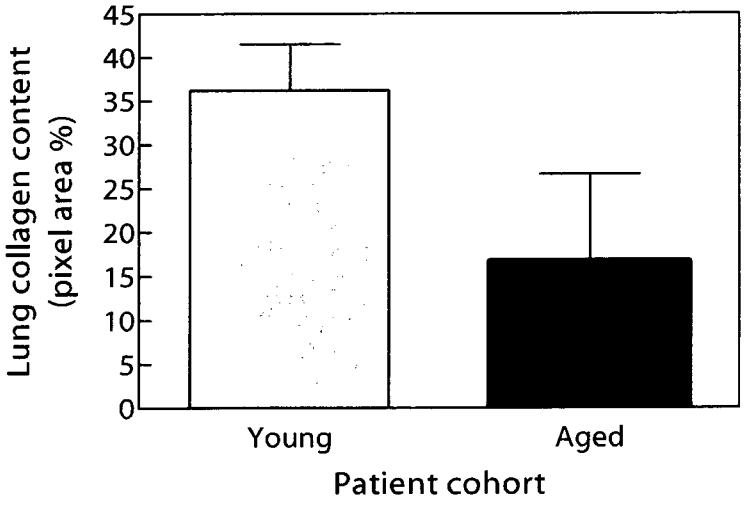
Lung collagen content
(pixel area %)
45
40
35
30
25
20
15
10
5
0
Young
Aged
Patient cohort

Figure 18: Collagen is less abundant in aged lung tissues.

Panel (A) shows lung tissue stained with Masson's trichrome for collagen, stained dark blue. Patient ages in years are shown. More intense staining is visually noted in younger patient samples. (B) Quantitative analysis reveals significantly more collagen stain by pixel count. p=0.0012, two tailed t-test with Welch's correction, n=2 for young patient, n=3 for aged patients, error bars = SD.

DISCUSSION

This thesis represents a unique assessment of the molecular and functional changes occurring in lung tissue at the extremes of age.

MOUSE LUNG STUDIES

PUBLISHED MODELS OF MOUSE PULMONARY METASTASES ARE INADEQUATE

Metastatic disease patterns were examined at three separate time points: (i) 14 days, (ii) at endpoint, and (iii) every 48h for 30 days to understand this phenomenon in extremely old mice. Early patterns of spread at 14 days after tumour cell injections did not demonstrate significant differences in number of tumour deposits (Figure 4A) or in tumour size (data not shown). Absence of differences after histological analysis (Figure 4C) was further confirmed by assessing a separate population of mice for the presence of GFP+ lung cells after injection of $CT26^{fLUC+}$ tumours using flow cytometry; no difference in cell proportions was noted (Figure 5). Pulmonary blood flow was not different between the two age groups (Figure 4F), which removed the possibility of differential tumour delivery to the lungs as a confounding factor. A previous study has examined intravenous metastases in 30-month old mice, finding a larger number of tumours in the aged cohort (48). Greater tumour burden has also been reported in 18-month old mice (7,152), while others have found reduced tumour counts in aged mice up to 22 months of age (66). Comparison to literature reports is challenging (Table 1), and these inconsistent reports may reflect the inbred genetic background of the mice used, or the wide variety of tumour types administered.

Two studies (98,152) used tumour cells resuspended in tissue culture media containing 10% bovine serum, raising the possibility that the reaction to foreign serum proteins could modulate immune responses and alter tumour spread. Distinctly different patterns of metastatic disease were noted; discrete tumour nodules more often seen in younger mice, while diffuse and ill-defined deposits were characteristic of older lungs. These patterns have also been noted by Hirayama and colleagues (66), albeit at earlier time points than reported herein. Most studies in Table 1 reported number of pulmonary metastases as the number of surface nodules counted. A more accurate estimate of tumour burden is reported here.

OVERALL SURVIVAL AFTER PULMONARY METASTASES IS REDUCED IN AGED MICE

Arbitrary experimental endpoints (as outlined above) do not truly reflect the full course of metastatic disease *in vivo.* Important information on the ability to resist tumour colonization and to adapt to physiologic stresses associated with disseminated pulmonary disease can only be assessed in a survival study. Two separate cohorts of mice were treated with CT26 and observed until death or predetermined weight loss/respiratory distress endpoints were reached. The median survival of 30-month mice was 47 days, while the younger mice had not yet reached the point of 50% attrition (Figure 4E) by 70 days, at which point the study was concluded. This may represent a 'normal' rate of attrition in the aged cohort when comparing to younger animals. Regardless of experimental treatment, there was no survival difference in the aged cohort – indeed, the survival curves are superimposable, which underlines the importance of non-cancer factors in the demise of

the oldest mice (chronic pulmonary infections or reduced cardiopulmonary reserve). This is opposite to the decreased survival of younger mice observed after induction of pulmonary metastases. It is possible that the results are explained by age-related reductions in pulmonary and respiratory capacity, however, no studies addressing these issues in hybrid CB6F1 mice have been published to date. Inbred mice, while providing genetic uniformity, are subject to strain-specific pathologies that may limit interpretability of experimental manipulations. In aging research, it has been advantageous to use hybrid strains (106), where genetic uniformity within the colony is preserved due to known and defined parental lineages. These first generation offspring manifest longer lifespan and fewer strain-specific pathologies. Turning to the parental strains, one finds that studies of BALB/c lung mechanics have only considered mice up to 2 months of age (13). In C57BL/6J mice, 26-month old mouse lungs were characterized by increased alveolar spaces, decreased lung resistance, decreased elastic fibre content and an increase in collagen deposition (69). Analogous changes were also seen in aged rat lungs up to ages of 36 months (161). It is likely that similar loss of pulmonary reserve with advancing age is present in CB6F1 mice, and responsible for the observed survival differences.

PATTERNS OF PULMONARY METASTASES ARE ALTERED WITH INCREASING AGE IN MICE

Having established significantly reduced survivorship in extremely old mice, we examined the pattern of metastatic spread. Significantly more tumour deposits developed in older mice, and this trend was consistent after normalizing counts for total lung area examined (Figure 4D). There was a trend for metastases to be smaller in size (measured by pixel

count) in older mice, although this trend was not statistically significant (data not shown). The long time course of this study allows for consideration of potential modifiers of disease course. In contrast to assessments at early time points, the longer-term viability of metastases depends on a sequence of adhesion, extravasation and establishment of a microenvironment (42). When considering a longer timescale, additional proliferation and angiogenesis steps are likely required for successful continued growth of metastatic colonies.

The engraftment of tumour cells was also examined in a time-dependent manner exploiting in-vivo luminescent capture techniques. A lentiviral vector containing a biscistronic reporter construct (Figure 5A) was used to infect CT26 cells. GFP was used to purify the cells to >95% homogeneity using FACS. Luciferase expression was confirmed prior to mouse injections using in-vitro assays, and further confirmed at endpoint by extracting total protein from a $CT26^{fLUC+}$ lung nodule (Figure 5B). Luminescent detection has been previously used to follow the kinetics of tumour metastases (102) and oncolytic virus replication (117). Figure 5C qualitatively shows early increases in signal intensity in older mice. Younger mice are delayed by 2 days in reaching equivalent intensity values. When quantified (Figure 5D), the luminescent data demonstrate an apparent disease burden peak at 15 days in old mice, with continued log phase growth in younger mice. Miller *et al.* (98) showed that clonogenic doubling time of metastatic tumours was greater in older mice at 8 days, which is consistent with the luminescent data we present. The interpretation of in-vivo imaging data must be done cautiously: In our study, luminescent data were only interpretable in half of all mice treated with $CT26^{fLUC+}$ cells. Mice included for analysis had

sustained luminescent signals detectable at day 20 after injection. The apparent loss of signal in the 30-month group of mice was not 'loss' of tumour burden, since robust tumour colonies were found on autopsy. In order to explain these curious finding, we challenged young BALB/c mice with identical doses of tumour cells. Luciferase assays were able to detect luminescent activity in ex-vivo tumours. In some mice, increasing the dose of luciferin substrate and delaying imaging for up to 45 minutes allowed for partial recovery of luminescence. Flow cytometry of cells from single, isolated tumour nodules confirmed that the tumour colonies were composed of clones of both wild-type and luciferase positive cancer cell (Figure 6). It is most likely that a lack of clonal proliferation of luciferase-expressing cells *in-vivo,* coupled with tumour core hypoxia (54) act together in order to attenuate the magnitude of luminescent signal. In the face of such limitations, we feel that in-vivo imaging analysis can only be considered to be reliable over shorter time intervals.

TRANSCRIPTS RELATED TO ANGIOGENESIS ARE ALTERED WITH AGE IN MOUSE LUNGS

Employing microarray methodology and validating selected transcripts, we characterized significantly altered patterns of gene expression in aged lung tissues. We present transcriptional evidence (Table 3and Figure 8A) for age-related inhibition of angiogenesis, mediated by Narg-1 (51). The Narg-1 gene product is a negative regulator of angiogenesis, as knockout mice display proliferative vascular retinopathy (112,156). Ephrin B2 is a membrane-bound ligand of the ephrin receptor tyrosine kinase family that has been identified as having a essential role in stimulating angiogenesis (80). At a transcriptional level, the gene product for Ephrin B2 is upregulated in older mouse lung (Figure 8A), while

the protein levels are found to be reduced (Figure 8B). These opposed findings may represent a response to lung injury or inflammation. An examination of $CD31^+$ endothelial progenitor cell populations (35) (Figure 9A) did not show any differences between the two age groups. Vascular endothelial growth factor receptor 1 (VEGFR1) has been shown to determine targeting organ specificity of metastases and involved in establishing the premetastatic niche (74). In aged mice, adoptive transfer of bone marrow from aged mice into young recipients slowed the growth of B16 melanoma cells (36). These published reports suggest a role for angiogenic activity mediated by hematopoietic cells as central to progression of metastatic disease.

Pulmonary metastases have been shown to recruit blood supply exclusively from the pulmonary circulation, the bronchial circulation or both (100) and is a key step in promoting tumour growth (43). The loss of VEGF signalling reported in advanced age (122,123), taken with our findings of increased levels of Narg-1 and reduced Ephrin B2 levels suggest a reduced capacity for angiogenesis. We propose that this would limit the size of metastatic tumour deposits by virtue of reduced tumour neovascularization and provide a plausible explanation for the smaller and more numerous tumour deposits in the older lungs, which could be explored by using a model of primary lung cancer and examining tumour growth parameters over a range of mouse ages.

MARKERS OF IMMUNE FUNCTION ARE PERTURBED IN AGED MOUSE LUNG TISSUE

Anti-tumour immune surveillance also modifies metastatic spread: Macrophages (157), natural killer (NK) cells (39,142) and cytotoxic $CD4^+$ and $CD8^+$ T-cells (116,153) have all been

shown to mediate the anti-tumour response. NK cell activation and proliferation was found to be reduced in aged mice 22 days after tumour injection (48) as well as after a 12h period of restraint stress . Younger mice restrained in a similar fashion showed a limited and reversible decrease in NK activity as compared to older mice. Metastases were found to be larger in young mice after the restraint stress, while no difference in tumour size was observed in older mice. It is unlikely that the stress of restraint would alter the patterns of metastatic spread reported herein, given that the total duration of restraint for all experimental manipulations was less than two minutes per mouse. An assessment of lung-resident lymphocytes (Figure 9B) did not reveal any differences between the two age groups; assays of immune cell-mediated lytic activity and enumeration of NK cell populations were not performed.

Transcriptional patterns observed clearly suggest age-related alteration of the immune system. In non-perfused mouse tissues, transcripts associated with the activation of lymphocytes (Table 2) were markedly upregulated in aged lungs. This prominent signature is absent when compared to the transcriptional profile of perfused lung tissues, and suggests enhanced recruitment of immune cells to the aged lung. A different profile of transcripts (Table 4) was noted in perfused lung tissue: Rather than relating exclusively to immune cell activation and signalling, the transcriptional profile favours innate immune mechanisms. Upregulated transcripts include toll-like receptor 1 (TLR1), macrophage recruitment and activation (MPA2L) and the complement regulating decay-activating factor (Daf1). Plekstrin, found to be increased at the protein level, has been shown to be phosphorylated in neutrophils, and is thought to act as an adaptor molecule in the

inflammatory response. This is consistent with observations of chronic inflammation in aged lung tissues, and suggests a partial compensation mechanism in aging lung tissue to counteract humoral immunosenescence.

Several transcripts in the perfused tissue arrays encode proteins that mediate DNA repair (Table 5). The transcript with the highest fold-change, although identified using the gene ontology term for DNA repair, Ste20-like kinase (Slk) has many other roles including apoptosis (127), cell motility (155) and cell cycle progression (109). Yes-associated protein (YAP) interacts with the Src-family proto-oncogene *Yes* (85) that has proliferative and pro-apoptotic function. A decrease in a pro-apoptotic mediator such as YAP may represent a carcinogenic stimulus. As recently reported, hematopoietic stem cells require functional DNA repair pathways in order to maintain their replicative lifespan (108); the upregulation of such transcripts as ATM and Slk may serve to maintain multipotency in the face of increasing DNA damage.

We have demonstrated a significant age-dependent alteration in survival, in the patterns of pulmonary metastases and in the patterns of gene expression. Considering the prevalent use of experimental models of metastases in all aspects of cancer research, it is important to note that most studies use inbred or immune deficient strains of mice at considerably younger ages than those used in this study. One must interpret data from studies of pulmonary metastases with the knowledge that young inbred mice in prime health do indeed exhibit metastatic disease differently from older hybrid mice, and the effects of

immune activation in aged lung tissues would not be accounted for in an immune-deficient host.

TRANSCRIPTIONAL PROFILE OF HUMAN LUNG AGING

Inclusion and exclusion criteria (Table 7) were selected to achieve a wide separation in chronological age between the young and aged cohorts; and to examine lung parenchyma that is free from genetic, carcinogenic or inflammatory changes that would interfere with the detection of an aging effect. The demographic data in Table 8, despite the small number of patients recruited, demonstrates that our recruitment objectives have been achieved.

THE MYC PROBLEM

MYCBP, found to be upregulated in this study, has been reported as a co-activator of MYC (72). MYC is an oncogene found to be amplified and overexpressed in up to 30% of SCLC and up to 10% of NSCLC cases (104). Overexpression of MYC induces entry into S-phase, however uncontrolled cellular proliferation requires additional oncogenic stimulus such as mutations in KRAS or pRB (166). The role of MYC (in concert with RAF) in promoting the development of lung cancer metastases has recently been demonstrated (120).

MYCBP was found to be significantly upregulated at the mRNA level in association with advanced age, both by microarray and PCR (Figure 12). Using tissues from study patients and from a commercial tissue microarray (TMA), MYCBP levels were unchanged between young and older tissue (Figure 13 and 14). An assessment of downstream MYCBP effectors

was undertaken, and tissue levels of MYC were found to be invariant between young and old tissue (Figure 16). The discrepancy between RNA and protein levels may relate to cellular proliferation rates. The cellular marker Ki-67 is found abundantly in proliferating cells, and was considered to be an estimate of cellular proliferation. Using a commercial TMA stained for Ki-67, no difference in proliferation rates between young, intermediate and older tissue samples was noted (Figure 14). The observed absence of MYCBP accumulation in normal aged lung tissue and with the lack of Ki-67 staining suggests that the overexpression of MYCBP is not driving cellular proliferation. This may also explain the lack of MYC staining, as only proliferating cells would accumulate MYC. The effect of sub cellular localization must be considered: MYC must translocate to the nucleus in order drive cell proliferation. No histochemical evidence of MYC localization to the nucleus was observed. In fact, only MYCBP was found to localize to the nucleus in samples of lung tumour (Figure 15).

It is possible that alternate pathways are being activated with advanced age; the Wnt/β-catenin pathway has been implicated in MYCBP signalling at Tcf/Lef sites in the MYCBP promoter, as it has been demonstrated that increased Wnt signalling is associated with NSCLC progression (68). The microRNA Let-7 has been shown to decrease MYC activity in cases of Burkitt's lymphoma(132), and overexpression suppresses NSCLC proliferation (81).

It may also be the case that the temporal sequence of events leading to cellular proliferation had passed, and that transient changes readily observed at the mRNA level were not detected at a protein level. Our data may also demonstrate an independent role

for MYCBP in the development of lung cancers, and that translocation of MYCBP to the nucleus represents activation of a yet unidentified transcription factor responsible for cancer cell proliferation.

It is also possible that antibody specificity is not as complete as outlined in the antibody technical data. This issue will be analysed more carefully in the context of ongoing histochemical analyses.

AGED LUNG IS CHARACTERIZED BY A FIELD DEFECT

The alterations and mutations identified in the context of smoking-induced carcinogenesis have been considered to represent field cancerization (62). The application of this paradigm to the genetic alterations accumulated with advancing age has so far not been considered to be a field defect. We present data herein in support of advancing age as a progressive field defect.

The retinoic acid receptor β (RARB) has been found to be methylated in normal pulmonary tissues, and is expressed mainly in the larger airways (34). Retinoid target genes are transcribed in a step-wise process (6) which involves recruitment of histone acetyltransferase activity to open chromatin and methyltransferase activity to unmask promoter sequences. Retinoid receptors are found bound to DNA sequences in complexes containing histone deacetylases (HDAC). RAR responder element 1 (RARRES1), found to be downregulated in this study, is a putative tumour suppressor. It has been identified as a target of retinoic acid signalling and an effector of differentiation and apoptosis in in-vitro

leukemia models. RARRES1 has been found in high levels in prostatic and lung tissues (164). Examined in multiple cancer cell lines, decreased RARRES1 expression was correlated with promoter CpG motif hypermethylation. Expression was reestablished after treatment with the demethylating agent 5-aza-deoxycytidine (164), via induction of proteasomal degradation of the maintenance methyltransferase, DNMT1 (53). A study of normal gastric mucosa in patients over a wide age range demonstrated increased promoter methylation with advancing age of both LOX and RARRES1 (140). High levels of RARRES1 have been found in colonic adenomas; corresponding losses in RARRES1 expression have been noted in dedifferentiated and advanced stage colon cancers (160). RARRES1 regulatory sequences are methylated in many human cancer tissues including gastric, endometrial, head & neck, colorectal, squamous oesophageal and prostate cancer, as demonstrated by reduced mRNA levels. Reduced RARRES1 transcripts have been associated with advanced age in normal gastric mucosa. Decreased RARRES1 in lung tissue could be considered evidence of field cancerization.

SPARC negatively regulates angiogenesis and plays a role in regulation of myofibroblast activation, with overexpression changing the nature of tumour stroma to a non-permissive environment (27). SPARC expression has been found to be decreased in colonic, pancreatic, ovarian, endometrial and lung cancers (15,23,111,124,129,133,141,147,162) through methylation of promoter sequences. Reestablishment of normal methylation status reduced precancerous changes.

LOX has been found to be hypermethylated in lung cancers in 95% of tissues examined, compared to methylation levels of 20% in normal lung tissue (134). There are controversial reports implicating over and underexpression of LOX and LOX family members with either tumour suppression or metastasis (12,101,137).

Sulfatase 1 and 2, found to be downregulated in our gene list, modify heparan sulfated proteoglycans (HSPG) by removal of *O*-linked sulfate groups (105). Such modification of HSPG alter signal transduction, decreasing tumour proliferation (46). SULF1 was found to be downregulated in a series of cancer cell lines, with forced overexpression reducing tumorigenesis and invasiveness (82,83), presumably by inhibition of cellular proliferation and angiogenesis (107). The SULF1 promoter has been noted to be hypermethylated in serum samples of patients with breast and gastric cancers (25), while SULF2 regulatory sequences were hypermethylated in NSCLC (151).

Phospholipase A2 (PLA2GA), found to downregulated by SAM analysis but not validated, has been shown to be a target gene of the β-catenin/Tcf-Lef pathway and found to inhibit the invasiveness and metastasis of gastric cancer (49). Its promoter sequences have also been found to be hypermethylated in prostate and leukemia cell lines (96). Phospholipase A2 is thought to control cell growth, differentiation and apoptosis by release of bioactive lipid mediators.

An examination of tumour and matched normal lung tissue demonstrated significant methylation in a panel of genes (80% rate) versus an 8% rate in normal tissue (41). The patients in this study were smokers and the analysis was not stratified with regards to age.

Current tobacco use is considered to cause field cancerization (62), yet the methylation status of the normal tissues was minimal.

TRANSCRIPTS RELATED TO TISSUE REPAIR ARE DOWNREGULATED WITH AGE

Lung airways and alveoli are supported by a parenchyma composed of collagen, elastic fibres, proteoglycans with a cellular subpopulation of fibro- and myofibroblasts (146). Senescent lung fibroblasts in culture have been found to synthesize less collagen than younger cells (64), which is concordant with loss of elastic fibres and collagen cross-linking observed in aged lung tissues, see also Figure 18.

A significant downregulation of multiple collagen isoforms occurs with advancing age at the transcript and protein levels. Most of the isoforms identified are present in ECM. Collagen 18, downregulated but not validated in this study, has been identified as an inhibitor of angiogenesis by virtue of a C-terminal peptide, endostatin (92). Concomitant reductions in ECM-modifying enzymes such as sulfatases (SULF1, 2), peptidylprolyl isomerases (PPIC, PCOLCE), and lysyl oxidases (LOX, LOXL2) were also noted in the gene list. An inhibitor of matrix metalloproteinases, TIMP1 was also found to have reduced transcript levels. Lysyl oxidase (LOX) is a copper amine oxidase and the prototype member of a multigene family which includes LOXL2. These serve to mature collagen and elastin in the extracellular matrix by covalent cross-linking (115). SPARC was found to be downregulated in aged lung tissues. This protein has been identified as a collagen chaperone is a matricellular protein with diverse and controversial roles(17-19) and a collagen chaperone (93). SPARC null mice

demonstrate accelerated degenerative disc disease (56)and poorly-organized collagen matrices (16).

An examination of transcriptional alteration with age has been described in a subgroup analysis of cadaveric lung tissues (57) using Affymetrix microarray technology. The subgroup consisted of lung tissues from 13 donors (n=6, mean age 69 years; and n=7, mean age 29 years) whose smoking status was not provided. The authors identify 40 significantly altered transcripts (22 downregulated and 18 upregulated) between the groups. A comparison of the published gene list to data presented herein reveals 4 common transcripts, all upregulated collagen isoforms in the aged group. The changes observed are in contrast to our findings of a more global downregulation of both collagen isoforms and remodelling enzymes with advanced age. The study used lungs deemed not suitable for transplantation, and were thus perfused with cold organ perfusion solution. The use of this preservative has been associated with upregulation of cytokine transcripts in lung tissues (26), it is unclear if preservative solution would alter other classes of transcripts as well. As counterpoint, a microarray analysis of aged inbred aged mouse tissues did demonstrate downregulation of a large panel of collagen isoforms (103), consistent with the findings of our human study.

It is important to consider an alternative explanation for the experimental results noted: The young lung tissue samples are taken from injured lung tissues, and the transcriptional profile may represent exaggerated fibrosis, rather than age-related decreases in collagen

and synthetic enzyme transcripts. This may only be adequately addressed with an increased number of young patient samples being analyzed.

When using microarray analysis technique, it has been noted that discordant gene lists are found for similar cancer types or tissue types. A recent study of breast-cancer microarray profiles (38) demonstrated association of several independently determined gene lists and survival data, yet when the individual lists were compared, very few transcripts were in fact concordant. It is perhaps more appropriate to consider a microarray profile as specific to a certain condition, and that a collection of gene profiles become specific to an overall behaviour or overall prognosis – that is, the individual transcript identities may vary as tissue conditions are subtly altered, yet the global pattern retains predictive power.

In an attempt to integrate both transcriptional data from mouse tissues and human tissues, we propose a model of age-related field cancerization (Figure 19). The intent is to begin to explain the progression from normal lung tissue, though precancerous lesions (atypical andeomatous hyperplasia, AAH) and carcinoma-in-situ (bronchoalveolar carcinoma, BAC) to invasive cancer. Age increases from left to right and frames the circumstances under which the genetic alterations reported in this thesis could form a field defect.

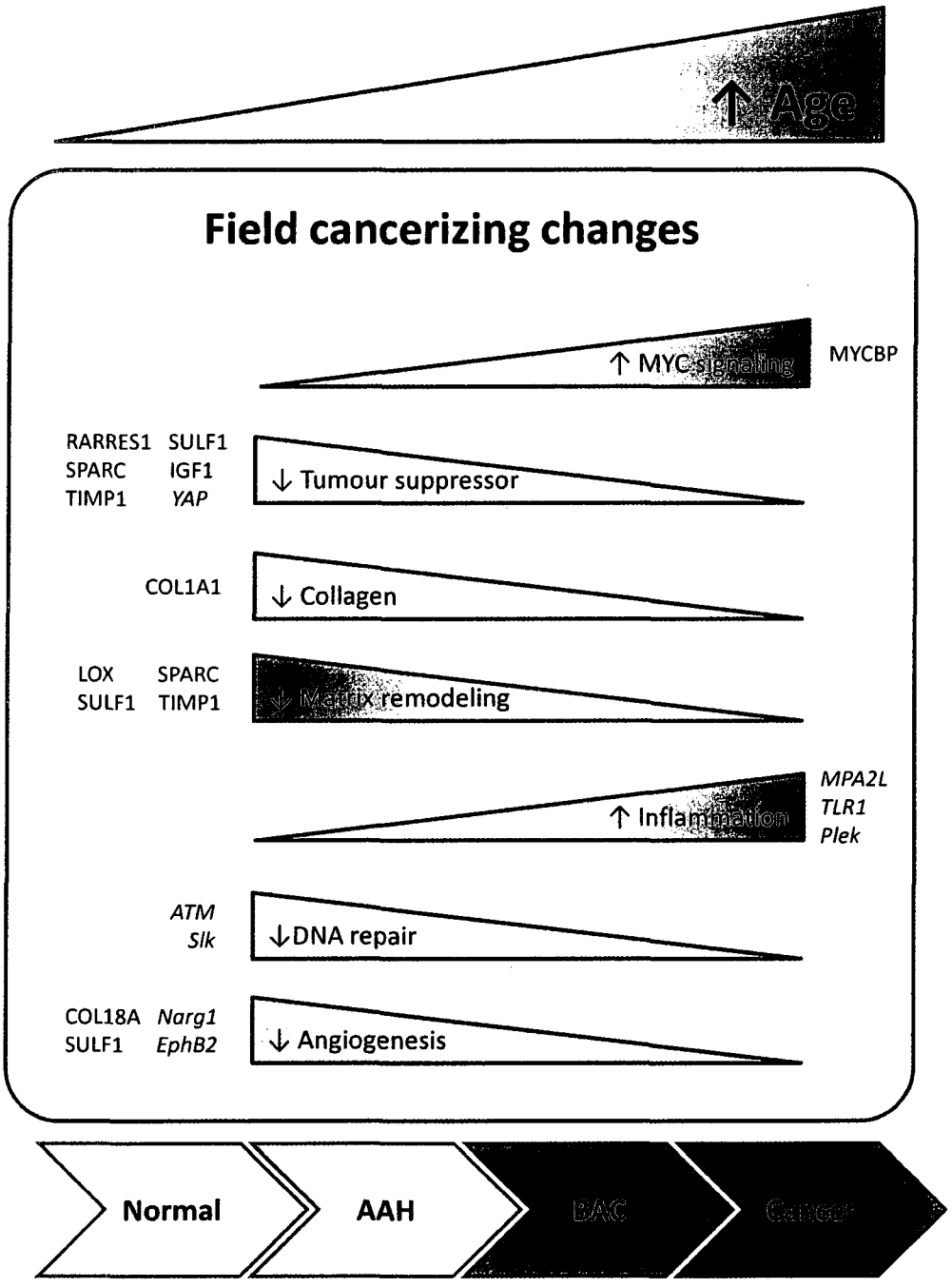
↑ Age
Field cancerizing changes
↑ MYC signaling
MYCBP
RARRES1 SULF1
SPARC IGF1
TIMP1 YAP
↓ Tumour suppressor
COL1A1
↓ Collagen
LOX SPARC
SULF1 TIMP1
↓ Matrix remodeling
↑ Inflammation
MPA2L
TLR1
Plek
ATM
Slk
↓DNA repair
COL18A Narg1
SULF1 EphB2
↓ Angiogenesis
Normal
AAH
BAC
Cancer

Figure 19: Proposed integrated model of field cancerization in normal lung tissue related to advancing age.

The model integrates the transcriptional data from mouse and human studies presented herein. The bottom sequence in the figure shows the stepwise progression from normal lung tissues, through the preneoplastic lesion atypical adenomatous hyperplasia (AAH) and the carcinoma-in-situ lesion bronchoalveolar carcinoma (BAC) to culminate in invasive adenocarcinoma. The uppermost sequence shows advancing age. Within the mid-figure box are outlined relevant changes identified in our study that support field cancerization. Shaded gradients demonstrate the increase or decrease in transcript function with advancing age. Data from mouse microarray studies are listed in *ITALICS*, while data from human microarray studies are in normal block type. ***ATM,*** *ataxia-telangiectasia mutated homolog;* **COL**, collagen; ***EphB2,*** *ephrin B2*; **IGF**, insulin-like growth factor; **LOX**, lysyl-oxidase; ***MPA2L,*** *macrophage activation 2 like*; **MYCBP**, MYC binding protein; ***Narg1,*** *NMDA receptor-regulated gene 1*; ***Plek,*** *plekstrin*; **RARRES1**, Retinoic acid receptor response element 1; **SPARC**, secreted protein, acidic rich in cysteine; ***Slk,*** *Ste20-like kinase*; **SULF1**, sulfatase 1; **TIMP1**, tissue inhibitor of metalloproteinase 1; ***YAP,*** *Yes-associated protein*.

CONCLUSIONS

We have demonstrated that aged lung tissue differs significantly from younger tissues. The transcriptional profiles are unique, and are concordant with observations of tissue aging in other organs.

Significant lung alterations occur with increased age: Together, these would suggest that an unfavourable environment is present in aged mouse lungs, which modulates the pattern and spread of metastatic disease. Metastases colonize more quickly and form more foci in older mice. Histologically, older lungs show more diffuse and confluent tumour deposits. Survival is decreased as compared to younger mice with identical disease, and is most likely related to reduced physiologic reserve. A selection/survival bias likely exists, as evidenced by the equivalence of angiogenic, immune and progenitor cells populations in the lung. At a transcriptional level, patterns consistent with immune cell activation and recruitment within the lung tissues are seen. Negative regulators of angiogenesis are upregulated at the mRNA level, and evidence of activation of certain DNA repair pathways was observed. We feel the evidence presented herein suggests that age-related changes exist in mouse lung tissues, and that these alterations have a functional impact on the spread of metastases in an experimental model.

The transcriptional alterations noted in normal human lung tissue suggest that a field defect exists in aged lung. It is striking that many of the downregulated transcripts found in our study have been identified as tumour suppressors in other organ types and been found in other cancers. The predominance of collagen isoforms in our gene list and the validation of

decreased collagen in older tissues is striking. Many modulators of tissue repair, namely LOX and SPARC have been doubly implicated in epigenetically controlled tumorigenesis.

MYCBP was found in our study to be transcriptionally upregulated with advanced age and localized to the nucleus in tumour tissues. The exact mechanisms whereby MYCBP contributes to the field defect are as yet unclear, but are very suggestive of cellular proliferation being implicated.

The field defect we identify most may represent a 'chronic wound' environment in the aged lung with the attendant risk to cancerous changes. Inflammation was also observed in mouse lung tissue in this study.

Thus, changes observed in aging lung tissues do indeed fulfill the criteria for field cancerization, and most likely being to explain the age-related risks of NSCLC.

FUTURE DIRECTIONS

Further work is required to fully assess the molecular alteration occurring in lung tissue with advancing age, especially with regards to the development of lung neoplasms. Areas of further work are outlined below.

ONGOING PATIENT RECRUITMENT

The results presented and discussed herein will need further validation. Patient accrual will continue through the currently approved protocol. At a minimum, one additional young patient is needed to allow for three biologic replicates in each age cohort. Based on the results of the SAM algorithm, it would seem prudent to recruit as many patients as possible into the study so as to minimize the transcriptional variability, as evidenced by the high estimated false discovery rate. At the current rate of accrual, we will require several more years before the current study numbers could be doubled.

TRANSCRIPTIONAL PROFILE OF TUMOUR TISSUES

Once formal results are available from the pilot study, extending the transcriptional profiling to tumour tissue will allow for a testing of the assertion that the aging lung harbours a field defect. The comparison will encompass old normal lung compared to tumour tissue. The Affymetrix HG U133 2.0+ platform will be used to ensure appropriate comparisons can be made.

EXPLORING THE ROLE OF ALTERNATE MYC AND MYCBP SIGNALING IN AGING LUNG TISSUE

An important binding partner of MYC has been identified as being upregulated in aging lung tissues. There has been no association with cellular proliferation , as measured by Ki-67. The levels of MYC present in lung tissue samples, although not found to differ in histochemical analyses, will need to be assessed using more sensitive techniques. Correlation with cell-cycle markers will also be required in order to explain and further elucidate the relationship between MYCBP and MYC noted in our study. Alternate pathways, including the Tcf/Lef pathway may need to be scrutinized in light of binding sites in the promoter region of the MYCBP gene. An examination of MYC knock-out mice and the creation of a MYCBP knock-out line would be valuable in further characterizing MYC signalling in aging lung tissues.

ASSESSING METHYLATION STATUS OF ALTERED TRANSCRIPTS

The preponderance of downregulated transcripts that have been implicated as tumour suppressor genes in other tissues suggests that an examination of the methylation status of the gene in lung tissues is required. This would further confirm the transcriptional findings presented herein and support the assertion that field cancerization plays a role in the aging lung. It will be important to examine tumour tissues at the same time in order to document the spectrum of tumour suppressor gene silencing in lung tumours in a non-smoking cohort, as this has not yet been described in the literature.

DETERMINING THE ROLE OF BASCS IN LUNG AGING AND CANCER

The capacity of an organ system to regenerate in the face of injury is highly variable and specific to the tissue type. In organs with high cellular turnover such as the hematopoietic system, the integument and the gastrointestinal tract, regenerative potential is high and related to significant cellular contribution from stem cells. In organ systems with low cellular turnover such as neural tissue and lung, the regenerative potential is low, as is the contribution of stem cells (119). Lung-resident stem cells (referred to as bronchoalveolar stem cells – BASC) repopulate alveolar and bronchiolar epithelia from their location at the bronchoalveolar junction (BAJ). BASC are characterized by the expression of both surfactant protein C, a type II pneumocyte (AT2) marker, and CC-10, a Clara-cell marker. In injury models using either bleomycin to deplete AT2 cells or naphthalene to deplete Clara cells, BASC were found to proliferate at the BAJ. These lung progenitor cells were initially identified with the surface marker profile Sca-1+CD31-CD45- (76). Subsequent identification of fetal cells with the Sca-1+CD34+Oct-4+SSEA-1+CK7+ profile also found co-expression of SpC and CC-10; this subpopulation was found to be susceptible to SARS coronavirus infection, suggesting that the devastating severity of SARS pneumonitis might be related to impaired epithelial repair mechanisms(24,88). Expansion of the BASC population by KRAS expression alone or in combination with naphthalene injury, led to increased numbers of adenomas and areas of hyperplasia in the BAJ region (76). No reports studying Sca-1+CD31-CD45- BASC populations in young and extremely old mice have been reported to date, and it is unknown if the tissue repair mediated by these lung progenitor cells varies with advancing age. The capacity of lung tissue to repair after injury has been

attributed to Sca-1+CD31-CD45- cells. The proportion of lung progenitor cells in extremely old mice does not show a significant decrease compared to younger mice.

We propose the use of bleomycin in a mouse lung-injury model. This animal model will be used to explore the use of lung-derived progenitor cells to limit/reverse lung injury.

The capacity of an organ system to regenerate in the face of injury is highly variable and specific to the tissue type. In organs with high cellular turnover such as the hematopoietic system, the integument and the gastrointestinal tract, regenerative potential is high and related to significant cellular contribution from stem cells. In organ systems with low cellular turnover such as neural tissue and lung, the regenerative potential is low, as is the contribution of stem cells. (119)

This may explain, in part, the devastating clinical manifestations of acute lung injury. Acute respiratory distress syndrome (ARDS) is a clinical syndrome of acute and persistent lung inflammation. Most patients meeting the criteria for ARDS are quite ill and require mechanical ventilation. The clinical course develops over a period of 4-48 hours and persists for days to weeks. Diffuse alveolar damage and resultant fibrosis are major pathologic features of ARDS. The age-adjusted incidence is 64/100 000, with a significant mortality rate of 41% (126). Several etiologies have been implicated in the pathogenesis of ARDS, including systemic infection (sepsis), pneumonia, aspiration of gastric contents, acute pancreatitis and more than 60 others (61). The final common pathway involves inflammatory mediators, excess recruitment and activation of neutrophils and macrophages, followed by excessive lung damage (136,148). A related syndrome,

idiopathic pulmonary fibrosis, has been attributed to aberrant healing rather than sustained injury (55). Available therapies to date are limited and supportive in nature – there have been no treatments consistently able to reverse or mitigate the process of lung injury.

Acute lung inflammation caused by bleomycin is a long-standing and widely accepted model of pulmonary injury and fibrosis (5,139,144). In mice, high-dose intratracheal or intranasal injection of bleomycin at a dose of 7.5 mg/kg body weight produces a predictable injury: Focal areas of cellular influx in the alveoli occur within 24h, followed by progressive alveolar septal thickening and lymphocytic and neutrophilic infiltrates which peak at 7 days. Resolution of inflammation and fibrotic repair occur within 14 days.

The treatment of injury in an organ system with low cellular turnover, such as the lung, can encompass recruitment of multipotent stem cells derived from bone marrow; or can attempt to expand the population of organ-resident progenitor cells.

Firstly, bone marrow-derived (BMD) cells have been studied as a potential source of progenitor cells for lung repair, and several subpopulations have been identified: Cells depleted of CD16 and CD32 mitigate bleomycin-induced injury in C56BL/6 mice (110), while cytokeratin+CD45- subpopulations have been observed to engraft as type I pneumocytes (78). Side population (SP) cells, based on Hoechst dye efflux properties, were found to engraft in several organs outside of the marrow space – those identified in lung expressed lung progenitor-specific surfactant protein B mRNA (79). Another bone marrow subpopulation expressing SSEA1 has also demonstrated lung engraftment (2). There is a suggestion that the great diversity seen in stem cell surface markers is a result of cell-cycle

specific marker expression; differentially labelled subpopulations may in fact be identical (118). At present, there are no consistent reports of a particular cell population successfully mitigating lung injury. There is also considerable controversy regarding engraftment of BMD cells in the lung as type 2 alveolar (AT2) progenitor cells: SP cells injected at doses of 200 cells/mouse failed to engraft when assayed using a sensitive FACS-based strategy to detection of donor cells.

Human studies have demonstrated that circulating CD34+AC133+ cells were reduced in patients with severe lung disease (37), and that high circulating levels of colony-forming progenitor cells conferred survival benefits in cases of ALI (20).

Secondly, lung-resident stem cells (referred to as bronchoalveolar stem cells – BASC) are characterized by their ability to repopulate alveolar and bronchiolar epithelia from their location at the bronchoalveolar junction (BAJ). Identified by Kim et al. (76), expression of both surfactant protein C, an AT2 marker, and CC-10, a Clara-cell marker, is co localized. In injury models using either bleomycin to deplete AT2 cells or naphthalene to deplete Clara cells, BASC were found to proliferate at the BAJ; migration was not noted, however. The surface marker profile Sca-1+CD34+CD31-CD45- was used to characterize the BASC fraction in FACS analyses. A recent study also determined that Sca-1+CD34+Oct-4+SSEA-1+CK7+ACE-2+ cells in pulmonary tissue expressed both SpC and CC-10 . Interestingly, this group found that the SARS coronavirus targeted and killed this subpopulation of cells, indicating that the devastating severity of SARS pneumonitis might be related to severely

impaired epithelial repair mechanisms. No reports of Sca-1+CD34+ BASC cells being used to treat acute lung injury have been noted to date.

We will determine what role Sca-1+CD34+ BASC cells play in mitigating severe lung injury by applying a 3-log dose range, with the lowest dose (100 cells) based on published data in studies using SP cells (77,88). Based on the known kinetics of bleomycin (28,150) injury, a single intravenous injection of purified GFP+ BASC administered 24 hours after injury might be expected to mitigate inflammation and reduce the degree of lung fibrosis. The proportion of all lung cells which exhibit Sca-1+CD31-CD45- marking has been reported as 0.4%, with 2-16% of these also staining for CD34+. In our hands, we find that 0.3% of all lung cells stain for Sca-1 and CD34, yielding approximately 2000 stem cells per donor mouse. To produce enough purified stem cells for the dose ranging study, we anticipate 40 GFP+ FVB/N mice will be required.

We will examine lung tissue at predefined time points: At 72h, early inflammation is expected. At 7 days, the peak inflammation will be seen, while resolution and fibrosis will be evident at 14 days. At each time point, mice will be anaesthetized and lungs will be harvested to determine (i) the degree of lung injury and (ii) the degree of BASC migration and proliferation. Standard trichrome histochemical staining will highlight collagen deposition, immunofluorescence for GFP, CC-10 and SpC will allow for identification and localization of adoptively transferred BASC. Flow cytometry will accurately quantify the number of GFP cells present in the injured lung. Whichever dose minimizes lung injury will be selected for further study.

The second proposed study has 4 arms. Mice are initially treated with either bleomycin or phosphate-buffered saline. Each cohort is then treated with either a stem cell suspension at a dose determined during the pilot study, or phosphate-buffered saline. We feel that this study design provides the required treatment and control groups to accurately assess the true contribution of BASC to lung repair after bleomycin injury. Sampling is expanded to include replicates, and analysis will proceed using the same methods outlined for the pilot study.

TABLES

Table 1: Relevant literature reports of the effect of mouse age on metastatic spread of intravenously-administered cell suspensions.

Study	Age (mo)	Strain	Sex	Cell line(s) used in study	Distribution of lung metastases compared to young mice	Other comments
Shimuzu et al.(2008) (135)	2, 8	SAMP10	NS	K1735M2 melanoma	Greater number in aged mice at 21d	
Kanno et al. (1997) (73)	3-4, 18-21	C57BL/6	F	B16 F10 melanoma	Smaller number in aged mice at 21d	Also examined effect of restraint stress
Hirayama et al. (1993) (65)	1.5, 22	C57BL/6	F	B16 F10 melanoma	Smaller number in aged mice at 21d	Also examined effect of parabiosis
Gabrilovac et al. (1990) (48)	1.5, 6, 30	CBA, C57BL/6	F	B16 melanoma; mammary carcinoma	Greater number in aged mice at 22d	
Baumgart and Zippel (1991) (7)	3, 12, 18	C57BL/6	F	B16 melanoma	Greater number, smaller size in aged mice at 21d	Also examined effect of immunosuppression.
Miller et al. (1991) (98)	4, 18	C57BL	F	4T07 mammary carcinoma	Slower tumour growth in aged mice up to 8 days post injection	Injected cells suspended in culture medium with bovine serum
Thompson (1976) (152)	4, 18	C3H	both	Erlich ascites (ELD); mammary carcinoma	Greater number in aged males at 14d (for ELD) and 42d (mammary carcinoma)	Injected cells suspended in culture medium with bovine serum

NS-not specified, Results selected from published studies spanning 1976-present. If more than one treatment or outcome was studied, results relating to age are reported.

Table 2: Differentially expressed transcripts, upregulated in unperfused, aged mouse lung tissues, grouped by over-represented GO terms.

GO identifier	GO term	Gene names	Number in submitted gene list	Number in genome database	p value
GO:0002376	immune system process	SYK; THY1; LCK; IL7R; TLR1; CD79A; IRF4; MR1; HCLS1; CCL5; IGJ; MS4A1; IL16; CCL8; PTPRC; CD8B1; DOCK2; TWSG1; PODXL; IGL-V1	20	757	1.22E-10
GO:0006955	immune response	SYK; THY1; LCK; TLR1; CCL8; CD79A; IRF4; PTPRC; CD8B1; MR1; CCL5; IGJ; IGL-V1	13	505	3.00E-06
GO:0045321	leukocyte activation	SYK; THY1; LCK; TLR1; IRF4; PTPRC; CD8B1; DOCK2; MS4A1	9	199	4.53E-06
GO:0050851	antigen receptor-mediated signalling pathway	SYK; THY1; LCK; CD79A; PTPRC	5	28	5.32E-06
GO:0001775	cell activation	SYK; THY1; LCK; TLR1; IRF4; PTPRC; CD8B1; DOCK2; MS4A1	9	215	5.32E-06
GO:0002429	immune response-activating cell surface receptor signalling pathway	SYK; THY1; LCK; CD79A; PTPRC	5	32	6.96E-06
GO:0002768	immune response-regulating cell surface receptor signalling pathway	SYK; THY1; LCK; CD79A; PTPRC	5	34	6.96E-06
GO:0002757	immune response-activating signal transduction	SYK; THY1; LCK; CD79A; PTPRC	5	34	6.96E-06
GO:0042110	T cell activation	SYK; CD8B1; THY1; LCK; DOCK2; IRF4; PTPRC	7	118	6.96E-06
GO:0002764	immune response-regulating signal transduction	SYK; THY1; LCK; CD79A; PTPRC	5	36	6.96E-06
GO:0046649	lymphocyte activation	SYK; THY1; LCK; IRF4; PTPRC; CD8B1; DOCK2; MS4A1	8	182	6.96E-06
GO:0048534	hemopoietic or lymphoid organ development	SYK; LCK; HCLS1; DOCK2; IL7R; TWSG1; IRF4; PTPRC	8	230	3.57E-05
GO:0030217	T cell differentiation	SYK; LCK; DOCK2; IRF4; PTPRC	5	56	4.43E-05

GO:0050853	B cell receptor signalling pathway	SYK; CD79A; PTPRC	3	7	4.52E-05
GO:0002520	immune system development	SYK; LCK; HCLS1; DOCK2; IL7R; TWSG1; IRF4; PTPRC	8	245	4.52E-05
GO:0002274	myeloid leukocyte activation	SYK; THY1; TLR1; IRF4	4	29	7.56E-05
GO:0030097	hemopoiesis	SYK; LCK; DOCK2; HCLS1; TWSG1; IRF4; PTPRC	7	206	0.000142

Table 3: Differentially expressed transcripts related to angiogenesis (GO:0001525) in perfused mouse lung tissues.

Probe	Fold Change	Symbol	Name
1418022_at	10.631	Narg1	NMDA receptor-regulated gene 1
1418024_at	9.009	Narg1	NMDA receptor-regulated gene 1
1416942_at	2.972	Arts1	type 1 tumour necrosis factor receptor shedding aminopeptidase regulator
1452649_at	1.619	Rtn4	reticulon 4

Fold changes greater than 0.5 represent upregulated transcripts.

Table 4: Differentially expressed transcripts related to the immune response (GO:0006955) in perfused mouse lung tissues.

Probe	Fold Change	Symbol	Name
1418776_at	15.619	5830443L24Rik	RIKEN cDNA 5830443L24 gene
1447927_at	13.609	Mpa2l	macrophage activation 2 like
1427098_at	9.704	Wwp1	WW domain containing E3 ubiquitin protein ligase 1
1418762_at	4.823	Daf1	decay accelerating factor 1
1452231_x_at	4.761	LOC545386	similar to Interferon-activatable protein 205 (IFI-205) (D3 protein)
1429707_at	4.504	Plaa	phospholipase A2, activating protein
1417493_at	4.411	Pcgf4	polycomb group ring finger 4
1420549_at	4.256	Gbp1	guanylate nucleotide binding protein 1
1450915_at	4.190	Ap3b1	adaptor-related protein complex 3, beta 1 subunit
1429399_at	3.476	Rnf125	ring finger protein 125
1426906_at	3.383	LOC545386	similar to Interferon-activatable protein 205 (IFI-205) (D3 protein)
1438999_a_at	2.951	Nfat5	nuclear factor of activated T-cells 5
1449049_at	2.909	Tlr1	toll-like receptor 1
1417540_at	2.810	Elf1	E74-like factor 1
1448736_a_at	2.625	Hprt1	hypoxanthine guanine phosphoribosyl transferase 1
1435001_at	2.174	Plaa	phospholipase A2, activating protein
1451086_s_at	1.719	Rac1	RAS-related C3 botulinum substrate 1
1435890_at	1.714	5730596K20Rik	RIKEN cDNA 5730596K20 gene
1451931_x_at	1.704	H2-D1	histocompatibility 2, D region locus 1
1427651_x_at	1.639	H2-D1	histocompatibility 2, D region locus 1
1451784_x_at	1.614	H2-D1	histocompatibility 2, D region locus 1
1425545_x_at	1.575	H2-D1	histocompatibility 2, D region locus 1
1459151_x_at	0.635	Ifi35	interferon-induced protein 35
1460737_at	0.563	Igbp1	immunoglobulin (CD79A) binding protein 1

Fold changes greater than 0.5 represent upregulated transcripts.

Table 5: Differentially expressed transcripts related to DNA repair (GO:0006281) in perfused mouse lung tissues.

Probe	Fold Change	Symbol	Name
1449336_a_at	8.645	Slk	STE20-like kinase (yeast)
1417831_at	2.738	Smc1l1	SMC (structural maintenance of chromosomes 1)-like 1 (S. cerevisiae)
1438289_a_at	2.726	Sumo1	SMT3 suppressor of mif two 3 homolog 1 (yeast)
1416161_at	2.601	Rad21	RAD21 homolog (S. pombe)
1417609_at	2.503	Ube2a	ubiquitin-conjugating enzyme E2A, RAD6 homolog (S. cerevisiae)
1421205_at	2.471	Atm	ataxia telangiectasia mutated homolog (human)
1433999_at	2.279	Slk	STE20-like kinase (yeast)
1455935_at	0.736	2410131K14Rik	RIKEN cDNA 2410131K14 gene
1424105_a_at	0.486	Pttg1	pituitary tumour-transforming 1
1416378_at	0.483	Pnkp	polynucleotide kinase 3'- phosphatase
1417093_a_at	0.483	Gtf2h4	general transcription factor II H, polypeptide 4
1419433_at	0.472	Nthl1	nth (endonuclease III)-like 1 (E.coli)
1436886_x_at	0.388	Xab2	XPA binding protein 2
1450921_at	0.383	Aptx	aprataxin

Fold changes greater than 0.5 represent upregulated transcripts.

Table 6: Primer sequences for mouse microarray transcript validation.

Primer name	NCBI accession	Primer sequence (5'-3')	
		Forward	Reverse
β-Actin (ACTB)	NM_007393	GCTACAGCTTCACCACCACA	AAGGAAGGCTGGAAAAGAGC
macrophage activation 2 like (Mpa2l)	NM_194336	TGGAGCAGCTGCATTATGTC	GCATTCTGGGTTTGTCACCT
Toll-like receptor 1 (TLR1)	NM_030682	GGACCTACCCTTGCAAACAA	GGTGGCACAAGATCACCTTT
NMDA receptor regulated gene 1 (Narg1)	NM_053089	CGAGGCTGATACAGCAAACA	TCCGTTGCTGCTTTTCTTTT
Ataxia telangiectasia mutated homolog (ATM)	NM_007499	TTACGATGGCAACAGCAGAG	TCCAGTTCTCGCTGAACCTT
Ste20-like kinase (SLK)	NM_009289	TTCTCAGGCGTCAGGAACTT	TCGTCTCTCAGGCGGTTAGT
Plekstrin (Plek)	NM_019549	ACTTTGCAAACGGATGTTC	TTCTTGCAAACTTCTGGCCT
Yes-associated protein (YAP)	NM_009534	ATCCACGAGGTCAGGTTGAG	CCAAACTACCCCACACTTGCT

Table 7: Inclusion and exclusion criteria for patient selection and enrolment into the human lung aging study.

Inclusion Criteria		Exclusion Criteria
Young Patients	**Aged patients**	**All patients**
• 30 years of age or less • Able to provide consent • Non smoker • Spontaneous pneumothorax fulfilling criteria for surgical intervention • Undergoing either open or thoracoscopic apical bullectomy and pleurectomy	• 65 years of age or more • No significant comorbidities • Non smoker for 10 continuous preceding years • Stage I, II, III or IV NSCLC • Undergoing elective pulmonary resection	• Evidence of intrinsic pulmonary disease such as severe asthma requiring oral steroid use, cystic fibrosis, idiopathic pulmonary fibrosis • Current or past smoker within 10 years • Any autoimmune disorder such as Systemic Lupus Erythematosus, Wegner's Granulomatosis or Goodpasture's Disease • Past history of exposure to pulmonary toxins such as bleomycin, asbestos, silica • Any past history of thoracic irradiation • Any active pulmonary infection • Any immunocompromise • Any familial cancer syndrome

NSCLC, non-small cell lung cancer. All patients recruited to date are of male gender.

Table 8: Demographics of human lung aging study population.

	Patient cohort	
	Aged	**Young**
Number (n)	3	2
Median age (range)	63 (60-71)	22.5 (19-26)
Lung cancer (n)	3	0
Histologic subtype (n)	Squamous cell (1) Adenocarcinoma (2)	n/a
Stage (n)	I (2) IIIa (1)	n/a
Smoking exposure, pack-years (range)	22 (0-40)	0
Years non-smoking (range)	22 (14-24)	22.5 (19-26)

N/A, not applicable; Pack-year, daily cigarette consumption (in packs of 20 cigarettes) multiplied by total years exposure. All patients analyzed are of male gender.

Table 9: List of significantly altered transcripts in aging human lung tissue.

Fold change	Gene Symbol	Gene Title	q.value	Probeset
1.182	MYCBP	MYC binding protein	0.174	203359_s_at
0.953	HIF3A	Hypoxia inducible factor 3, alpha subunit	0.304	232669_at
0.949	TTLL5	tubulin tyrosine ligase-like family, member 5	0.302	210539_at
0.949	SUHW3	suppressor of hairy wing homolog 3 (Drosophila)	0.344	235520_at
0.943	RAN	RAN, member RAS oncogene family	0.308	200750_s_at
0.940	40787	Septin 11	0.308	216147_at
0.938	RPL3	ribosomal protein L3	0.342	212039_x_at
0.938	LACTB	lactamase, beta	0.342	1552486_s_at
0.926	GINS1	GINS complex subunit 1 (Psf1 homolog)	0.233	206102_at
0.918	MIB2	Mindbomb homolog 2 (Drosophila)	0.373	241541_at
0.915	BOLA2 BOLA2B	bolA-like 2 (E. coli) bolA-like 2B (E. coli)	0.281	209836_x_at
0.909	MMP11	matrix metallopeptidase 11 (stromelysin 3)	0.342	203876_s_at
0.908	ALOX5	Arachidonate 5-lipoxygenase	0.178	232607_at
0.898	OGT	O-linked N-acetylglucosamine (GlcNAc) transferase	0.358	212307_s_at
0.895	TIAL1	TIA1 cytotoxic granule-associated RNA binding protein-like 1	0.342	202405_at
0.890	RPL17	ribosomal protein L17	0.233	214291_at
0.879	CLDN15	claudin 15	0.358	219640_at
0.870	BOLA1	bolA-like 1 (E. coli)	0.368	219345_at
0.864	SPARC	secreted protein, acidic, cysteine-rich (osteonectin)	0.377	200665_s_at
0.864	PLK2	polo-like kinase 2 (Drosophila)	0.358	201939_at
0.861	IKBKB	inhibitor of kappa light polypeptide gene enhancer in B-cells, kinase beta	0.339	209342_s_at
0.857	CAV2	caveolin 2	0.304	213426_s_at
0.844	MCM2	MCM2 minichromosome maintenance deficient 2, mitotin (S. cerevisiae)	0.362	202107_s_at
0.844	GGTLA1	gamma-glutamyltransferase-like activity 1	0.308	205582_s_at
0.842	PPIC	peptidylprolyl isomerase C (cyclophilin C)	0.179	204518_s_at
0.833	RAP2B	RAP2B, member of RAS oncogene family	0.174	227897_at
0.831	NENF	Neuron derived neurotrophic factor	0.339	214072_x_at
0.831	PDE1A	phosphodiesterase 1A, calmodulin-dependent	0.179	208396_s_at
0.831	PRSS23	protease, serine, 23	0.221	202458_at
0.827	TPM4	tropomyosin 4	0.358	212481_s_at
0.820	STMN3	stathmin-like 3	0.228	222557_at
0.816	HOXC6	homeobox C6	0.342	206858_s_at
0.813	COL6A1	collagen, type VI, alpha 1	0.380	213428_s_at
0.810	COL6A3	collagen, type VI, alpha 3	0.129	201438_at
0.802	COL1A2	collagen, type I, alpha 2	0.246	202403_s_at
0.802	ANGPT2	angiopoietin 2	0.315	205572_at

Fold change	Gene Symbol	Gene Title	q.value	Probeset
0.791	TIMP1	TIMP metallopeptidase inhibitor 1	0.372	201666_at
0.785	COL18A1	collagen, type XVIII, alpha 1	0.362	209082_s_at
0.772	PI15	peptidase inhibitor 15	0.375	229947_at
0.771	KRT5	keratin 5	0.344	201820_at
0.763	CFH CFHR1	complement factor H complement factor H-related 1	0.179	215388_s_at
0.755	CFI	complement factor I	0.358	203854_at
0.750	PCOLCE	procollagen C-endopeptidase enhancer	0.304	202465_at
0.731	SULF2	sulfatase 2	0.342	233555_s_at
0.731	TPBG	trophoblast glycoprotein	0.339	203476_at
0.725	PTGFRN	prostaglandin F2 receptor negative regulator	0.310	224937_at
0.712	FAM38B	family with sequence similarity 38, member B	0.362	219602_s_at
0.694	COL5A1	collagen, type V, alpha 1	0.260	203325_s_at
0.692	LOXL2	lysyl oxidase-like 2	0.342	202998_s_at
0.690	FMO1	flavin containing monooxygenase 1	0.096	205666_at
0.673	FLRT2	fibronectin leucine rich transmembrane protein 2	0.246	204359_at
0.673	COL1A1	collagen, type I, alpha 1	0.342	1556499_s_at
0.667	WT1	Wilms tumour 1	0.304	206067_s_at
0.647	COL3A1	collagen, type III, alpha 1 (EDS type IV, AD)	0.174	215076_s_at
0.646	COL5A2	collagen, type V, alpha 2	0.214	221729_at
0.644	GAS1	growth arrest-specific 1	0.308	204457_s_at
0.638	NID2	nidogen 2 (osteonidogen)	0.344	204114_at
0.637	COL5A1	collagen, type V, alpha 1	0.267	212488_at
0.636	COL1A2	collagen, type I, alpha 2	0.304	202404_s_at
0.627	CFI	complement factor I	0.178	1555564_a_at
0.614	COL5A1	collagen, type V, alpha 1	0.344	212489_at
0.607	C1S	complement component 1, s subcomponent	0.233	1555229_a_at
0.604	COL3A1	collagen, type III, alpha 1 (EDS type IV, AD)	0.175	201852_x_at
0.586	COL3A1	collagen, type III, alpha 1 (EDS type IV, AD)	0.304	211161_s_at
0.585	TFPI2	tissue factor pathway inhibitor 2	0.179	209278_s_at
0.579	THBS2	thrombospondin 2	0.304	203083_at
0.573	COL1A1	collagen, type I, alpha 1	0.179	202310_s_at
0.569	SULF1	sulfatase 1	0.174	212344_at
0.567	COL5A2	collagen, type V, alpha 2	0.174	221730_at
0.561	LOX	lysyl oxidase	0.250	215446_s_at
0.550	RARRES1	retinoic acid receptor responder (tazarotene induced) 1	0.179	206392_s_at
0.523	IGF1	insulin-like growth factor 1 (somatomedin C)	0.362	209541_at
0.501	ALDH1A2	aldehyde dehydrogenase 1 family, member A2	0.169	207016_s_at
0.486	PRG4	proteoglycan 4	0.174	206007_at
0.477	PLA2G2A	phospholipase A2, group IIA (platelets, synovial fluid)	0.129	203649_s_at

EDS, Ehlers-Danlos syndrome; AD, autosomal dominant; shaded entries were seleceted for validation.

Table 10: Primer sequences for human transcript validation by quantitative PCR.

Primer name	NCBI accession	Primer sequence (5'-3')	
		Forward	Reverse
β-Actin (ACTB)	NM_001101	GATGAGATTGGCATGGCTTT	CACCTTCACCGTTCCAGTTT
Collagen 1A1 (COL1A1)	NM_000088	GTGCTAAAGGTGCCAATGGT	ACCAGGTTCACCGCTGTTAC
Insulin-like growth factor 1 (IGF1)	NM_000618	TGGATGCTCTTCAGTTCGTG	CCTGCACTCCCTCTACTTGC
Lysyl oxidase (LOX)	NM_002317	CCCCAAAGAGTGAAAAACCA	CCAGGACTCAATCCCTGTGT
MYC-binding protein (MYCBP)	NM_012333	AGCTGCTTCGCCTAGAACTG	CCTATTCAGCACGCTTCTCC
Retinoic acid receptor response element 1 (RARRES1)	NM_206963	GAGCGCTACAACCCAGAGTC	GAAAGCCAAATCCCAGATGA
Secreted protein, acidic, rich in cysteine (SPARC)	NM_003118	GTGCAGAGGAAACCGAAGAG	TCATTGCTGCACACCTTCTC
Sulfatase 1 (SULF1)	NM_015170	AAGTGACGGGTTCTTGGTTG	GGCAAGGTCAAATGAGGTGT
Tissue factor pathway inhibitor 2 (TFPI2)	NM_006528	CGCACCAAAGAAAATTCCAT	ATTGTCATTCCCTCCACAGC
Tissue inhibitor of metalloproteinase 1 (TIMP1)	NM_003254	AATTCCGACCTCGTCATCAG	TGCAGTTTTCCAGCAATGAG

Table 11: Chromosomal locations of validated human transcripts.

Transcript	NCBI accession	Chromosome
Collagen 1A1 (COL1A1)	NM_000088	17q21
Insulin-like growth factor 1 (IGF1)	NM_000618	12q22
Lysyl oxidase (LOX)	NM_002317	5q23
MYC-binding protein (MYCBP)	NM_012333	1p33
Retinoic acid receptor response element 1 (RARRES1)	NM_206963	3q25
Secreted protein, acidic, rich in cysteine (SPARC)	NM_003118	5q31
Sulfatase 1 (SULF1)	NM_015170	8q13
Tissue factor pathway inhibitor 2 (TFPI2)	NM_006528	7q22
Tissue inhibitor of metalloproteinase 1 (TIMP1)	NM_003254	Xp11

Table 12: Summary of validation studies for significant alterations in lung tissue observed with advancing age in both mouse and human models.

Transcript	Microarray	Mouse study PCR	Western blot	Tissue
EPHB2	downregulated	downregulated	downregulated	-
PLEK	upregulated	downregulated	upregulated	-
ATM	downregulated	downregulated	-	-
SLK	upregulated	upregulated	-	-
MPA2L	upregulated	upregulated	-	-
TLR1	upregulated	upregulated	-	-
NARG1	upregulated	upregulated	-	-
YAP	downregulated	-	downregulated	-

Transcript	Microarray	Human study PCR	Western Blot	Tissue
MYCBP	upregulated	upregulated	-	no difference
MYC	-	-	-	no difference
COL1A1	downregulated	downregulated	-	downregulated
SPARC	downregulated	downregulated	-	-
SULF1	downregulated	downregulated	-	-
LOX	downregulated	downregulated	-	-
RARRES1	downregulated	downregulated	-	-
IGF1	downregulated	downregulated	-	-
TIMP1	downregulated	downregulated	-	-

ATM, ataxia-telangiectasia mutated homolog; **COL**, collagen; **EphB2**, ephrin B2; **IGF**, insulin-like growth factor; **LOX**, lysyl-oxidase; **MPA2L**, macrophage activation 2 like; **MYCBP**, MYC binding protein; **Narg1**, NMDA receptor-regulated gene 1; **Plek**, plekstrin; **RARRES1**, Retinoic acid receptor response element 1; **SPARC**, secreted protein, acidic rich in cysteine; **Slk**, Ste20-like kinase; **SULF1**, sulfatase 1; **TIMP1**, tissue inhibitor of metalloproteinase 1; **YAP**, Yes-associated protein.

REFERENCES

1. **Abrams, H., R. Spiro, and N. Goldstein**. 1949. Metastases in carcinoma. Analysis of 1000 autopsied cases. Cancer **3**:74-85.

2. **Anjos-Afonso, F., E. K. Siapati, and D. Bonnet**. 2004. In vivo contribution of murine mesenchymal stem cells into multiple cell-types under minimal damage conditions. J Cell Sci **117**:5655-5664.

3. **ARMITAGE, P. and R. DOLL**. 1954. The age distribution of cancer and a multi-stage theory of carcinogenesis. Br. J. Cancer **8**:1-12.

4. **Ashburner, M., C. A. Ball, J. A. Blake, D. Botstein, H. Butler, J. M. Cherry, A. P. Davis, K. Dolinski, S. S. Dwight, J. T. Eppig, M. A. Harris, D. P. Hill, L. Issel-Tarver, A. Kasarskis, S. Lewis, J. C. Matese, J. E. Richardson, M. Ringwald, G. M. Rubin, and G. Sherlock**. 2000. Gene ontology: tool for the unification of biology. The Gene Ontology Consortium. Nat. Genet. **25**:25-29.

5. **Aso, Y., K. Yoneda, and Y. Kikkawa**. 1976. Morphologic and biochemical study of plumonary changes induced by bleomycin in mice. Laboratory Investigation **35**:558-568.

6. **Bastien, J. and C. Rochette-Egly**. 2004. Nuclear retinoid receptors and the transcription of retinoid-target genes. Gene **328**:1-16.

7. **Baumgart, J. and D. Zippel**. 1991. Age-dependent experimental tumor dissemination of murine melanoma B16. Archivum Immunologiae et Therapiae Experimentalis **39**:489-494.

8. **Beissbarth, T.** 2006. [18] Interpreting Experimental Results Using Gene Ontologies, p. 340-352. *In* Alan Kimmel and Brian Oliver (ed.), Methods in Enzymology DNA Microarrays, Part B: Databases and Statistics. Academic Press.

9. **Beissbarth, T. and T. P. Speed**. 2004. GOstat: find statistically overrepresented Gene Ontologies within a group of genes. Bioinformatics **20**:1464-1465.

10. **Belinsky, S. A.** 2005. Silencing of genes by promoter hypermethylation: key event in rodent and human lung cancer. Carcinogenesis **26**:1481-1487.

11. **Boedtker, H., F. Fuller, and V. Tate**. 1983. The structure of collagen genes. Int. Rev. Connect. Tissue Res **10**:1-63.

12. **Bouez, C., C. Reynaud, E. Noblesse, A. Thepot, C. Gleyzal, J. Kanitakis, E. Perrier, O. Damour, and P. Sommer**. 2006. The lysyl oxidase LOX is absent in basal and

squamous cell carcinomas and its knockdown induces an invading phenotype in a skin equivalent model. Clin Cancer Res **12**:1463-1469.

13. **Bozanich, E. M., R. A. Collins, C. Thamrin, Z. Hantos, P. D. Sly, and D. J. Turner.** 2005. Developmental changes in airway and tissue mechanics in mice. J Appl Physiol **99**:108-113.

14. **Braakhuis, B. J., M. P. Tabor, J. A. Kummer, C. R. Leemans, and R. H. Brakenhoff.** 2003. A genetic explanation of Slaughter's concept of field cancerization: evidence and clinical implications. Cancer Res **63**:1727-1730.

15. **Brabender, J., R. V. Lord, R. Metzger, J. Park, D. Salonga, K. D. Danenberg, P. V. Danenberg, A. H. Holscher, and P. M. Schneider**. 2003. Differential SPARC mRNA expression in Barrett's oesophagus. Br. J. Cancer **89**:1508-1512.

16. **Bradshaw, A. D., P. Puolakkainen, J. Dasgupta, J. M. Davidson, T. N. Wight, and S. E. Helene**. 2003. SPARC-null mice display abnormalities in the dermis characterized by decreased collagen fibril diameter and reduced tensile strength. J. Invest Dermatol. **120**:949-955.

17. **Bradshaw, A. D., M. J. REED, J. G. CARBON, E. M. M. E. PINNEY, R. A. BREKKEN, and E. H. Sage**. 2001. Increased fibrovascular invasion of subcutaneous polyvinyl alcohol sponges in SPARC-null mice. Wound Repair and Regeneration **9**:522-530.

18. **Bradshaw, A. D., M. J. REED, and E. H. Sage**. 2002. SPARC-null Mice Exhibit Accelerated Cutaneous Wound Closure. J. Histochem. Cytochem. **50**:1-10.

19. **Bradshaw, A. D. and E. H. Sage**. 2001. SPARC, a matricellular protein that functions in cellular differentiation and tissue response to injury. J. Clin. Invest. **107**:1049-1054.

20. **Burnham, E., R. Taylor, A. Quyyumi, M. Rojas, K. Brigham, and M. Moss**. 2005. Increased circulating endothelial progenitor cells are associated with survival in acute lung injury. American Journal of Respirology and Critical Care Medicine **172**:854-860.

21. Canadian Cancer Society Steering Committee. Canadian Cancer Statistics 2009. 2009. Toronto, ON, Canadian Cancer Society.
Ref Type: Serial (Book,Monograph)

22. **Carbon, S., A. Ireland, C. J. Mungall, S. Shu, B. Marshall, and S. Lewis**. 2009. AmiGO: online access to ontology and annotation data. Bioinformatics. **25**:288-289.

23. **Cheetham, S., M. J. Tang, F. Mesak, H. Kennecke, D. Owen, and I. T. Tai**. 2008. SPARC promoter hypermethylation in colorectal cancers can be reversed by 5-Aza-

2'deoxycytidine to increase SPARC expression and improve therapy response. Br. J. Cancer **98**:1810-1819.

24. **Chen, Y., V. S. Chan, B. Zheng, K. Y. Chan, X. Xu, L. Y. To, F. P. Huang, U. S. Khoo, and C. L. Lin**. 2007. A novel subset of putative stem/progenitor CD34+Oct-4+ cells is the major target for SARS coronavirus in human lung. J. Exp. Med **204**:2529-2536.

25. **Chen, Z., J. Q. Fan, J. Li, Q. S. Li, Z. Yan, X. K. Jia, W. D. Liu, L. J. Wei, F. Z. Zhang, H. Gao, J. P. Xu, X. M. Dong, J. Dai, and H. M. Zhou**. 2009. Promoter hypermethylation correlates with the Hsulf-1 silencing in human breast and gastric cancer. Int. J. Cancer **124**:739-744.

26. **Chiang, C. H., C. P. Yu, C. P. Wu, H. C. Yan, and W. C. Perng**. 2001. Cytokine up-regulation in ischaemic/reperfused lungs perfused with University of Wisconsin solution and normal saline. Clin Sci. (Lond) **101**:285-294.

27. **Chlenski, A., L. J. Guerrero, Q. Yang, Y. Tian, R. Peddinti, H. R. Salwen, and S. L. Cohn**. 2007. SPARC enhances tumor stroma formation and prevents fibroblast activation. Oncogene.

28. **Chua, F., J. Gauldie, and G. Laurent**. 2005. Pulmonary fibrosis - Searching for model answers. American Journal of Respiratory Cell and Molecular Biology **33**:9-13.

29. **Corsini, E., A. Giani, S. Peano, M. Marinovich, and C. L. Galli**. 2004. Resistance to silica-induced lung fibrosis in senescent rats: role of alveolar macrophages and tumor necrosis factor-[alpha] (TNF). Mechanisms of Ageing and Development **125**:145-146.

30. **Coussens, L. M. and Z. Werb**. 2002. Inflammation and cancer. Nature **420**:860-867.

31. **Cowling, V. H. and M. D. Cole**. 2006. Mechanism of transcriptional activation by the Myc oncoproteins. Semin. Cancer Biol **16**:242-252.

32. **De Jong, W. K., G. F. Verpooten, H. Kramer, J. Louwagie, and H. J. Groen**. 2009. Promoter methylation primarily occurs in tumor cells of patients with non-small cell lung cancer. Anticancer Res **29**:363-369.

33. **Ding, L., G. Getz, D. A. Wheeler, E. R. Mardis, M. D. McLellan, K. Cibulskis, C. Sougnez, H. Greulich, D. M. Muzny, M. B. Morgan, L. Fulton, R. S. Fulton, Q. Zhang, M. C. Wendl, M. S. Lawrence, D. E. Larson, K. Chen, D. J. Dooling, A. Sabo, A. C. Hawes, H. Shen, S. N. Jhangiani, L. R. Lewis, O. Hall, Y. Zhu, T. Mathew, Y. Ren, J. Yao, S. E. Scherer, K. Clerc, G. A. Metcalf, B. Ng, A. Milosavljevic, M. L. Gonzalez-Garay, J. R. Osborne, R. Meyer, X. Shi, Y. Tang, D. C. Koboldt, L. Lin, R. Abbott, T. L. Miner, C. Pohl, G. Fewell, C. Haipek, H. Schmidt, B. H. Dunford-Shore, A. Kraja, S. D. Crosby, C. S. Sawyer, T. Vickery, S. Sander, J. Robinson, W. Winckler, J. Baldwin, L. R. Chirieac, A. Dutt, T. Fennell, M. Hanna, B. E. Johnson, R. C. Onofrio, R. K.**

Thomas, G. Tonon, B. A. Weir, X. Zhao, L. Ziaugra, M. C. Zody, T. Giordano, M. B. Orringer, J. A. Roth, M. R. Spitz, I. I. Wistuba, B. Ozenberger, P. J. Good, A. C. Chang, D. G. Beer, M. A. Watson, M. Ladanyi, S. Broderick, A. Yoshizawa, W. D. Travis, W. Pao, M. A. Province, G. M. Weinstock, H. E. Varmus, S. B. Gabriel, E. S. Lander, R. A. Gibbs, M. Meyerson, and R. K. Wilson. 2008. Somatic mutations affect key pathways in lung adenocarcinoma. Nature **455**:1069-1075.

34. **Dolle, P.** 2009. Developmental expression of retinoic acid receptors (RARs). Nucl. Recept. Signal. **7**:e006.

35. **Durr, E., J. Yu, K. M. Krasinska, L. A. Carver, J. R. Yates, J. E. Testa, P. Oh, and J. E. Schnitzer**. 2004. Direct proteomic mapping of the lung microvascular endothelial cell surface in vivo and in cell culture. Nat Biotech **22**:985-992.

36. **Ershler, W., A. Moore, H. Shore, and R. Gamelli**. 1984. Transfer of age-associated restrained tumour growth in mice by old-to-young bone marrow transplantation. Cancer Research **44**:5677-5680.

37. **Fadini, G. P., M. Schiavon, M. Cantini, I. Baesso, M. Facco, M. Miorin, M. Tassinato, S. V. d. Kreutzenberg, A. Avogaro, and C. Agostini**. 2006. Circulating Progenitor Cells Are Reduced in Patients with Severe Lung Disease. Stem Cells **24**:1806-1813.

38. **Fan, C., D. S. Oh, L. Wessels, B. Weigelt, D. S. Nuyten, A. B. Nobel, L. J. van't Veer, and C. M. Perou**. 2006. Concordance among gene-expression-based predictors for breast cancer. N. Engl. J. Med **355**:560-569.

39. **Faunce, D. E., J. L. Palmer, K. K. Paskowicz, P. L. Witte, and E. J. Kovacs**. 2005. CD1d-Restricted NKT Cells Contribute to the Age-Associated Decline of T Cell Immunity. J Immunol **175**:3102-3109.

40. **Fearon, E. R. and B. Vogelstein**. 1990. A genetic model for colorectal tumorigenesis. Cell **61**:759-767.

41. **Feng, Q., S. E. Hawes, J. E. Stern, L. Wiens, H. Lu, Z. M. Dong, C. D. Jordan, N. B. Kiviat, and H. Vesselle**. 2008. DNA methylation in tumor and matched normal tissues from non-small cell lung cancer patients. Cancer Epidemiol. Biomarkers Prev. **17**:645-654.

42. **Fidler, I.** 2003. The pathogenesis of cancer metastasis: the 'seed and soil' hypothesis revisited. Nature Reviews Cancer **3**:1-6.

43. **Folkman, J.** 2006. Angiogenesis. Annu. Rev. Med **57**:1-18.

44. **Fraga, M. F., R. Agrelo, and M. Esteller**. 2007. Cross-talk between aging and cancer: the epigenetic language. Ann. N. Y. Acad. Sci. **1100**:60-74.

45. **Fraser, H. B., P. Khaitovich, J. B. Plotkin, S. bo, and M. B. Eisen**. 2005. Aging and Gene Expression in the Primate Brain. PLoS Biology **3**:e274.

46. **Frese, M. A., F. Milz, M. Dick, W. C. Lamanna, and T. Dierks**. 2009. Characterization of the human sulfatase sulf1 and its high-affinity heparin/heparan sulfate interaction domain. J. Biol. Chem.

47. **Fulop, T., A. Larbi, N. Douziech, I. Levesque, A. Varin, and G. Herbein**. 2006. Cytokine receptor signalling and aging. Mechanisms of Ageing and Development **127**:526-537.

48. **Gabrilovac, J., M. Radacic, M. Osmak, and M. Boranic**. 1990. Opposing influence of age on the growth and colony-forming ability of mouse melanoma B16 and mammary adenocarcinoma: correlation with natural killer activity. Cancer Immunology Immunotherapy **32**:45-50.

49. **Ganesan, K., T. Ivanova, Y. Wu, V. Rajasegaran, J. Wu, M. H. Lee, K. Yu, S. Y. Rha, H. C. Chung, B. Ylstra, G. Meijer, K. O. Lian, H. Grabsch, and P. Tan**. 2008. Inhibition of gastric cancer invasion and metastasis by PLA2G2A, a novel beta-catenin/TCF target gene. Cancer Res **68**:4277-4286.

50. **Gatenby, R. A. and R. J. Gillies**. 2008. A microenvironmental model of carcinogenesis. Nat. Rev. Cancer **8**:56-61.

51. **Gendron, R. L., L. C. Adams, and H. Paradis**. 2000. Tubedown-1 A novel acetyltransferase associated with blood vessel development. Developmental Dynamics **218**:300-315.

52. **Gentleman, R. C., V. J. Carey, D. M. Bates, B. Bolstad, M. Dettling, S. Dudoit, B. Ellis, L. Gautier, Y. Ge, J. Gentry, K. Hornik, T. Hothorn, W. Huber, S. Iacus, R. Irizarry, F. Leisch, C. Li, M. Maechler, A. J. Rossini, G. Sawitzki, C. Smith, G. Smyth, L. Tierney, J. Y. Yang, and J. Zhang**. 2004. Bioconductor: open software development for computational biology and bioinformatics. Genome Biol. **5**:R80.

53. **Ghoshal, K., J. Datta, S. Majumder, S. Bai, H. Kutay, T. Motiwala, and S. T. Jacob**. 2005. 5-Aza-deoxycytidine induces selective degradation of DNA methyltransferase 1 by a proteasomal pathway that requires the KEN box, bromo-adjacent homology domain, and nuclear localization signal. Mol. Cell Biol. **25**:4727-4741.

54. **Gordan, J. D. and M. C. Simon**. 2007. Hypoxia-inducible factors: central regulators of the tumor phenotype. Current Opinion in Genetics & Development **17**:71-77.

55. **Gross, T. and G. Hunninghake**. 2001. Idiopathic pulmonary fibrosis. New England Journal of Medicine **345**:517-525.

56. **Gruber, H. E., E. H. Sage, H. J. Norton, S. Funk, J. Ingram, and E. N. Hanley, Jr.** 2005. Targeted deletion of the SPARC gene accelerates disc degeneration in the aging mouse. J. Histochem. Cytochem. **53**:1131-1138.

57. **Gruber, M. P., C. D. Coldren, M. D. Woolum, G. P. Cosgrove, C. Zeng, A. E. Baron, M. D. Moore, C. D. Cool, G. S. Worthen, K. K. Brown, and M. W. Geraci.** 2006. Human lung project: evaluating variance of gene expression in the human lung. Am. J. Respir. Cell Mol. Biol. **35**:65-71.

58. **Gruver, A. L., L. L. Hudson, and G. D. Sempowski.** 2007. Immunosenescence of ageing. J. Pathol. **211**:144-156.

59. **Halpern, M. T., B. W. Gillespie, and K. E. Warner.** 1993. Patterns of absolute risk of lung cancer mortality in former smokers. J. Natl. Cancer Inst. **85**:457-464.

60. **Hanahan, D. and R. A. Weinberg.** 2000. The Hallmarks of Cancer. Cell **100**:57-70.

61. **Hansen-Flaschen, J. and M. Siegel.** 2006. Acute respiratory distress syndrome: Definition, epidemiology, diagnosis and etiology. UpToDate **Online 14.1**.

62. **Hecht, S. S., F. Kassie, and D. K. Hatsukami.** 2009. Chemoprevention of lung carcinogenesis in addicted smokers and ex-smokers. Nat. Rev. Cancer **9**:476-488.

63. **Herbst, R. S., J. V. Heymach, and S. M. Lippman.** 2008. Lung cancer. N. Engl. J. Med **359**:1367-1380.

64. **Hildebran, J. N., M. Absher, and R. B. Low.** 1983. Altered rates of collagen synthesis in in vitro aged human lung fibroblasts. In Vitro **19**:307-314.

65. **Hirayama, R., K. Hirokawa, and T. Makinodan.** 1985. Change in the metstatic mode of B16 malignant melanoma in C57BL/6 mice with ageing and sex. IARC Sci Publ **58**:85-96.

66. **Hirayama, R., K. Takemura, Z. Nihei, W. Ichikawa, Y. Takagi, Y. Mishima, M. Utsuyama, and K. Hirokawa.** 1993. Differential effect of host microenvironment and systeminc humoral factors on the implantation and the growth rate of metastatic tumor in parabiotic mice constructed between young and old mice. Mechanisms of Ageing and Development **71**:213-221.

67. **Hornsby, C., K. M. Page, and I. P. Tomlinson.** 2007. What can we learn from the population incidence of cancer? Armitage and Doll revisited. Lancet Oncol. **8**:1030-1038.

68. **Huang, C. L., D. Liu, S. Ishikawa, T. Nakashima, N. Nakashima, H. Yokomise, K. Kadota, and M. Ueno.** 2008. Wnt1 overexpression promotes tumour progression in non-small cell lung cancer. Eur. J. Cancer **44**:2680-2688.

69. **Huang, K., R. Rabold, B. Schofield, W. Mitzner, and C. G. Tankersley**. 2007. Age-dependent changes of airway and lung parenchyma in C57BL/6J mice. J Appl Physiol **102**:200-206.

70. **Ito, M., G. Ito, M. Kondo, M. Uchiyama, T. Fukui, S. Mori, H. Yoshioka, Y. Ueda, K. Shimokata, and Y. Sekido**. 2005. Frequent inactivation of RASSF1A, BLU, and SEMA3B on 3p21.3 by promoter hypermethylation and allele loss in non-small cell lung cancer. Cancer Lett. **225**:131-139.

71. **Jackson, E. L., N. Willis, K. Mercer, R. T. Bronson, D. Crowley, R. Montoya, T. Jacks, and D. A. Tuveson**. 2001. Analysis of lung tumor initiation and progression using conditional expression of oncogenic K-ras. Genes Dev. **15**:3243-3248.

72. **Jung, H. C. and K. Kim**. 2005. Identification of MYCBP as a [beta]-catenin/LEF-1 target using DNA microarray analysis. Life Sciences **77**:1249-1262.

73. **Kanno, J., A. Wakikawa, M. Utsuyama, and K. Hirokawa**. 1997. Effect of restraint stress on immune system and experimental B16 melanoma metastasis in aged mice. Mechanisms of Ageing and Development **93**:107-117.

74. **Kaplan, R. N., R. D. Riba, S. Zacharoulis, A. H. Bramley, L. Vincent, C. Costa, D. D. MacDonald, D. K. Jin, K. Shido, S. A. Kerns, Z. Zhu, D. Hicklin, Y. Wu, J. L. Port, N. Altorki, E. R. Port, D. Ruggero, S. V. Shmelkov, K. K. Jensen, S. Rafii, and D. Lyden**. 2005. VEGFR1-positive haematopoietic bone marrow progenitors initiate the pre-metastatic niche. Nature **438**:820-827.

75. **Karamouzis, M. V., P. A. Konstantinopoulos, and A. G. Papavassiliou**. 2007. Epigenomics in respiratory epithelium carcinogenesis: prevention and therapeutic challenges. Cancer Treat. Rev. **33**:284-288.

76. **Kim, C. F., E. L. Jackson, A. E. Woolfenden, S. Lawrence, I. Babar, S. Vogel, D. Crowley, R. T. Bronson, and T. Jacks**. 2005. Identification of bronchioalveolar stem cells in normal lung and lung cancer. Cell **121**:823-835.

77. **Kotton, D., A. Fabian, and R. Mulligan**. 2005. Failure of bone marrow to reconstitute lung epithelium. American Journal of Respiratory Cell and Molecular Biology **33**:328-334.

78. **Kotton, D., B. Ma, W. Cardoso, E. Sanderson, R. Summer, M. Williams, and A. Fine**. 2001. Bone marrow-derived cells as progenitors of lung alveloar epithelium. Development **128**:5181-5188.

79. **Krause, D. S., N. D. Theise, M. I. Collector, O. Henegariu, S. Hwang, R. Gardner, S. Neutzel, and S. J. Sharkis**. 2001. Multi-Organ, Multi-Lineage Engraftment by a Single Bone Marrow-Derived Stem Cell. Cell **105**:369-377.

80. **Kuijper, S., C. J. Turner, and R. H. Adams**. 2007. Regulation of angiogenesis by Eph-ephrin interactions. Trends Cardiovasc. Med **17**:145-151.

81. **Kumar, M. S., S. J. Erkeland, R. E. Pester, C. Y. Chen, M. S. Ebert, P. A. Sharp, and T. Jacks**. 2008. Suppression of non-small cell lung tumor development by the let-7 microRNA family. Proc. Natl. Acad. Sci. U. S. A **105**:3903-3908.

82. **Lai, J. P., D. S. Sandhu, A. M. Shire, and L. R. Roberts**. 2008. The Tumor Suppressor Function of Human Sulfatase 1 (SULF1) in Carcinogenesis. J. Gastrointest. Cancer **39**:149-158.

83. **Lai, J. P., C. Yu, C. D. Moser, I. Aderca, T. Han, T. D. Garvey, L. M. Murphy, M. M. Garrity-Park, V. Shridhar, A. A. Adjei, and L. R. Roberts**. 2006. SULF1 inhibits tumor growth and potentiates the effects of histone deacetylase inhibitors in hepatocellular carcinoma. Gastroenterology **130**:2130-2144.

84. **Lamm, W. J. E., S. L. Bernard, W. W. Wagner, Jr., and R. W. Glenny**. 2005. Intravital microscopic observations of 15-{micro}m microspheres lodging in the pulmonary microcirculation. Journal of Applied Physiology **98**:2242-2248.

85. **Lapi, E., A. S. Di, S. Donzelli, H. Gal, E. Domany, G. Rechavi, P. P. Pandolfi, D. Givol, S. Strano, X. Lu, and G. Blandino**. 2008. PML, YAP, and p73 are components of a proapoptotic autoregulatory feedback loop. Mol. Cell **32**:803-814.

86. **Lee, M. L. T., F. C. Kuo, G. A. Whitmore, and J. Sklar**. 2000. Importance of replication in microarray gene expression studies: Statistical methods and evidence from repetitive cDNA hybridizations. Proceedings of the National Academy of Sciences of the United States of America **97**:9834-9839.

87. **Licchesi, J. D., W. H. Westra, C. M. Hooker, and J. G. Herman**. 2008. Promoter hypermethylation of hallmark cancer genes in atypical adenomatous hyperplasia of the lung. Clin Cancer Res **14**:2570-2578.

88. **Ling, T. Y., M. D. Kuo, C. L. Li, A. L. Yu, Y. H. Huang, T. J. Wu, Y. C. Lin, S. H. Chen, and J. Yu**. 2006. Identification of pulmonary Oct-4+ stem/progenitor cells and demonstration of their susceptibility to SARS coronavirus (SARS-CoV) infection in vitro. Proc Natl. Acad. Sci U. S. A **103**:9530-9535.

89. **Linton, P. J. and K. Dorshkind**. 2004. Age-related changes in lymphocyte development and function. Nat. Immunol. **5**:133-139.

90. **Liu, Z., J. Zhao, X. F. Chen, W. Li, R. Liu, Z. Lei, X. Liu, X. Peng, K. Xu, J. Chen, H. Liu, Q. H. Zhou, and H. T. Zhang**. 2008. CpG island methylator phenotype involving tumor suppressor genes located on chromosome 3p in non-small cell lung cancer. Lung Cancer **62**:15-22.

91. **Ljubuncic, P. and A. Z. Reznick**. 2009. The evolutionary theories of aging revisited--a mini-review. Gerontology **55**:205-216.

92. **Marneros, A. G. and B. R. Olsen**. 2005. Physiological role of collagen XVIII and endostatin. FASEB J. **19**:716-728.

93. **Martinek, N., J. Shahab, J. Sodek, and M. Ringuette**. 2007. Is SPARC an evolutionarily conserved collagen chaperone? J. Dent. Res **86**:296-305.

94. **Masoro, E.** 2006. Are Age-associated Diseases an Integral Part of Aging?, p. 43-62. *In* E. Masoro and S. Austad (ed.), Handbook on the Biology of Aging. Academic Press, Burlington, MA.

95. **Matsuo, Y., S. Amano, M. Furuya, K. Namiki, K. Sakurai, M. Nishiyama, T. Sudo, K. Tatsumi, T. Kuriyama, S. Kimura, and Y. Kasuya**. 2006. Involvement of p38{alpha} Mitogen-activated Protein Kinase in Lung Metastasis of Tumor Cells. J. Biol. Chem. **281**:36767-36775.

96. **Menschikowski, M., A. Hagelgans, H. Kostka, G. Eisenhofer, and G. Siegert**. 2008. Involvement of epigenetic mechanisms in the regulation of secreted phospholipase A2 expressions in Jurkat leukemia cells. Neoplasia. **10**:1195-1203.

97. **Meyer, K. C.** 2004. Lung infections and aging. Ageing Res Rev. **3**:55-67.

98. **Miller, F., C. Aslakson, and D. McEachern**. 1991. Modulation of host resistance to metastasis in the lungs of aged retired breeder mice. Invasion Metastasis **11**:233-240.

99. **Miller, R., S. Austad, D. Burke, C. Chrisp, R. Dysko, A. Galecki, A. Jackson, and V. Monnier**. 1999. Exotic mice as models for aging research: polemic and prospectus. Neurobiology of Aging **20**:217-231.

100. **Milne, E. N. and E. A. Zerhouni**. 1987. Blood supply of pulmonary metastases. J. Thorac. Imaging **2**:15-23.

101. **Min, C., Z. Yu, K. H. Kirsch, Y. Zhao, S. R. Vora, P. C. Trackman, D. B. Spicer, L. Rosenberg, J. R. Palmer, and G. E. Sonenshein**. 2009. A Loss-of-Function Polymorphism in the Propeptide Domain of the LOX Gene and Breast Cancer. Cancer Res.

102. **Minn, A. J., G. P. Gupta, P. M. Siegel, P. D. Bos, W. Shu, D. D. Giri, A. Viale, A. B. Olshen, W. L. Gerald, and J. Massague**. 2005. Genes that mediate breast cancer metastasis to lung. Nature **436**:518-524.

103. **Misra, V., H. Lee, A. Singh, K. Huang, R. K. Thimmulappa, W. Mitzner, S. Biswal, and C. G. Tankersley**. 2007. Global expression profiles from C57BL/6J and DBA/2J mouse lungs to determine aging-related genes. Physiol Genomics **31**:429-440.

104. **Mitsuuchi, Y. and J. R. Testa**. 2002. Cytogenetics and molecular genetics of lung cancer. Am. J. Med Genet. **115**:183-188.

105. **Morimoto-Tomita, M., K. Uchimura, Z. Werb, S. Hemmerich, and S. D. Rosen**. 2002. Cloning and characterization of two extracellular heparin-degrading endosulfatases in mice and humans. J. Biol. Chem. **277**:49175-49185.

106. **Nadon, N. L.** 2007. Animal models in gerontology research. Int. Rev. Neurobiol. **81**:15-27.

107. **Narita, K., J. Staub, J. Chien, K. Meyer, M. Bauer, A. Friedl, S. Ramakrishnan, and V. Shridhar**. 2006. HSulf-1 inhibits angiogenesis and tumorigenesis in vivo. Cancer Res **66**:6025-6032.

108. **Nijnik, A., L. Woodbine, C. Marchetti, S. Dawson, T. Lambe, C. Liu, N. P. Rodrigues, T. L. Crockford, E. Cabuy, A. Vindigni, T. Enver, J. I. Bell, P. Slijepcevic, C. C. Goodnow, P. A. Jeggo, and R. J. Cornall**. 2007. DNA repair is limiting for haematopoietic stem cells during ageing. Nature **447**:686-690.

109. **O'Reilly, P. G., S. Wagner, D. J. Franks, K. Cailliau, E. Browaeys, C. Dissous, and L. A. Sabourin**. 2005. The Ste20-like Kinase SLK Is Required for Cell Cycle Progression through G2. J. Biol. Chem. **280**:42383-42390.

110. **Ortiz, L., F. Gambelli, C. McBride, D. Gaupp, M. Baddoo, N. Kaminsky, and D. Phinney**. 2003. Mesenchymal stem cell engraftment in lung is enhanced in response to bleomycin exposure and ameliorates its fibrotic effects. Proceedings of the National Academy of Science **100**:8407-8411.

111. **Pan, M. R., H. C. Chang, L. Y. Chuang, and W. C. Hung**. 2008. The nonsteroidal anti-inflammatory drug NS398 reactivates SPARC expression via promoter demethylation to attenuate invasiveness of lung cancer cells. Exp. Biol. Med (Maywood.) **233**:456-462.

112. **Paradis, H., C.-Y. Liu, S. Saika, M. Azhar, T. Doetschman, W. V. Good, R. Nayak, N. Laver, C. W. Kao, W. W. Kao, and R. L. Gendron**. 2002. Tubedown-1 in Remodeling of the Developing Vitreal Vasculature in Vivo and Regulation of Capillary Outgrowth in Vitro. Developmental Biology **249**:140-155.

113. **Parman, C. and C. Halling**. 2009. affyQCReport: A package to generate QC reports for affymetrix array data. Bioconductor Vignettes.

114. **Pawelec, G., S. Koch, H. Griesemann, A. Rehbein, K. Hahnel, and C. Gouttefangeas.** 2006. Immunosenescence, suppression and tumour progression. Cancer Immunol. Immunother. **55**:981-986.

115. **Payne, S. L., M. J. Hendrix, and D. A. Kirschmann.** 2007. Paradoxical roles for lysyl oxidases in cancer--a prospect. J. Cell Biochem. **101**:1338-1354.

116. **Perez-Diez, A., N. T. Joncker, K. Choi, W. F. Chan, C. C. Anderson, O. Lantz, and P. Matzinger.** 2007. CD4 cells can be more efficient at tumor rejection than CD8 cells. Bloodblood-2006.

117. **Power, A. T., J. Wang, T. J. Falls, J. M. Paterson, K. A. Parato, B. D. Lichty, D. F. Stojdl, P. A. Forsyth, H. Atkins, and J. C. Bell.** 2007. Carrier cell-based delivery of an oncolytic virus circumvents antiviral immunity. Mol. Ther. **15**:123-130.

118. **Quesenberry, P., G. Colvin, M. Abedi, G. Dooner, M. Dooner, J. Aliotta, P. Keaney, L. Luo, D. Demers, A. Peterson, B. Foster, and D. Greer.** 2005. The stem cell continuum. Annals of the New York Academy of Sciences **1044**:228-235.

119. **Rando, T. A.** 2006. Stem cells, ageing and the quest for immortality. Nature **441**:1080-1086.

120. **Rapp, U. R., C. Korn, F. Ceteci, C. Karreman, K. Luetkenhaus, V. Serafin, E. Zanucco, I. Castro, and T. Potapenko.** 2009. MYC is a metastasis gene for non-small-cell lung cancer. PLoS. One. **4**:e6029.

121. **Rauch, T. A., X. Zhong, X. Wu, M. Wang, K. H. Kernstine, Z. Wang, A. D. Riggs, and G. P. Pfeifer.** 2008. High-resolution mapping of DNA hypermethylation and hypomethylation in lung cancer. Proc. Natl. Acad. Sci. U. S. A **105**:252-257.

122. **Rivard, A., L. Berthou-Soulie, N. Principe, M. Kearney, C. Curry, D. Branellec, G. L. Semenza, and J. M. Isner.** 2000. Age-dependent Defect in Vascular Endothelial Growth Factor Expression Is Associated with Reduced Hypoxia-inducible Factor 1 Activity. J. Biol. Chem. **275**:29643-29647.

123. **Rivard, A., J. E. Fabre, M. Silver, D. Chen, T. Murohara, M. Kearney, M. Magner, T. Asahara, and J. M. Isner.** 1999. Age-Dependent Impairment of Angiogenesis. Circulation **99**:111-120.

124. **Rodriguez-Jimenez, F. J., T. Caldes, P. Iniesta, J. A. Vidart, J. L. Garcia-Asenjo, and M. Benito.** 2007. Overexpression of SPARC protein contrasts with its transcriptional silencing by aberrant hypermethylation of SPARC CpG-rich region in endometrial carcinoma. Oncol. Rep. **17**:1301-1307.

125. **Rodwell, G. E. J., R. Sonu, J. M. Zahn, J. Lund, J. Wilhelmy, L. Wang, W. Xiao, M. Mindrinos, E. Crane, E. Segal, B. D. Myers, J. D. Brooks, R. W. Davis, J. Higgins, A. B.**

Owen, and S. K. Kim. 2004. A Transcriptional Profile of Aging in the Human Kidney. PLoS Biology **2**:e427.

126. **Rubenfeld, G., E. Caldwell, E. Peabody, J. Weaver, D. Martin, M. Neff, E. Stern, and L. Hudson**. 2005. Incidence and outcomes of acute lung injury. New England Journal of Medicine **353**:1693.

127. **Sabourin, L. A. and M. A. Rudnicki**. 1999. Induction of apoptosis by SLK, a Ste20-related kinase. Oncogene **18**:7566-7575.

128. **Saeed, A. I., V. Sharov, J. White, J. Li, W. Liang, N. Bhagabati, J. Braisted, M. Klapa, T. Currier, M. Thiagarajan, A. Sturn, M. Snuffin, A. Rezantsev, D. Popov, A. Ryltsov, E. Kostukovich, I. Borisovsky, Z. Liu, A. Vinsavich, V. Trush, and J. Quackenbush**. 2003. TM4: a free, open-source system for microarray data management and analysis. Biotechniques **34**:374-378.

129. **Said, N., M. J. Socha, J. J. Olearczyk, A. A. Elmarakby, J. D. Imig, and K. Motamed**. 2007. Normalization of the ovarian cancer microenvironment by SPARC. Mol. Cancer Res **5**:1015-1030.

130. **Sakamuro, D. and G. C. Prendergast**. 1999. New Myc-interacting proteins: a second Myc network emerges. Oncogene **18**:2942-2954.

131. **Saltzstein, S. and C. Behling**. 1998. Features of cancer in nonagenarians and centarians. Journal of the Americal Geriatrics Society **46**:994-998.

132. **Sampson, V. B., N. H. Rong, J. Han, Q. Yang, V. Aris, P. Soteropoulos, N. J. Petrelli, S. P. Dunn, and L. J. Krueger**. 2007. MicroRNA let-7a down-regulates MYC and reverts MYC-induced growth in Burkitt lymphoma cells. Cancer Res **67**:9762-9770.

133. **Sato, N., N. Fukushima, N. Maehara, H. Matsubayashi, J. Koopmann, G. H. Su, R. H. Hruban, and M. Goggins**. 2003. SPARC/osteonectin is a frequent target for aberrant methylation in pancreatic adenocarcinoma and a mediator of tumor-stromal interactions. Oncogene **22**:5021-5030.

134. **Shames, D. S., L. Girard, B. Gao, M. Sato, C. M. Lewis, N. Shivapurkar, A. Jiang, C. M. Perou, Y. H. Kim, J. R. Pollack, K. M. Fong, C. L. Lam, M. Wong, Y. Shyr, R. Nanda, O. I. Olopade, W. Gerald, D. M. Euhus, J. W. Shay, A. F. Gazdar, and J. D. Minna**. 2006. A genome-wide screen for promoter methylation in lung cancer identifies novel methylation markers for multiple malignancies. PLoS. Med **3**:e486.

135. **Shimizu, K., S. N. Kinouchi, T. Asai, H. Tsukada, and N. Oku**. 2008. Enhanced experimental tumor metastasis with age in senescence-accelerated mouse. Biol. Pharm. Bull. **31**:847-851.

136. **Siegel, M.** 2006. Acute respiratory distress syndrome: Pathophysiology, clinical manifestations and prognosis. UpToDate **Online 14.1**.

137. **Sion, A. M. and W. D. Figg**. 2006. Lysyl oxidase (LOX) and hypoxia-induced metastases. Cancer Biol. Ther. **5**:909-911.

138. **SLAUGHTER, D. P., H. W. SOUTHWICK, and W. SMEJKAL**. 1953. Field cancerization in oral stratified squamous epithelium; clinical implications of multicentric origin. Cancer **6**:963-968.

139. **Sleijfer, S.** 2001. Bleomycin-induced pneumonitis. Chest **120**:617-624.

140. **So, K., G. Tamura, T. Honda, N. Homma, T. Waki, N. Togawa, S. Nishizuka, and T. Motoyama**. 2006. Multiple tumor suppressor genes are increasingly methylated with age in non-neoplastic gastric epithelia. Cancer Sci. **97**:1155-1158.

141. **Socha, M. J., N. Said, Y. Dai, J. Kwong, P. Ramalingam, V. Trieu, N. Desai, S. C. Mok, and K. Motamed**. 2009. Aberrant promoter methylation of SPARC in ovarian cancer. Neoplasia. **11**:126-135.

142. **Solana, R. and E. Mariani**. 2000. NK and NK/T cells in human senescence. Vaccine **18**:1613-1620.

143. **Spira, A., J. Beane, V. Shah, G. Liu, F. Schembri, X. Yang, J. Palma, and J. S. Brody**. 2004. Effects of cigarette smoke on the human airway epithelial cell transcriptome. Proc Natl. Acad. Sci U. S. A **101**:10143-10148.

144. **Starcher, B. and C. Kuhn**. 2003. Combining histology and biochemical measurements of connective tissue components in small samples of lung: application to bleomycin-induced fibrosis in the mouse. Experimental Lung Research **29**:179-194.

145. **Steeg, P. S.** 2006. Tumor metastasis: mechanistic insights and clinical challenges. Nat Med **12**:895-904.

146. **Suki, B., S. Ito, D. Stamenovic, K. R. Lutchen, and E. P. Ingenito**. 2005. Biomechanics of the lung parenchyma: critical roles of collagen and mechanical forces. J Appl Physiol **98**:1892-1899.

147. **Suzuki, M., C. Hao, T. Takahashi, H. Shigematsu, N. Shivapurkar, U. G. Sathyanarayana, T. Iizasa, T. Fujisawa, K. Hiroshima, and A. F. Gazdar**. 2005. Aberrant methylation of SPARC in human lung cancers. Br. J. Cancer **92**:942-948.

148. **Taggart, C., C. Green, T. Carroll, S. O'Neill, and N. McElvaney**. 2005. Elastolytic proteases: Inflammation resolutionand dysregulation in chronic infective lung disease. Am J Respir Crit Care Med **171**:1070-1076.

149. **Taira, T., J. Maeda, T. Onishi, H. Kitaura, S. Yoshida, H. Kato, M. Ikeda, K. Tamai, S. M. Iguchi-Ariga, and H. Ariga**. 1998. AMY-1, a novel C-MYC binding protein that stimulates transcription activity of C-MYC. Genes Cells **3**:549-565.

150. **Teder, P., R. W. Vandivier, D. Jiang, J. Liang, L. Cohn, E. Pure, P. M. Henson, and P. W. Noble**. 2002. Resolution of Lung Inflammation by CD44. Science **296**:155-158.

151. **Tessema, M., Y. Y. Yu, C. A. Stidley, E. O. Machida, K. E. Schuebel, S. B. Baylin, and S. A. Belinsky**. 2009. Concomitant promoter methylation of multiple genes in lung adenocarcinomas from current, former and never smokers. Carcinogenesis **30**:1132-1138.

152. **Thompson, S.** 1976. Effect of age and sex on lung-colony-forming efficiency of injected mouse tumour cells. British Journal of Cancer566-570.

153. **Tomita, Y., H. Mayumi, M. Eto, and K. Nomoto**. 1990. Tumor allograft rejection is mainly mediated by CD8+ cytotoxic T lymphocytes stimulated with class I alloantigens in cooperation with CD4+ helper T cells recognizing class II alloantigens. J Immunol **144**:2425-2435.

154. **Tusher, V. G., R. Tibshirani, and G. Chu**. 2001. Significance analysis of microarrays applied to the ionizing radiation response. Proc. Natl. Acad. Sci. U. S. A **98**:5116-5121.

155. **Wagner, S., T. A. Flood, P. O'Reilly, K. Hume, and L. A. Sabourin**. 2002. Association of the Ste20-like Kinase (SLK) with the Microtubule. ROLE IN Rac1-MEDIATED REGULATION OF ACTIN DYNAMICS DURING CELL ADHESION AND SPREADING. J. Biol. Chem. **277**:37685-37692.

156. **Wall, D. S., R. L. Gendron, W. V. Good, E. Miskiewicz, M. Woodland, K. Leblanc, and H. Paradis**. 2004. Conditional Knockdown of Tubedown-1 in Endothelial Cells Leads to Neovascular Retinopathy. Invest. Ophthalmol. Vis. Sci. **45**:3704-3712.

157. **Wallace, P., T. Eisenstein, J. Meissler Jr, and P. Morahan**. 1995. Decreases in macrophage mediated antitumor activity with aging. Mechanisms of Ageing and Development **77**:169-184.

158. **Wistuba, I. I. and A. F. Gazdar**. 2006. Lung cancer preneoplasia. Annu. Rev. Pathol. **1**:331-348.

159. **Wistuba, I. I. and M. Meyerson**. 2008. Chromosomal deletions and progression of premalignant lesions: less is more. Cancer Prev. Res (Phila Pa) **1**:404-408.

160. **Wu, C. C., R. Y. Shyu, J. M. Chou, S. W. Jao, P. C. Chao, J. C. Kang, S. T. Wu, S. L. Huang, and S. Y. Jiang**. 2006. RARRES1 expression is significantly related to tumour differentiation and staging in colorectal adenocarcinoma. Eur. J. Cancer **42**:557-565.

161. **Yamamoto, Y., A. Tanaka, A. Kanamaru, S. Tanaka, H. Tsubone, Y. Atoji, and Y. Suzuki**. 2003. Morphology of aging lung in F344/N rat: Alveolar size, connective tissue and smooth muscle markers. The Anatomical Record Part A **272A**:538-547.

162. **Yang, E., H. J. Kang, K. H. Koh, H. Rhee, N. K. Kim, and H. Kim**. 2007. Frequent inactivation of SPARC by promoter hypermethylation in colon cancers. Int. J. Cancer **121**:567-575.

163. **Yoshida, S., B. M. Yashar, S. Hiriyanna, and A. Swaroop**. 2002. Microarray Analysis of Gene Expression in the Aging Human Retina. Invest. Ophthalmol. Vis. Sci. **43**:2554-2560.

164. **Youssef, E. M., X. Q. Chen, E. Higuchi, Y. Kondo, G. Garcia-Manero, R. Lotan, and J. P. Issa**. 2004. Hypermethylation and silencing of the putative tumor suppressor Tazarotene-induced gene 1 in human cancers. Cancer Res **64**:2411-2417.

165. **Zahn, J. M., R. Sonu, H. Vogel, E. Crane, K. Mazan-Mamczarz, R. Rabkin, R. W. Davis, K. G. Becker, A. B. Owen, and S. K. Kim**. 2006. Transcriptional Profiling of Aging in Human Muscle Reveals a Common Aging Signature. PLoS Genetics **2**:e115.

166. **Zajac-Kaye, M.** 2001. Myc oncogene: a key component in cell cycle regulation and its implication for lung cancer. Lung Cancer **34 Suppl 2**:S43-S46.

CONTRIBUTION OF COLLABORATORS

- Masson's trichrome staining was performed by the University of Ottawa Pathology department technicians.
- Madison Gray (summer student) acquired raw pixel count data from tissue microarrays stained for MYCBP and Ki67.
- Melanie Duquette (honours research student) and Matthew Tang (graduate student) performed RNA extraction and a preliminary microarray analysis for unperfused mouse lung tissues. The Affymetrix MOE430A chip set was employed. They also performed quantitative PCR and Western Blotting for *Yes*-associated protein, ephrin B2 and plekstrin. These data formed the basis for the structured reanalysis and validation presented herein.
- **Appendix 4** outlines the histochemical staining protocol employed by Mei Zhang (Senior Histochemical Technician) on study tissues and tissue microarrays.
- **Appendix 5** outlines Paul Krzyzanowski's contribution of to the mouse microarray analysis. The second round of analysis using perfused lung tissues was hybridized using MOE430 2.0 chips, which possess denser probeset architecture as well as additional probesets. The collaboration aimed to explore the feasibility of combing probeset data from two different chipsets to boost the number of biologic replicated analysed. Appendix 5 outlines the attempted analysis. Ultimately, Paul reanalyzed and performed gene ontology mining of the gene list from the perfused sample set, results of which are presented herein.

- Isolation protocols for lung bronchoalveolar stem cells (BASC) were adapted from (76) and optimized in collaboration with Dr. Josée Coulombe (Senior Research Associate).
- The flow cytometry data for lung CD31+, CD4+, CD8+ and BASC cell populations were acquired by Caroline Vergette, Flow Cytometry Technician the StemCore facility.
- Veterinary manipulations were performed by the veterinary technicians Jennifer Sparling, Theresa Falls and Steve Nantel.

APPENDICES

1. RNA QUALITY ASSURANCE, HUMAN LUNG SAMPLES

The quality of the isolated RNA from each sample was assessed by the StemCore facility (OHRI) using an Agilent Bioanalyzer (Santa Clara CA, USA). Samples with an A260/280 ratio of 1.8 or better were submitted for chromatography. Samples were used for hybridization to microarray chips when intact 18S and 28S peaks were observed on the bioanalyzer tracings with intact baselines.

Sample ID	rRNA Ratio [28S / 18S]	Trace
01N	1.29	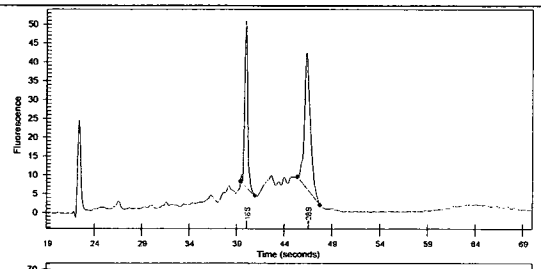
02N	1.07	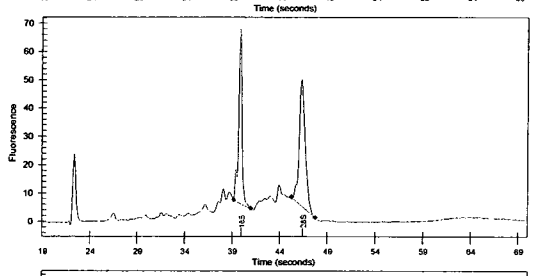
03N	1.19	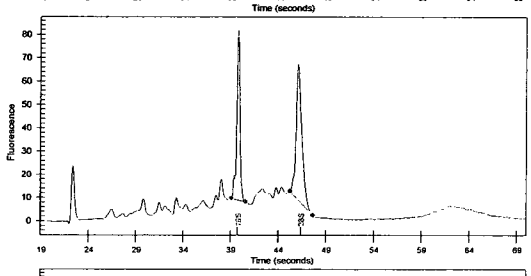
04N	1.36	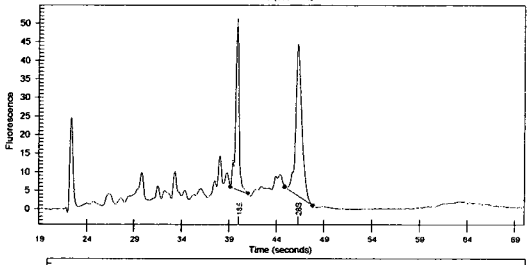
05N	1.91	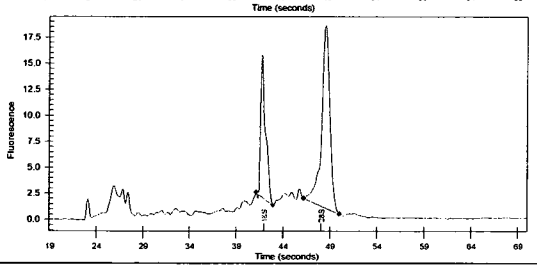

2. MOUSE POST-HYBRIDIZATION QUALITY CONTROL

A

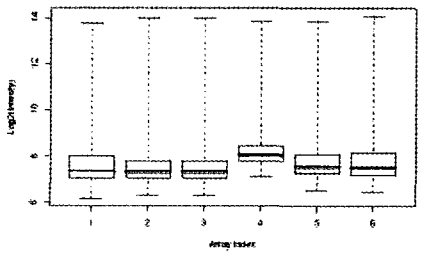

B

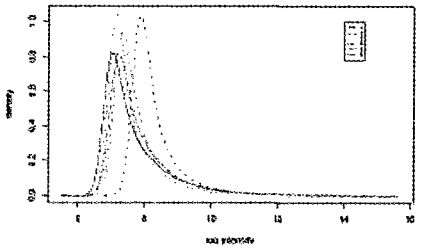

C

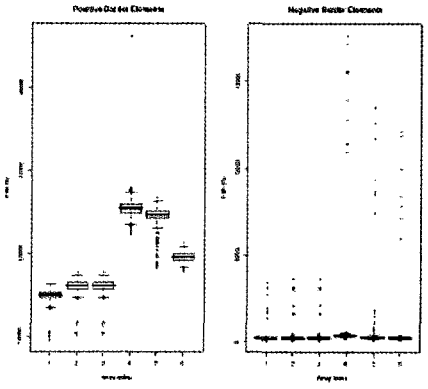

D

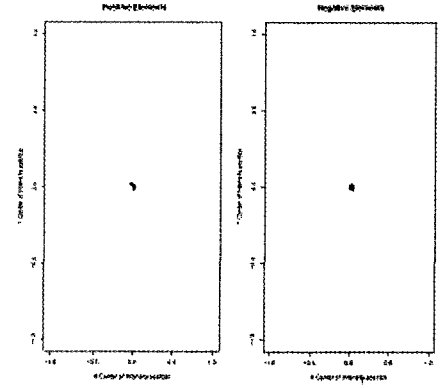

E

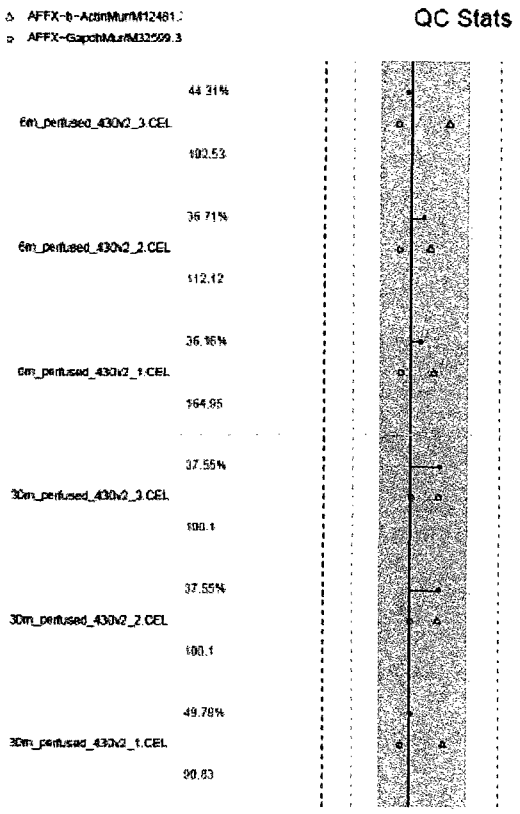

F

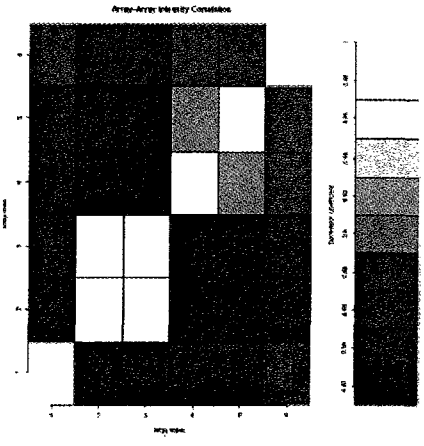

Panels A-F are generated using the Bioconductor (52) package *affyQCReport (113)*. This allows for a visual assessment of the quality of hybridization within a batch of microarray chips and is run under R on RMA normalized data. Panels (A and B) represent intensity data from perfect match (PM) calls from the microarray. One notices that both the box-whisker plots (A) and the log intensity graphs (B) cluster without evidence of outliers. This represents a technically successful hybridization. Panel (C) assess arbitrary positive (left panel) and negative elements (right panel) present on the physical microarray chip for non-uniform hybridization. The box-whisker plots cluster between age cohorts with no evidence of outliers. This indicates the chip used were intact and that the hybridization was successful, with little background. Panel (D) assesses the overall chip intensity for hot spots, even hybridization will cluster in the centre. Panel (E) examines the positive controls beta-actin and glyceraldehyde-3-phosphate dehydrogenase (GAPDH) and determines to assess intensity levels of ubiquitously expresses transcripts. Panel (F) shows a Spearman rank correlation matrix. This is primarily used to assess similarity between sets of technical replicates, as biological replicates will show low correlation – the variation is especially seen in the three 30 month samples.

Taken together, the hybridizations used for the mouse microarray analysis are technically valid and acceptable.

3. HUMAN POST-HYBRIDIZATION QUALITY CONTROL

A

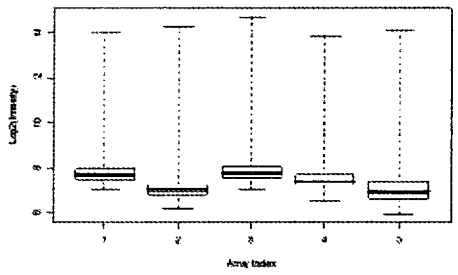

B

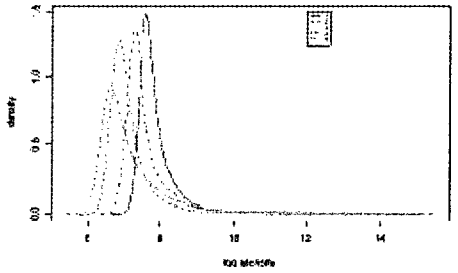

C

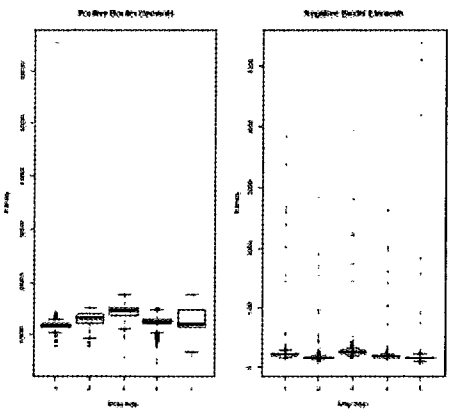

D

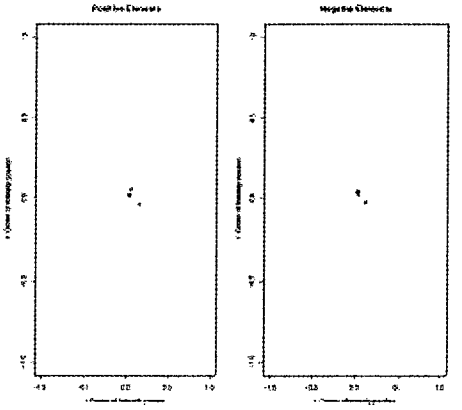

E

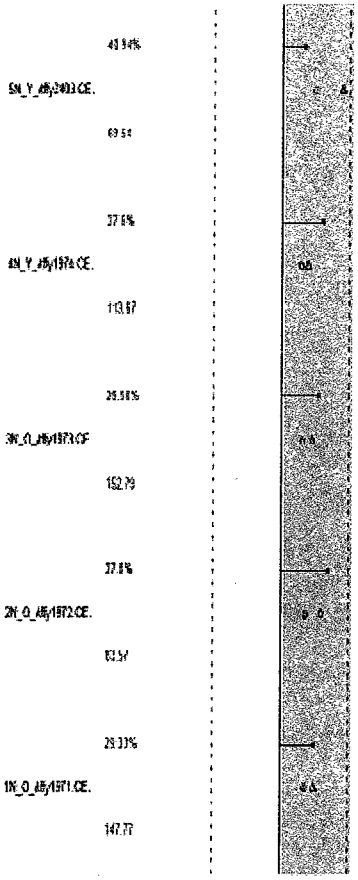

F

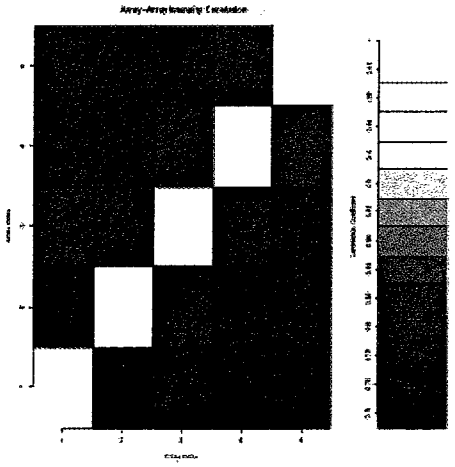

Panels A-F are generated using the Bioconductor (52) package *affyQCReport (113)*. This allows for a visual assessment of the quality of hybridization within a batch of microarray chips and is run under R on RMA normalized data. Panels (A and B) represent intensity data from perfect match (PM) calls from the microarray. One notices that both the box-whisker plots (A) and the log intensity graphs (B) cluster without evidence of outliers. This represents a technically successful hybridization. Panel (C) assess arbitrary positive (left panel) and negative elements (right panel) present on the physical microarray chip for non-uniform hybridization. The box-whisker plots cluster with no evidence of outliers. This indicates the chip used were intact and that the hybridization was successful, with little background. Panel (D) assesses the overall chip intensity for hot spots, even hybridization will cluster in the centre. Panel (E) examines the positive controls beta-actin and glyceraldehyde-3-phosphate dehydrogenase (GAPDH) and determines to assess intensity levels of ubiquitously expresses transcripts. Panel (F) shows a Spearman rank correlation matrix. This is primarily used to assess similarity between sets of technical replicates, as biological replicates will show low correlation.

Taken together, the hybridizations used for the human microarray analysis are technically valid and acceptable.

3. GO TERM ANALYSIS OF HUMAN GENE LIST

	Part GOs (Max: 50)	Genes	Count 41	Total 38972	P-Value
Collagen	GO:0005581	col1a1 col1a2 col6a3 col5a1 col6a1 col3a1 col18a1 col5a2	8	54	1.32e-12
Extracellular matrix part	GO:0044420	col1a1 col1a2 col6a3 col5a1 col6a1 nid2 col3a1 col5a2 col18a1	9	131	1.36e-11
Fibrillar collagen	GO:0005583	col1a1 col1a2 col3a1 col5a1 col5a2	5	11	1.85e-10
Proteinaceous extracellular matrix	GO:0005578	col1a1 col1a2 col6a3 col5a1 thbs2 timp1 col6a1 col3a1 nid2 col5a2 col18a1	11	431	3.19e-10
Phosphate transport	GO:0006817	col1a1 col1a2 col6a3 col5a1 col6a1 col3a1 col18a1 col5a2	8	143	8.33e-10
Inorganic anion transport	GO:0015698	col1a1 col1a2 cav2 col6a3 col5a1 col6a1 col3a1 col5a2 col18a1	9	260	2.24e-09
Extracellular region part	GO:0044421	col1a1 prg4 col1a2 col6a3 col5a1 thbs2 timp1 col6a1 col3a1 nid2 col5a2 col18a1 sulf1	13	910	2.56e-09
Anion transport	GO:0006820	col1a1 col1a2 cav2 col6a3 col5a1 col6a1 col3a1 col5a2 col18a1	9	323	1.15e-08
Extracellular matrix structural component	GO:0005201	col1a1 col1a2 col3a1 col18a1 col5a1 col5a2	6	123	5.44e-07
Collagen	GO:0005589	col6a1 col6a3	2	2	8.61e-05
	GO:0005588	col5a1 col5a2	2	3	0.000215
	GO:0005584	col1a1 col1a2	2	3	0.000215
	GO:0005814	col1a1 col18a1	2	4	0.000357
Cytoplasm	GO:0005737	glns1 col6a3 col5a1 fmo1 nan hid1 sult1 col5a2 col1a1 rpl17 col1a2 cav2 ppic ikbkb mib2 pla2g2a aldh1a2 tgm1 col6a1 col3a1 col18a1	21	7482	0.000625
Biological adhesion	GO:0022610	col6a1 col5a1 thbs2 tpbg cldn11 col6a1 nid2 col18a1	8	960	0.000625
Cell adhesion	GO:0007155	col6a1 col5a1 thbs2 tpbg cldn11 col6a1 nid2 col18a1	8	960	0.000625
Ion transport	GO:0006811	col1a1 col1a2 cav2 col6a3 col5a1 col6a1 col3a1 col5a2 col18a1	9	1364	0.00103

Anchoring collagen	GO:0030934	col6a1 col6a3	2	9	0.00171
Organ development	GO:0048513	col1a1 col1a2 cav2 col6a3 timp1 col3a1 col5a2 col18a1	8	1141	0.0018
Protein binding	GO:0005515	ginS1 plk2 pde1a col6a3 tpbg thbs2 timp1 ran pcolce col1a1 mcm2 col1a2 ppic hdac1 cav2 ikbkb mib2 tpm4 cldn15 col6a1 nid2 col18a1	22	9005	0.00506
Collagen binding	GO:0005518	pcolce nid2	2	19	0.00692
Multicellular organismal development	GO:0048518	mib2 cfl plk2 timp1 ran cav2 tial1	7	1062	0.00699
Developmental process	GO:0007275	col1a1 ginS1 col1a2 cav2 col6a3 timp1 pcolce col3a1 col5a2 col18a1	10	2299	0.00816
Anatomical structure development	GO:0048434	col1a1 cav2	2	22	0.00816
Developmental process	GO:0032502	col1a1 ginS1 col1a2 cav2 col6a3 timp1 pcolce col3a1 sulf1 col5a2 col18a1 tial1	12	3347	0.0103
Anatomical structure development	GO:0048856	col1a1 ginS1 col1a2 cav2 col6a3 timp1 col3a1 col18a1 col5a2	9	2005	0.0125
System development	GO:0048731	col1a1 col1a2 cav2 col6a3 timp1 col3a1 col5a2 col18a1	8	1605	0.013
Response to steroid hormone stimulus	GO:0048545	col1a1 cav2	2	37	0.0196
Positive regulation of cellular process	GO:0048522	mib2 plk2 timp1 ran cav2 tial1	6	954	0.0196
Localization	GO:0051179	col1a1 col1a2 cav2 col6a3 col5a1 fmo1 tpbg tpm4 ran col6a1 col3a1 col5a2 col18a1	13	4481	0.0213

4. IMMUNOHISTOCHEMICAL STAINING PROTOCOLS

This work was performed by Mei Zhang, senior research technician.

MYC, MYCBP: The sections were deparaffinized and then heated in 10 mM sodium citrate buffer (pH7.6) in microwave oven for 10 min to unmask the antigen. Endogenous peroxide activity was blocked by incubation in methanol containing 3% hydrogen peroxide for 20 min. The sections were incubated for 30 min with 1.5% normal goat serum in 0.1M PBS (pH7.4) to block nonspecific binding. They were then incubated overnight at 4ºC with rabbit

anti-MYCBP 1:600 diluted in blocking solution. After being washed with PBS, the sections were exposed for 30 min by using Dako EnVision+System-HRP Labelled Polymer anti-rabbit kit. The reaction product was visualized by applying substrate-chromogen. Cell nuclei were counter stained with hematoxylin.

Ki67: The sections were deparaffinized and then heated in 10 mM sodium citrate buffer (pH7.6) in microwave oven for 10 min to unmask the antigen. Endogenous peroxide activity was blocked by incubation in methanol containing 3% hydrogen peroxide for 20 min. The sections were incubated for 30 min with 1.5% normal goat serum in 0.1M PBS (pH7.4) to block nonspecific binding. They were then incubated overnight at 4ºC with mouse anti-Ki67 1:60 diluted in blocking solution. After being washed with PBS, the sections were exposed for 30 min to Biotinylated horse anti-mouse immunoglobulin G diluted 1:200 in blocking solution. The reaction product was visualized by the avidin biotin peroxidase method with an ABC Elite kit. Cell nuclei were counter stained with hematoxylin.

5. BIOINFORMATICS COLLABORATION REPORT

Report on microarray experiments that compare young mouse lung tissue versus old mouse lung tissues, with the objective of identifying genes that are active in old lung tissues and are responsible for aged phenotype lung tissues.

There are 12 hybridizations in total. One comparison consists of triplicates of old (30m) vs. young (6m) lung tissues on Affymetrix MOE430A chips. A new comparison is identical

except that the lung tissues have been perfused of blood and hybridization to the MOE430v2 platform.

The initial proposed arrangement of these data was to combine the MOE430A probe sets from the perfused MOE430v2 hybridization with the non-perfused MOE430A hybridization and to consider them as a large experiment with six replicates in each condition (6m and 30m). To test whether assembling the data in this way is reasonable, we processed the 12 CEL files with MAS5 in R, rearranged the hybridization values of probe sets common to both platforms into one matrix, and hierarchically clustered by columns (hybridizations). It was expected that the 30m lung tissue hybridizations would cluster together.

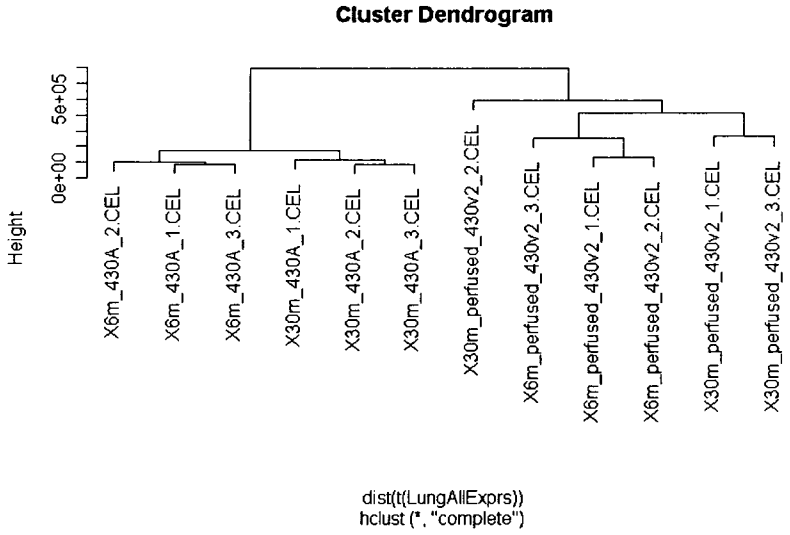

From the tree above, we see that 30m samples do not cluster together, indicating that the originally intended comparison would probably not be valid. The reason that we see two major branches forming is either due to i) the different chip platforms, ii) whether the samples were perfused of blood or not, or iii) some combination of both.

In order to still make use of both data, we attempted to identify genes involved in the aging process in each set of samples individually (perfused and non-perfused), and intersect those lists to focus on genes that are significant to both sets of samples. We reprocessed both sets of array data with GCRMA in Bioconductor and performed SAM using the 'siggenes' package of Bioconductor on each set of array data, comparison the 6m samples vs. the 30m ones. A delta cutoff for each set was chosen to produce a significant gene list with a FDR of 5%. Delta values of 3.4 and 2.6 produced gene lists of 1145 and 495 for MOE430v2 and MOE430A, respectively. Intersection of these lists identifies 15 probe sets common to both aging processes.

A separate spreadsheet, 'Significant genes in old lung.xls' contains the results of the two siggenes analyses as well as a short analysis of the 15 common probesets.

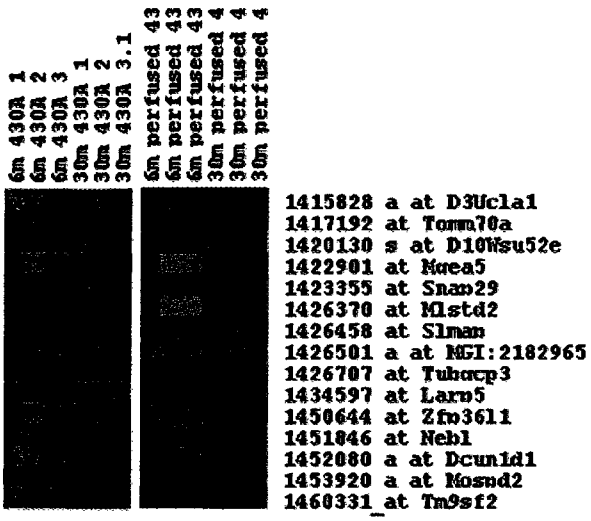

The heatmap above shows the relative expression values of these 15 probe sets. GCRMA expression values from both conditions were median centered and heatmaps were visualized with TreeView. We noted that most of these probe sets had expression changes that were in the same direction but that ones in the perfused MOE430v2 samples exhibited greater fold changes than the non-perfused samples. We believe that this was due to the higher purity of lung-tissue in the perfused samples.

To test whether these higher fold changes were generally seen, we calculated fold changes observed in common probe sets for the samples that were perfused and those that were not. The mean GCRMA hybridization values for each triplicate were used to determine the fold-change (e.g. mean 30m non-perfused vs. mean 6m non-perfused; and similarly for perfused), and the fold-changes were plotted against each other, below.

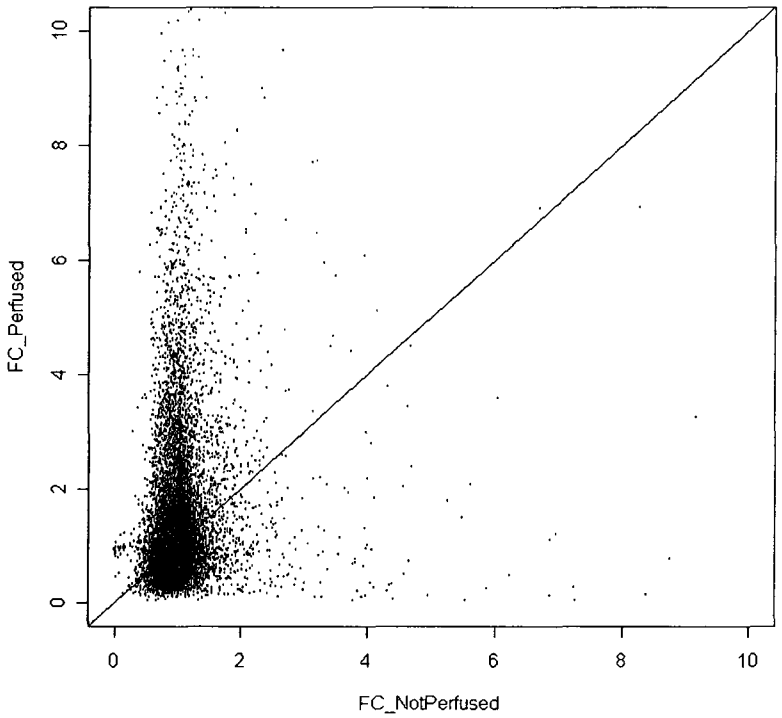

Each point represents a probe set, the line is y=x, and the axes are limited to 10x. It is clearly seen that high fold changing probe sets for the perfused comparison are more numerous and many of the probe sets that more than two-fold upregulated in the perfused samples are not highly upregulated in the non-perfused samples. We believe that this is likely being caused by the higher purity of tissue hybridized to the MOE430v2 arrays.

Since the MOE430v2 array encompasses all of the probe sets of the MOE430A platform and includes the 430B probe sets as well, we recommend the perfused sample data be used alone. We believe that combining both data sets will require assumptions to be made which will likely draw attention away from the biological conclusions of any publication.

We performed analysis of functional enrichments on the genes identified in the perfused samples, identifying Gene Ontology categories that are statistically over-represented in the list of probe sets. This will allow us to identify genes of interest to further study.

6. CURRICULUM VITAE

PATRICK JAMES VILLENEUVE, MDCM, FRCSC

Education

Biochemistry, University of Ottawa
PhD candidate — JUL 2004 – ongoing
RCPSC Clinical Investigator Program

Thoracic Surgery, University of Ottawa
Fellowship — JUL 2009 – JUN 2011

General Surgery, University of Ottawa
FRCSC — JUL 2002 – JUN 2009

Medicine, McGill University
MD, CM — SEP 1998 – APR 2002

Chemical Engineering, University of Ottawa
BASc, Biotechnology Option — SEP 1993 – APR 1998
Magna Cum Laude

Biochemistry, University of Ottawa
BSc Honours, Biotechnology Option — SEP 1993 – APR 1997
Magna Cum Laude

Awards

- Terry Fox Foundation / National Cancer Institute of Canada Clinical Research Fellowship (2005-2007; value $86,000)
- University of Ottawa National Excellence Scholarship (2005-2007; value $11,400)
- University of Ottawa PhD Admission Scholarship (2007-2009; value $6000/year)
- Outstanding Paper, Department of Surgery Collins Research Day (2007)
- Outstanding Resident Teacher Award, Department of Surgery (2003)
- Award for high score in yearly in-training (CAGS) exam (2002, 2003, 2009)
- Dean's Honour List, Faculty of Medicine (2000)
- Dean's Honour List, Faculty of Science (1995, 1997)
- University of Ottawa Merit Scholarship (1996)
- University of Ottawa Admission Scholarship (1994)
- Bell Canada Scholarship (1994)

Publications

Villeneuve PJ, Krzyzanowski PM, Duquette M, Tang MY, Coulombe J, Andrade-Navarro MA, Sundaresan RS and Gray DA (2009) Age-related alterations in patterns of pulmonary metastases and transcriptional profiles in extremely old mice [submitted to Lung Cancer].

Villeneuve PJ and Sundaresan RS (2009) Surgical Management of Colorectal Lung Metastasis. Clinics of Colon and Rectal Surgery 22(4) [in press].

Villeneuve PJ and Sundaresan RS (2006) Complications of Pulmonary Resection: Post-Pneumonectomy Pulmonary Edema and Post-Pneumonectomy Syndrome. Thoracic Surgery Clinics of North America 16(3): 223-234. [PMID: 17004550]

Villeneuve PJ (2002). The placebo standard in regulatory market approval: Why the Declaration of Helsinki has been ignored for 35 years. McGill Journal of Medicine 7: 52-55.

Presentations & Posters

Villeneuve PJ, *Gray DA* and Sundaresan RS (October 4-6, 2007) Age-related changes in the mouse and human lung and their relevance to lung cancer. Poster, European Conference on Cancer and Ageing, Warsaw, Poland.

Villeneuve PJ, Gray DA and Sundaresan RS (September 8, 2007) Patterns of pulmonary metastasis are modified by increased age. Presentation, Canadian Association of Thoracic Surgery, Canadian Surgical Forum, Toronto, ON

Villeneuve PJ, Gray DA and Sundaresan RS (April 2007) Patterns of pulmonary metastasis are modified by increased age. Presentation, Collins Surgical Research Day, Department of Surgery, University of Ottawa, Ottawa, ON.

Villeneuve PJ, Gray DA and Sundaresan RS (September 6, 2006) Patterns of pulmonary metastasis are modified by increased age. Presentation, Resident Research Retreat, Canadian Surgical Forum, Calgary AB

Villeneuve PJ, Gray DA and Sundaresan RS (October 18, 2005) Increased oxidative damage and compromised responses to oxidative stress may favour neoplasia in aging murine lungs. Poster, Ottawa Health Research Institute Research Day, Ottawa ON

Villeneuve PJ, Gray DA and Sundaresan RS (September 7, 2005) Aging murine lungs develop tissue microenvironments that may favour neoplasia. Presentation, Resident Research Retreat, Canadian Surgical Forum, Montreal QC

Villeneuve PJ, Gray DA and Sundaresan RS (September 9, 2004) Transcriptional changes in aging human lung associated with cancer susceptibility. Presentation, Resident Research Retreat, Canadian Surgical Forum, Ottawa ON

Villeneuve PJ and Fairfull-Smith RJ (September 18, 2003) A gender bias exists in the choice of operative approach in patients undergoing appendectomy. Poster and presentation, Canadian Surgical Forum, Vancouver BC

Research completed

Molson Medical Informatics Project (1999) – Website produced demonstrating embryologic development of the cardiovascular system in humans.
http://sprojects.mmi.mcgill.ca/embryology/cvs/default.html
Supervisor Dr. E. Daniels

Chemical engineering research thesis (1998) – Recombinant Pharmaceuticals from Plant Tissue Cultures: Bioreactor scale-up suitability of differentiated and de-differentiated cell cultures.
Thesis supervisors Drs. I. Altosaar, Z. Duvjnak

Biochemistry research thesis (1997) – Electroporation as an alternate transformation technique for use in Maize Endosperm Suspension Cultures.
Thesis supervisor Dr. I. Altosaar

Certification & Extracurricular

Advanced Trauma Life Support (recertified 2008)
Advanced Cardiac Life Support
American College of Surgeons Ultrasound Course for Residents (2009)
Interests: camping, canoeing, hiking, cross-country skiing, classical music, freshwater aquaria, scuba diving